Harmonic Emissions Assessment for common DC and AC Electric Vehicle Charging Station Architectures

by

Gagandeep Sharma

A thesis submitted to the
School of Graduate and Postdoctoral Studies in partial
fulfillment of the requirements for the degree of

Master of Applied Science

In

Electrical and Computer Engineering

ECE Department/Ontario Tech University/Dr. Vijay K. Sood

University of Ontario Institute of Technology (Ontario Tech University)

Oshawa, Ontario, Canada

October 2020

THESIS EXAMINATION INFORMATION

Submitted by: **Gagandeep Sharma**

Master of Applied Science (MASc) in Electrical Engineering

Thesis title: Harmonic Emissions Assessment for common DC and AC Electric Vehicle Charging Station Architectures

An oral defense of this thesis took place on **October 23, 2020** in front of the following examining committee:

Examining Committee:

Chair of Examining Committee	Dr. Ying Wang
Research Supervisor	Dr. Vijay K. Sood
Examining Committee Member	Dr. Walid Morsi Ibrahim
Thesis Examiner	Dr. Akramul Azim

The above committee determined that the thesis is acceptable in form and content and that a satisfactory knowledge of the field covered by the thesis was demonstrated by the candidate during an oral examination. A signed copy of the Certificate of Approval is available from the School of Graduate and Postdoctoral Studies.

ABSTRACT

Future transportation needs are going to be met by Electric Vehicles (EVs) because of global pollution by oil-based vehicles and climate change. In order to meet the charging demand and range anxiety of EV users, Fast Charging Stations (FCS) are required. As these FCS are grid-connected, they are going to be a new non-linear load for the host utility, which will impact its Power Quality (PQ).

In this thesis, Common DC and AC bus (CDCB and CACB) architectures for grid-connected FCS are examined. For both architectures, two-level Voltage Source Converter (VSC) is used to connect the EV FCS to the grid, and further cascaded DC-DC converters are used for voltage regulation at the charger end. The Unit Template (UTC) and dq-SRF control methods are implemented for switching control of the VSC. The Constant Current-Constant Voltage (CC-CV) method is used for the control of DC-DC converters. The simulations are run in MATLAB/Simulink®. The following studies are carried out:

- Comparison of CDCB & CACB architectures by varying load and transformer connections: - results show that CDCB architecture gives better performance in terms of charging and PQ, and the star-delta configuration of Distribution Transformer (DT) connections provides lower harmonics.

- Comparison of two control strategies for the VSC using UTC and dq-SRF control strategies: - results show that UTC strategy performs better than dq-SRF method for control and operation of VSC.

- Studying the impact of varying X/R ratio and MVA_{SC}: - results show that MVA_{SC} and X/R ratio has significant impact on a weak-grid operation connected with the FCS.

- Studying the system with and without PV-panel: - results show that inclusion of PV-panel increases the reliability and efficiency of the system. There is small increase in THD_V and THD_I due to inclusion of PV-panel, but is as per the IEEE-519 standards.

- Comparison of a Conventional-Capacitor (CC) with Super-Capacitor (SC) for the common DC bus: - results show that SC escalates the charging speed with fewer harmonics.

- Comparison of two architectures in Vehicle to Grid (V2G) mode: - results show low harmonic content and better State of Discharge (SoD) with CDCB architecture.

Keywords: Electric grid; Electric Vehicle (EV); FCS; power quality; harmonics.

AUTHOR'S DECLARATION

I hereby declare that this thesis consists of original work of which I have authored. This is a true copy of the thesis, including any required final revisions, as accepted by my examiners.

I authorize the University of Ontario Institute of Technology (Ontario Tech University) to lend this thesis to other institutions or individuals for the purpose of scholarly research. I further authorize University of Ontario Institute of Technology (Ontario Tech University) to reproduce this thesis by photocopying or by other means, in total or in part, at the request of other institutions or individuals for the purpose of scholarly research. I understand that my thesis will be made electronically available to the public.

_____ GAGANDEEP SHARMA

STATEMENT OF CONTRIBUTIONS

Part of the work described in the thesis has been published as:

A. Journal Paper

1. **Gagandeep Sharma**, Vijay K. Sood, Mohammad Saad Alam and Samir M. Shariff, "Comparison of Common DC and AC Bus Architectures for EV Fast Charging Stations and Impact on Power Quality", *Elsevier eTransportation*, Volume 5, August 2020.

B. Conference Paper and Book Chapter

2. **Gagandeep Sharma** and Vijay K. Sood, "Power quality problems in Grid-connected Electric Vehicle (EV) Fast charging Fast Charging Stations", 2020 Electric Power and Renewable Energy Conference (EPREC 2020), May 29-30, 2020 held at NIT, Jamshedpur (India) and accepted for publication in Scopus-indexed SPRINGER-Lecture Notes in Electrical Engineering (LNEE)in the book title "*Recent Advances in Power Electronics and Drives*".

C. Book Chapter

3. **Gagandeep Sharma** and Vijay K. Sood, "Impact of Electric Vehicle Charging Infrastructure on the Distribution Network Power Quality: Challenges and Opportunities", book-chapter accepted in the upcoming book titled "*Developing Charging Infrastructure and Technologies for Electric Vehicles"* to be published by IGI Global Publishers, USA.

I performed the majority of the synthesis, simulation, and writing of the manuscript.

Acknowledgments

Firstly, and foremost I like to pay my gratitude and sincere thanks to my supervisor Dr. Vijay K. Sood, for his continuous support, guidance, and valuable suggestions throughout this thesis work. He always been supportive and give me insight to do the work by adding technical and writing skills in a right manner. I am obliged for the opportunity he gave me to pursue my Masters in Ontario Tech. University, and for remarkable support in every aspect.

I acknowledge the support of Ontario Tech. University administration and support staff to help in a wonderful manner.

I am grateful to my examining committee members; Dr. Waleed Morsi Ibrahim, Dr. Akramul Azim and defence chair Dr. Ying Wang for taking time to review my work.

I am thankful to management of Canada Post to grant me leave to complete my studies and to being always supportive.

I would also like to thank my lab colleagues and fellow students for valuable discussions and great time we had together.

Last but not least, I would like to thank my family, friends and my son Aadit for love and support they gave me during my work.

CONTENTS

LIST OF FIGURES

LIST OF TABLES

LIST OF ACRONYMS

APF	Active Power Filter
BEV	Battery Electric Vehicles
BMS	Battery Management System
CC-CV	Constant Current-Constant Voltage
CCS	Combo Charging System
CACB	Common AC Bus
CDCB	Common DC Bus
DPF	Displacement Power Factor
DT	Distribution Transformer
ECM	Equivalent Circuit Model
ESS	Energy System Storage
EV	Electric Vehicles
EVSE	Electric Vehicle Supply Equipment
FCS	Fast Charging Station
FFT	Fast Fourier Transform
GHG	Green House Gases
G2V	Grid to Vehicle
HCC	Hysteresis Current Controller
HEV	Hybrid Electric Vehicles
ICE	Internal Combustion Engine
IGBT	Insulated-Gate Bipolar Transistor
NPC	Neutral Point Clamped
OCV	Open Circuit Voltage
PCC	Point of Common Coupling
PEV	Plug-in Electric Vehicles
PFC	Power Factor Control
PHEV	Plug-in Hybrid Electric Vehicles
PLL	Phase Locked Loop
SoC	State of Charge
SoD	State of Discharge
SRFT	Synchronous Reference Frame Theory
TDD	Total Demand Distortion
THD	Total Harmonic Distortion
UTC	Unit Template Control
VSC	Voltage Source Converter
V2G	Vehicle to Grid

CHAPTER 1

INTRODUCTION

1.1 Background

Pollution has become the world's biggest human-created problem. Climate change is now visibly affecting daily life. Air pollution was the earliest form of pollution which was introduced well before the age of modern industrialization [1]. As per World Health Organization (WHO) reports, there are 4.2 million deaths worldwide annually due to exposure to ambient air pollution and 91% of the world population presently lives in places where air quality exceeds WHO limits. Air pollution is now the fourth major cause of deaths in the world [2]. There are different sources for air pollution. Burning of wood and coal in earlier civilization and then vast industrialization introduced the World with huge air pollution. Massive air pollution increased the proportion of Green House Gases (GHG) in the environment which is resulting now into climate change.

Pollution due to transportation is playing a big role in increasing the GHG effect. There are strict regulations applied to emissions created by Internal Combustion Engine (ICE) vehicles, but, still a large proportion of carbon emissions are produced by the growing transport sector. These emissions include various concentrations of carbon dioxide, nitrogen oxides, particulate matter ($PM_{2.5}$ and PM_{10}), sulfur dioxide, carbon monoxide and Volatile Organic Compounds (VOCs) [3]. As per IEA reports, there is growth of about 1.7% annually in emissions by transport sector in past decade. Transportation sector is accountable for 24% of direct CO_2 emissions from fuel combustion [4].

Pollution due to the transportation sector is growing exponentially and on the other hand mobility is the need of society due to increase in urbanization and population. So, control of emissions by transport sector become focus of international and regional level controlling authorities. After the

Kyoto protocol (1997), Doha Amendment (2012), Paris Agreement (2015), COP24 (2018), and COP25 (2019), many countries are now willing to take steps towards adoption of green technology in mobility. Globally, pollution due to transportation accounts for one quarter of total emissions i.e. 8 giga tons per year as per Intergovernmental Panel for Climate Change (IPCC) [1][5][6]. Many countries are eager to take some serious steps to meet the challenges in the transportation sector and positive results are coming. Some proposed steps are mentioned in an engagement paper by the World Bank, as follows [7]:

- Norway wished all passenger cars, LCV and city buses should be zero emission by year 2025.
- United Kingdom and France offered a ban on sales of petrol and diesel vehicles after 2040.
- South Africa is willing to implement Draft Green Strategy by which the target is to 5% decrease in the production of GHG by 2050.
- Germany is working towards 1 million xEVs (Battery Electric Vehicles (BEV), Hybrid Electric Vehicles (HEV) and Plug Hybrid Electric Vehicles (HEV)) on the road by 2020.
- China is considering ban on sale of new petrol and diesel vehicles in near future.
- India is working on 15% vehicles to be EV by 2023.

Similarly, various countries and cities are working towards green mobility future and planning to reduce the ICE based transportation. These steps by the UN and leading nations motivated prominent car manufacturing companies to work towards the green EV technology. Several companies like Nissan, BMW, Ford, GM, Hyundai, Honda and Tesla etc. are producing and working on research and development of xEVs production on a mass scale. Stronger collaboration amongst the leading economies of the world can create real change in the transportation sector which is second largest emitting sector.

EVs produce zero emissions and are more efficient than Internal Combustion Engine (ICE) vehicles. The number of EVs (Battery Electric Vehicle (BEV) and Plugged Hybrid Electric Vehicle (PHEV)) is increasing worldwide. Still, there are few obstacles in the way of technology like range anxiety, reliable charging infrastructure, charging time, and impacts on the power quality due to chargers. Many consumers are still hesitant to accept EVs as they are range concerned (mileage and overnight charging). Electric Vehicles (EVs) will help in the future reduction of Green House Gases (GHG) emissions. According to IEA Global EV Outlook 2019, there was a 63% increase in EVs in the year 2018 compared to the previous year [8][9]. Predictions are that globally there will be 120 million EVs on the road by 2030. This increase in EV numbers will results in a surge for energy-demand. There is a forecast for an energy-demand increase to 280 billion kWh by the year 2030 in US, China and Europe [10]. This will require a vast investment in charging infrastructures and emphasizes the need of fast charging.

1.2 Levels and Standards of Charging

Battery Charging is the foremost important concern of xEV users. Range anxiety, compatibility, time duration for charging, battery depletion etc. are the major worries of EV users. Battery technology is improving day by day and new batteries with better range and more life are coming into the market. There are many factors which deplete the charging of battery like number of passengers, air-conditioning, road conditions, weather etc. [11]. EV charging needs reliable infrastructure for charging. Charging can be done with various methods like slow charging or overnight charging at homes, medium charging, fast charging at charging stations. We can understand charging methods as per Table 1.1:

Table 1.1: Different types of Charging levels and specifications [12-14]

Charger Description	**Level 1**	**Level 2**	**Level 3**
Charger Type	On-board	On-board	Off-board
Charging Speed	Slow-charging	Slow/semi-fast charging	Fast charging
Typical Use	Residential	Residential/office/work	Charging Station
Typical Charging Time	6-10 Hours (Overnight Charging)	30 Minute to 4 Hours	10 to 50 Minutes
Voltage Level	120 V	208 or 240 V	200-500 V_{DC}
Power Level	1.1 to 3.3 kW	3.3 to 19.2 kW	20-150 kW
Charger location	On-board	On board	Off-board
Miles of range per hour of charging	12-25 miles per hour depending upon rating of charger	3.5 hours for 80-mile battery 8 hours for 200-mile battery	80% charging within 30 minutes (depends upon power level of charger and car model
Number of Phases	1-Phase	1 and 3-Phase	3-Phase
Type of connectors & Standards	NEMA 5–15, SAEJ1772	IEC 62196, IEC 60309, SAEJ1772, IEC 62198-2-Mennekes and 62198-2-scame connectors	SAE J 1772 Combo, CHAdeMO and IEC 62196 Mennekes Combo
Equipment Type	 16 A, 110 V Source: evcharge solutions	 50 A, 208/240 V Source: Leviton	 200 A, 200-450 V DC Source: Blink

In Table 1.1, different Levels of EV charging and associated connectors are classified. Table 1.1 shows the voltage level, maximum current, maximum power and the types of connectors as proposed by the leading international agencies. The time of charging of EVs depends upon level of charging and type of connectors.

Several societies and researchers are working on other types of connectors too. Battery charger, EV Inlet and EV connector comes under the Electric Vehicle Supply Equipment (EVSE). Chargers

are specified according to Level (as given in Table 1.1) as Level 1, 2 and 3. EV Inlet is the physical connection between vehicle and EVSE connector. Other categorization of charging is according to the following four modes: -

- **Mode 1** is the slow charging by a household type socket without any safety feature and this mode is irrelevant in the context of EVs and is not allowed for EV charging in North America.
- **Mode 2** is also a household type charger but having an in-cable protection device for the protection of system.
- **Mode 3** may be slow or fast charging and having internet and communication technologies installed in it and devising control and protection features.
- **Mode 4** is a DC charging method and having excellent control and protection features included [15].

All DC fast charging levels use off-board charging equipment. Inclusive development of any technology requires suitable and widely accepted standards. Globally, different standards are developed by leading organizations for the development of EV charging stations and associated Electric Vehicle Supply Equipment (EVSE). The responsible organizations for the development of EV charging standards are International Electrotechnical Commission (IEC), Society of Automotive Engineers (SAE), IEEE and CHAdeMO.

The most famous standard under IEC is SAE J1772 which is known as J plug maintained by SAE. Another popular standard under IEC is “CHAdeMO” (CHArge de MOve) which is coined by the company of same name formed by Tokyo Electric Power Company (TEPCO) and other leading car makers of Japan [16-18]. There is a competitive race between both the technologies for

adaptation by the EV manufacturing companies and users. We can understand the few important standards which are governing the EV charging system with the help of following Table 1.2.

Table 1.2: Global Standards for Governing the EV Charging System [19]

Standards	**Series**	**Area/Scope**	**Method of Charging**
IEC 61851	IEC 61851-1	Defines cables and plug setups	Conductive
IEC 61851	IEC 61851-23	Describes electrical safety, harmonics, grid connection, and communication architecture for DCFC station (DCFCS)	Conductive
	IEC 61851-24	Explains digital communication for DC charging control	Conductive
IEC 62196	IEC 62196-1	Explains general requirements for EV connectors	Conductive
	IEC 62196-2	Describes coupler types for different charging modes	Conductive
	IEC 62196-3	Defines Connectors and Inlets for DCFCS	Conductive
IEC 60309	IEC 60309-1	Explains general requirement for Charging Station	Conductive
	IEC 60309-2	Describes different sizes of plugs and sockets with different number of pins based on current supply and number of phases, also defines color coded connector based on voltage range frequency	Conductive
IEC 60364		Describes about electrical installations for buildings	Conductive and Inductive
SAE J1772		Conductive charging system for define connectors for AC charging Describes new combo connector for DCFCS	Conductive
SAE J2847	SAE J2847-1	Describes the communication medium and criteria for the EV to connect to the utility for AC Level 1and AC Level 2energy transfer	Conductive and Inductive
	SAE J2847-2	Defines additional messages for DC energy transfer	Conductive and Inductive
SAE J2293	SAE J2293-1	Describes the total EV energy transfer system and allocates requirements to the EV or EVSE for the various system architectures	Conductive
SAE J2344		Describes guidelines for Electric vehicle safety	Conductive and Inductive
SAE J2954		Inductive charging under development	Inductive
IEC 61980	IEC 61980-1	Electric vehicle wireless power transfer (WPT) systems-Part 1: General requirements	Inductive
	IEC 61980-2	Specific requirements for communication between electric road vehicle (EV) and wireless power transfer (WPT) systems including general background and definitions	Inductive
	IEC 61980-3	Specific requirements for electric road vehicle (EV) magnetic field wireless power transfer (MP-WPT) systems including general background and definitions. (e.g. efficiency, electrical safety, EMC, EMF)	Inductive
IEC TS 62840-1	IEC TS 62840-1	Electric vehicle battery swap system –Part 1: General and guidance	Battery Swapping
SAE J1773		Specification is applicable to manually connected inductive charging for Levels 1 and 2 power transfer.	Inductive
SAE J2954		Wireless Power Transfer for Light-Duty Plug-In/Electric Vehicles and Alignment Methodology	Inductive
UL 2202		Electric Vehicle Charging Equipment	Conductive and Inductive
GB/T 20234.1-2011		Connection set of conductive charging for electric vehicles- Part 1:General requirements	Conductive

GB/T 20234.2-2011	Connection set of conductive charging for electric vehicles-Part2:AC Charging coupler	Conductive
GB/T 20234.3-2011	Connections set of conductive charging for electric vehicle Part3:DC charging coupler	Conductive
GB/T 27930-2011	Communication protocols between off-board conductive charger and battery management system for the electric vehicle	Conductive
GB/T 28569-2012	Electric energy metering for electric vehicle AC charging spot	Conductive
GB/T 29317-2012	The terminology of electric vehicle charging/battery swap infrastructure	Battery Swapping
GB/T 29318-2012	Electric energy metering for electric vehicle off-board charger	Conductive and Inductive
UL 9741 Ed. 1(2014)	Investigation For Bidirectional EV Charging System Equipment	Inductive
UL 2251	The standard for Safety for Plugs, Receptacles, and Couplers for Electric Vehicles.	Conductive
UL 2734 Ed. 3(2015)	Connectors And Service Plugs For Use With On-Board EV Charging Systems	Conductive
C601	Plugs and Receptacles for EV Charging	Conductive
G105:1993	Connector applicable to quick charging system	Conductive
G106:2000	EV Inductive charging system: General Requirement	Inductive
G107:2000	EV Inductive charging system : Manual Connection	Inductive
G108:2001	EV Inductive charging system: Software Interface	Inductive
G108:2001	EV Inductive charging system: General Requirement	Inductive

These standards are important to select the connectors for charging stations. Connector is very important device which connects the EVSE and Plug-In Electric Vehicle (PEV). SAE (USA), Japanese Auto standards development organization and Tesla electric automobiles etc. are working to develop reliable and efficient connectors [20].

The SAE J1772 type connectors are used in Japan and North America, and are comprise of 5 pins. Type-2 or Mennekes connectors, are used in Europe and having 7 pins. These connectors can also be used in 3-phase system. China is also using modified version of Mennekes connectors under the standard GB/T 20234.2-2015. Tesla has an exception to this regional bifurcation and uses SAE J1772 in North America, while uses Type-2 connectors in Europe. The addition of DC connector in the existing AC connector was developed in 2011 and is known as Combo Charging System (CCS). It uses the HomePlug GreenPHY communication protocol [21] [22].

Sufficient charging infrastructure is required for the expansion of EV vehicle technology. Fast and adequate charging stations are essential for the mass approval and to meet the anxiety of EV users. Car manufacturing companies have proposed different charging methods including Level-1 charger (slow charger), Level-2 charger (moderate charger), and Level-3 charger (DC Fast Charger). In these, Level-3 charger is considered as a fast charger, and installation can be made in car parks, either public or private. One of the solutions is to upgrade the legacy power grid system and consider the inclusion of fast chargers in it. The other way out is to develop the FCS infrastructure, which should connect to the grid at nearly Unity Power Factor (UPF). It would have a minimal impact on the power quality of the input grid current and fewer issues on the grid side [23]. These FCS should be installed at different places like parking lots, commercial sites, etc. akin to a fuel station.

The number of EVs are growing worldwide. They are expected to increase from 5 hundred thousand in 2012 to 10 million globally by year 2020 as already reaches up to 7.2 million in 2019. Bloomberg NEF also speculates that 1 in 10 vehicles will be an EV by 2025, and there will be a requirement for 12 million public FCS by 2040. These number of FCS need an estimated $ 400 billion in investments on infrastructure. The EV market is projected to rise from USD 146,902.20 Million in 2019 to USD 359,854.56 Million by the end of year 2025. The Compound Annual Growth Rate (CAGR) is expected to be 16.10% in the EV market. Fast charging stations components will also be a major part of this unprecedented development. CHAdeMO 4 charger is predicted to be the highest gainer in this period [24]. This EV growth rate is expected to continue in future years, and therefore FCS development is also required. There is a little decline in the CAGR (-3.3 %) of EV market in year 2020 due to COVID-19 pandemic.

Table 1.3 shows the current number of EV charging stations in few leading countries:

Table 1.3 Number of Charging Stations (leading EV user countries) as per 2019

Country	Number of Charging Stations
Norway	7,065 (approx. 400 FCS and semi FCS)
Canada	5,004 (approx. 772 FCS)
USA	78,500 (approx. 11,000 FCS)
China	4,96,000 (approx. 2,00,000 FCS)
United Kingdom	9,200 (approx. 1,600 FCS)

It has been predicted that AC supply is the source for most of the power required to charge the EV batteries. There are chances that power demand will increase to 300 Twh to charge the expected 130 million EVs by year 2030 [25]. FCS will emerge as a new load to utility companies. This higher amount of power demand may have a negative impact on the power quality (particularly harmonics) indices of the grid. The massive popularity of EVs and need of adequate charging infrastructure gave motivation for the said work.

1.3 Problem Formulation and Tasks

The study problem is formulated after doing an extensive literature survey (included in Chapter-2). It is understood that FCS are required to meet the anxiety and requirements of EV users. In this study, grid-connected common AC and DC bus architectures are proposed for FCS and their impact on power quality (harmonic assessment, in particular) is the focus of this study.

The following tasks are set for the research work:

1. Comprehensive literature survey related to EVs, architectures of FCS, power quality impacts (particularly harmonic assessment) on grid due to fast charging of EVs, different kinds of batteries used in EVs, battery management system, power electronic converters and their control algorithms.
2. To make Simulink model of common AC and DC bus FCS architectures.

3. Implementation of VSC and efficient control algorithm in the Simulink model of FCS.
4. Comparison of common AC and DC bus architectures in relation to harmonic assessment and impact of it on the electric-grid by using different transformer configurations in steady-state and impact on PCC voltages and current in dynamic-state during charging operation (G2V).
5. Inclusion of PV-panel into the FCS and comparison of grid-connected FCS with and without PV-panel.
6. To study the impact of varying X/R ratio and Short-circuit capacity (MVA_{SC}) on the performance of grid-connected FCS and harmonics.
7. Impact by replacing Conventional-Capacitor (CC) with Super-Capacitor (SC).
8. Comparison of CDCB and CACB during Vehicle to Grid (V2G) operation.

The results are compared in terms of SoC, PCC voltages, PCC currents, THD_V and THD_I.

1.4 Challenges and Assumptions

There are few challenges in performing these tasks are as follows:

1. The rating of FCS and selection of number of EVs for both the architectures.
2. Selection of appropriate control algorithm for AC/DC converter and DC-DC converter.
3. Selection of X/R ratios to determine the impact on weak-grid (low MVA_{SC}).
4. Computational limitations to run simulations for both the architectures.

Following assumptions are made to carry out the simulation work:

1. Ten number of EVs are assumed as full-load for both the architectures.
2. Parasitic inductance values are assumed.
3. The values of X/R is assumed as 0.2 (minimum value) and 10 (maximum value).
4. The parallel capacitance across the EV batteries.

CHAPTER 2

LITERATURE REVIEW

Electric Vehicles (EVs) are topics of research and interest for different disciplines of Science and Technology. Impacts of EV charging on the electric grid has becomes the field of research of many due to large scale deployment of EVs in present years and a possible future surge is predicted. In this chapter, a thorough literature review is presented to formulate the problem and to understand the concepts in detail. Literature review is divided into following sub-sections:

1. History of EVs and rejuvenation of the EV technology in the wake of increasing pollution due to automotive vehicles.
2. Inductive and Conductive Charging of EVs.
3. Common AC and DC Bus Charging Architectures for FCS.
4. Common Configurations of Converters used in FCS.
5. Power quality problems due to Grid-connected FCS.
6. Commonly used batteries in EVs, Battery Management System (BMS).
7. Parameter Estimation of the batteries.
8. Impact of variation in X/R ratio and Short circuit capacity (MVA_{SC}) on grid-connected FCS.

2.1 History of EVs and rejuvenation of the EV technology in the wake of increasing pollution due to automotive vehicles

EVs are not a recent technology. Early inventions in the transportation started with EVs, but the Internal Combustion Engine (ICE) technology took over the lead soon afterwards due to some revolutionary inventions and the oil lobby. Due to oil crisis and climate change impacts, countries and companies again started working towards the xEV (BEV, PHEV, HEVs etc.) technology. EV technology was firstly developed in 1884. The first U.S. successful EV was launched in 1891 and

the growth continued till the invention and implementation of starter of ICE in 1912 by Charles F. Kettering. ICE based vehicles grabbed the market and EV technology was not propelled due to efficient technique of fuel-based automobile, oil availability and limitations in the battery technology of EVs. Around about 1920, EVs lost their commercial viability and the market was grasped by ICE vehicles. Car manufacturing companies also become totally focussed on ICE vehicles [26] [27].

In 1965, an important report by U.S. President's science advisory committee titled "Restoring the Quality of our Environment" drew the attention of the world towards the problem of climate change and pollution [28]. Afterwards, due to oil embargo in 1973 and growth of power electronics devices and converters in 1970s [29], transformation in xEV technology began.

Power Electronic converters are playing a big role in popularity of modern day xEVs. xEVs need reliable and ample battery charging to meet with the anxiety of consumers and to compete with ICE technology. Thus, researchers and companies are focused on dependable charging infrastructure and the battery technology. EV batteries need fast and reliable charging infrastructure. Scientists and researchers are working on innovative battery technology as well as fast charging infrastructure.

Charging is a key part of xEV industry as it drives the interest of consumers, but reason of anxiety too. EV users worry about battery State of Charge (SoC), charging time, availability of chargers and time of charging.

2.2 Inductive and Conductive charging of EVs

a. Inductive Charging: Magnetic coupling is the principle behind the inductive charging. In this operation, power is initially converted to DC using a rectifier and then again converted to AC fit

for the transmitter placed on the ground. The receiver is placed on the vehicle chassis and charging power is transmitted to the vehicle by the method of magnetic resonance. Whenever there is need of charging, the vehicle is driven over the transmitter and the process of wireless transfer starts. Rectification progression happens again to convert AC to DC for battery charging. Higher switching frequency and power density is required for inductive charging. It is challenging task to achieve high efficiency at higher frequencies. There is need of appropriate voltage and current gain stages to attain these goals. Wireless technology is advantageous as compared to conductive charging in some aspects as it needs no physical connection, easy in operation, less infrastructure required, charging time is less. But, still it is not much popular and in developing stage due to few limitations like chances of loss of energy, sensitive, possible bad impact on humans etc. [30] [31].

b. Conductive Charging: In conductive charging, there is a physical link between xEV and electrical power system as a direct connection between EV to the electric power through extension cord and connectors. The type of connector employed plays an important role in this kind of charging. Conductive charging can be used in households, charging stations and public parking places. This sort of charging is simple, reliable and easy to implement [32].

In this work, conductive charging is used to study the system. Details and requirement of conductive charging are described next.

- **Different methods of Conductive Charging and Infrastructure requirement of EVs:** Charging is the first requirement of an EV user. There are many concerns which increases the anxiety of EV consumers like range anxiety, charging time, battery life, fear of battery drainage, location and availability of charging stations etc. The range and efficiency of new EVs are far better than their previous counter-parts. The new batteries having better life and vehicle can travel more in a single charge. But, in comparison to a typical gasoline car

which can travel around 500 kms with one full tank, the range of most of the EV battery full charging is only about 300 kms. There are many factors which deplete the battery charge like number of passengers, air-conditioning, weather, need to retain margin of battery charging etc. [33]. Therefore, xEV charging needs reliable and sufficient infrastructure for charging. EV charging can be done with various methods like slow charging or overnight charging at homes, medium charging, fast charging at charging stations as given in Table 1.1.

Many countries and car manufacturing companies are developing conductive charging infrastructure and policies to encourage adoption of EVs like; Norway implemented an aggressive approach to encourage the adoption of EVs as many kinds of incentives are given on the purchase of EVs and afterwards for the use of public parking and toll roads. Sales of Plug-in Electric Vehicles (PEVs) reached 49.1% (2018) and 56% (2019) in Norway [34] [35]. According to the Norway Road Traffic Information Office (OFV), the sale of new fossil fuel vehicles is plunge by 60% in Norway, and one from two car sales in Norway is electric [36]. The availability of charging infrastructure is a prime reason in it.

Predictions show that there will be a big surge in EV adoption in the coming decade. There are chances of about 350 new EV models will be launched by different vehicle manufacturing companies by 2025. The big worry and obstacle in front of future EV buyers is reliable charging infrastructure. After the cost and driving range, charging infrastructure is the third foremost concern of future EV buyers. Infrastructure development requirements vary as per geographical location and even on city planning. EV charging is different from ICE fueling as ICE fueling needs fueling stations, but, there are multiple options for EV charging, it can be done at home, workplace, public charging stations, highways charging structures and apartments parking. Paradigm is

shifting towards public and fast charging, and in the coming future, there will be big investments in infrastructure development [37]. This development needs proper economical and installation planning which can meet the future EV penetration. Improper planning can be a set back for the EV adoption. There is possibility to attract investment in the field of setting up of FCS. Planning model can help to offer greater opportunity to EV drive convenience and will provide security for investors [38].

Charging of EVs is also classified as on-board and off-board. On-board charger is inbuilt in the vehicle and off-board charger is situated outside the vehicle. On-board charger is developed for a particular type and size of battery which is used in the vehicle. Household AC voltage can be connected to the on-board charger inlet. Charging of large batteries is not possible by using on-board charger as the charging process is slow and capacity of converter is less. Off-board charging technology is faster and the converter is capable of charging large batteries in shorter time. Communication with the battery control system is required in case of off -board battery charging unit. Communication protocol depends upon the vehicle model and off-board charger are designed to accommodate different technologies. IEC, SAE and CHADeMO are continuously developing new communication protocols [39].

2.3 Common AC and DC bus Infrastructure for the Fast Charging Stations

Fast Charging Stations (FCS) are still not widespread. There is a need of more FCS with the increase in number of EVs on the road. The selection of a suitable architecture will play a vital role for it. Two common solutions to design the FCS are common AC bus and common DC bus. In the FCS infrastructure, common AC bus charging and common DC bus charging are popular conductive charging technologies. These two types of infrastructure can also be used in wireless

technology with different operating principles. Simple layouts of both of these infrastructures are as shown in Figs. 2.1 and 2.2.

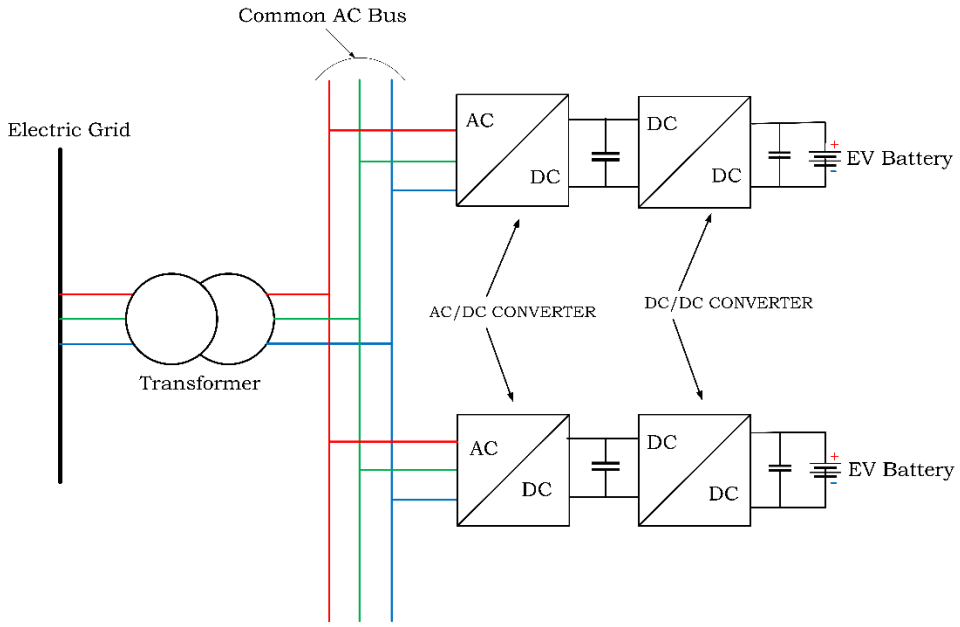

Figure 2.1. Schematic of Common AC Bus Charging

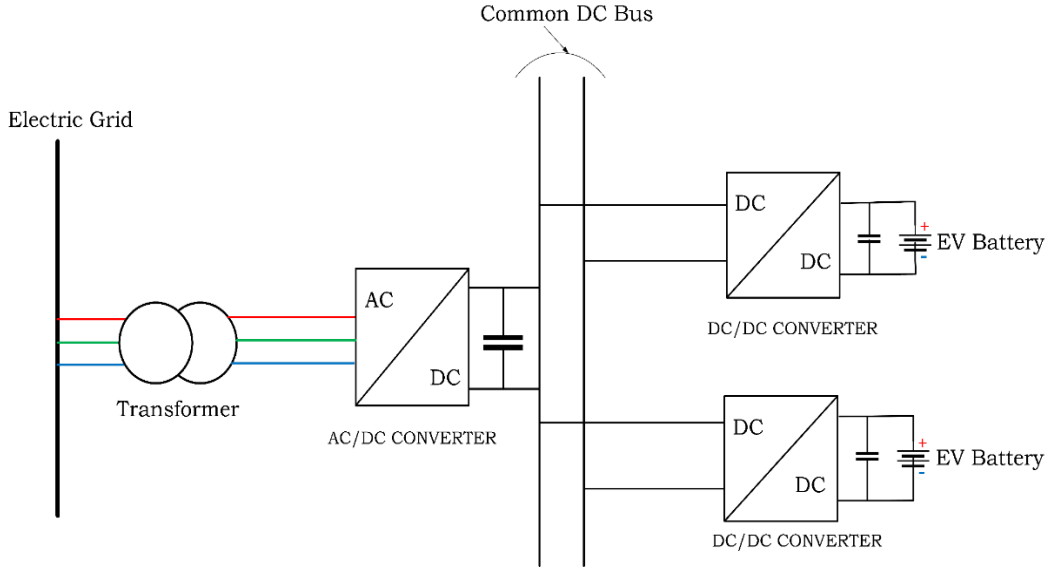

Figure 2.2. Schematic of Common DC Bus Charging

In Figs. 2.1 and 2.2, schematic of CACB and CDCB charging architectures is shown. Ref. [40] reviewed the existing state of EV charging infrastructure and concluded that FCS are a viable

solution to mitigate the impacts of EV charging on distribution grid, voltage fluctuations and harmonic distortions. Ref. [41] described two basic architectures for fast EV charging i.e. common AC bus charging and common DC bus charging. In the common AC bus architectures, all the chargers are having separate AC-DC converters and in common DC bus architecture, only one main AC-DC converter is required. The vehicles getting charged via household charging stations in a close neighbourhood can be considered as operating off a common AC bus. Ref. [42] proposed P-V control strategy for the control of converters in EV chargers. P-control is for the DC-DC converter and V-control is used for the AC-DC converters. Ref. [43] proposed cascaded control in dq-frame followed by PWM generator to send the gating pulses to converter to retain a constant DC voltage and CC-CV (Constant Current-Constant Voltage) Strategy for DC-DC converter for the battery charger. Ref. [44] did the EV load modelling for system stability and explained the associated equations and model to keep unity power factor operation. There is manipulation of q-axis current to achieve the unity power factor operation and d-axis current is manipulated to regulate the DC link voltage. Ref. [45] proposed a multi-objective off-board EV charging station which aims to enrich the operation of smart homes in smart grids, charging and discharging modes of EV battery through a DC interface, use of active and reactive conditioner to compensate power quality and reactive power management respectively.

It is evident from the literature review that AC-DC converters [46-48] are having paramount importance in the EV charging infrastructure irrespective of topology. In these converters, Voltage Source Converter (VSC) plays a vital role in the exchange of apparent power to and from the grid. The maximum amount of apparent power exchanged between the charger and grid is governed by the following equation [49]:

$$P_k^2 + Q_k^2 \leq \bar{S}^2 \tag{2.1}$$

Where $\bar{S}$ is the maximum apparent power of the inverter, P_k is the real power, and Q_k is the reactive power. The operating regions can be defined on the basis of signs of P_k and Q_k as shown in Fig. 2.3.

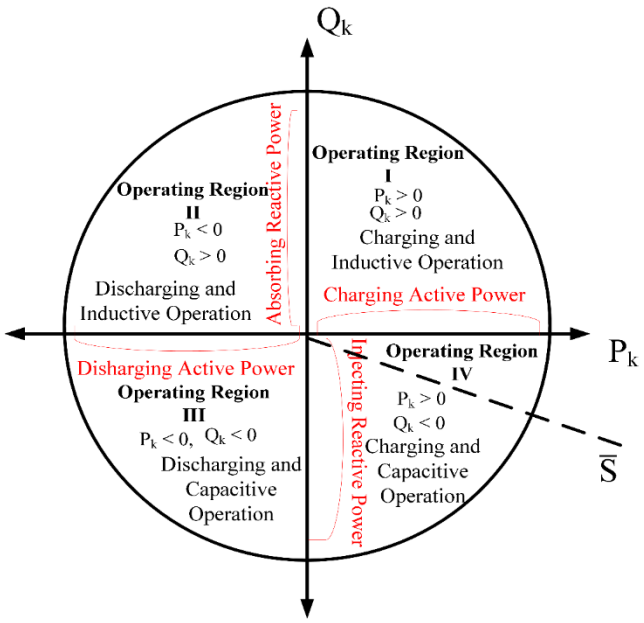

Figure 2.3. Operating region of the EV [49]

It is seen from Fig. 2.3 that operating regions of the EV depends upon the polarity of active and reactive power. Region I, is a charging operation, and both active and reactive power are positive. In Region II, the EV is supplying the load (or V2G operation), then active power is considered outgoing and reactive power is positive. Similarly, there are operating Regions III and IV, which support the injection of reactive power in the bi-directional operation of the charger.

Common AC and DC bus charging infrastructure is discussed in detail in next sub-sections.

2.3(a) Common AC Bus Charging system (CACBCS): In common AC bus, shared AC bus is used. MV-LV transformer is key equipment to supply the AC bus. Afterwards, there is separate AC-DC rectifier and DC-DC converter for each EV bay. The charging station can be combination of Level-2 (medium speed) and Level-3 chargers (fast speed) in common AC bus [50]. In CACBS, power electronic equipment can be used on-board and the solution will be inexpensive as compared to

common DC bus. Load management algorithm is needed for effective use of common AC bus charging system. Generally, IEC 62196 is used for connector standardization and IEC 61850-51 is used as communication standard [51] [52].

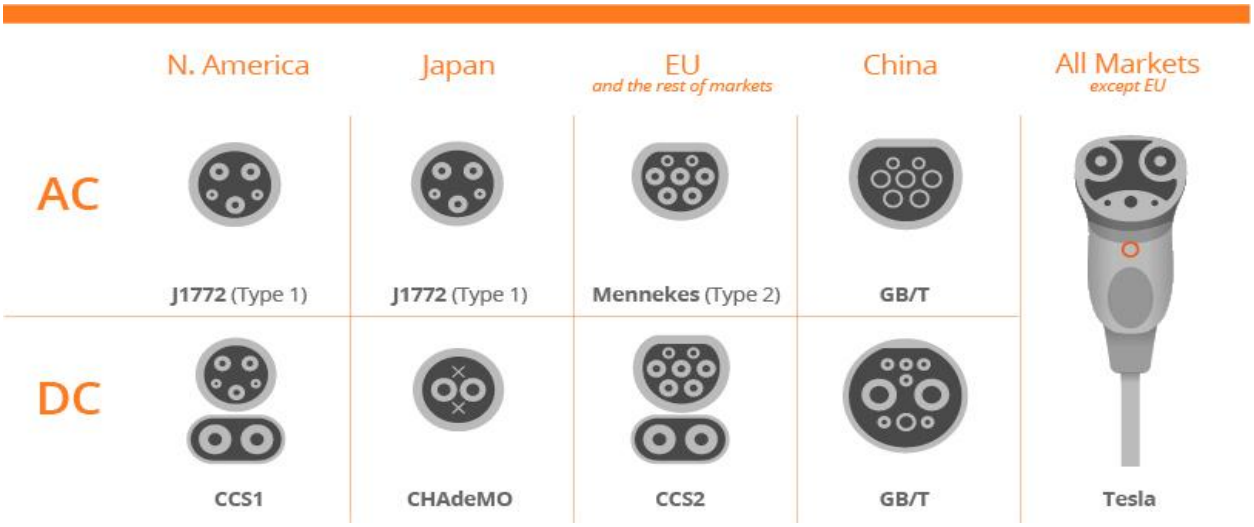

Figure 2.4. Different types of AC and DC connectors [53]

In Fig. 2.4, different types of AC and DC connectors for various regions of the world are shown which are commonly used in AC and DC bus infrastructure.

The literature shows that there are more conversion losses in case of AC bus architecture as compared to DC bus architecture. These are about 22% more conversion losses in AC bus architecture as compared to DC counterpart [54]. AC bus architecture can be used in public places, homes or at work. Dedicated EVSE is required which is governed by IEC 61851-1. AC dedicated charging come under Level-3 charging and there is provision by many car manufacturing companies that Level-2 accessories can be used in Level-3 charging accessory too. Three-phase system is generally available in European electrical distribution systems and they can use it for fast charging or can form AC common bus charging system [55].

Presently, most of the EV charging equipment are AC type Level-2 (90.5%). There are different standards which govern EV charging equipment. IEC 61851 is a common global standard which covers the general requirements of the chargers. Similarly, SAE J1772 and GB/T 18487 series covers general requirements of chargers in North America and China respectively [56]. The details of the standards are covered in Chapter 1.

AC common bus charging can also be classified as on-board charger and off-board chargers. On-board chargers are part of the vehicle and give flexibility to the user as not any specialized equipment is needed to carry. There are certain drawbacks of the on-board chargers related to size and capacity of the charger and usually chargers are found below the rating of 3.5 kW.

Off-board chargers are preferred for longer EV range (>100 km) and for large amount of energy (>20 kWh). The other solution proposed in the literature is to use available traction equipment i.e. motor and inverter of the vehicle to use as on-board charging infrastructure. These integrated chargers have less weight and more range and energy as compared to conventional on-board chargers [57].

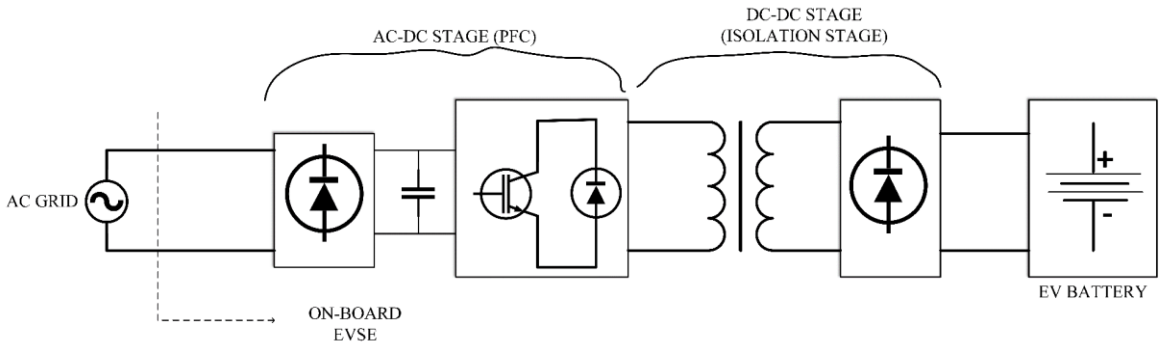

Figure 2.5. Two-stage on-board charger [58]

In Fig. 2.5, 2-stage on-board charger is shown. First is AC-DC stage which is used for Power Factor Correction (PFC) and second stage is isolation stage which is known as DC-DC stage. The EV battery is connected further with DC-DC converter. This all structure is compact and on-board.

There are no size and weight constraints for off-board chargers. These chargers can be used for fast and frequent high power charging. The bidirectional power flow that is grid-to-vehicle and vehicle-to-grid is possible with off-board chargers. Extra cost of power electronics and complex communication is disadvantage of off-board chargers. On-board chargers need lesser hardware and there are fewer interconnection issues [59]. Off-board chargers can be used both in CACB and CDCB charging stations.

There are different topologies proposed for bidirectional charging in off-board chargers. Traditionally, 2 or 3-stage architectures are used in it which consist of AC-DC bidirectional converter, bidirectional DC-DC converter to regulate the battery current and isolation transformer. There is also proposal of high-frequency transformer in the DC-DC stage instead of bulky LF transformer. HF transformer can provide higher power density and fast control in comparison to the LF transformer [60].

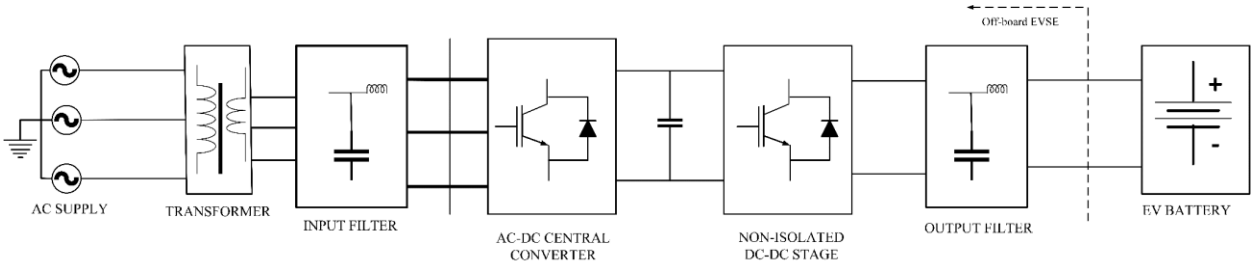

Figure 2.6. Off-board charger for fast charging stations [61]

In Fig. 2.6, a block diagram of the off-board charger is shown. This configuration is used in fast chargers (Level-3) and is connected to the grid through a 3-phase supply link. The shown configuration (Fig. 2.6) is considered as a low-frequency isolation as a transformer is used at the

source-end. It is known as high-frequency isolation if a transformer is used towards the EV-end. FCS comes under the off-board charging technique and therefore, can be installed only to a specific charging location. There is requirement of hardware infrastructure for the deployment of these charging stations. It includes of the 3-phase AC supply or DC supply, 208-600 $V_{AC,}$ 208-600 V_{DC} and time taken by PHEVs is 0.2 to 0.5 hours and 0.4 to 1 hours for BEVs to fully charge.

2.3(b) Common DC Bus Charging System (CDCBCS): Common DC bus charging is widely popular technology for xEV charging. It can be used for both conductive and inductive charging. The major advantage of common DC Bus charging station is the use of a single AC-DC conversion stage as compared to multiple converters in common AC bus charging or on-board chargers. CDCB charging station mostly consist of main AC-DC converter and further DC-DC converters for regulation. These charging stations can also incorporate renewable energy resources and Energy Storage System (ESS). There aim is to maintain the power quality indices of the system during charging of multiple EVs [62].

In Fig. 2.6, off-board charger structure is shown. In this system, structure is installed in a station and distribution/isolation transformer can be used to connect the structure with the AC grid. DC FCS comes under the off-board charging technique and therefore can be installed only to a specific charging location while on-board charging can be done at a place which is having only an electrical outlet. Even then, DC FCS are much needed to encourage people to adopt xEVs without worrying for charging and range anxiety [63].

Fast charging stations is an essential infrastructure to escalate the sale of EVs. Therefore, many companies are entering into this business such as; Charge Point, ABB, BP, Shell, Hyundai, Webasto, RWE, Daimler Mercedes-Benz, Siemens, EVgo etc. [64].

2.4 Common Configurations of Converters used in FCS

Common DC bus architecture can be realized by using 2-level VSCs or by using 3-level Neutral-Point-Clamped (NPC) converters. Unipolar or Bipolar DC architecture can be used as a common tie out point for EVs. Unipolar architecture is simple and easy to construct while Bipolar DC architecture offer more flexibility, increased power capacity, lower filtering requirement, better current performance and leading to lower dv/dt. Line to line voltage of 2-level VSC contains 3 voltage levels, while NPC converter yields 5 voltage levels and the corresponding switching frequency of the NPC converter is double the device switching frequency, leading to better current performance, lower dv/dt and lower filtering requirement. There is problem of imbalance of power between positive bus and negative DC bus because of difference between both of the DC buses and may be difference in loads of both the buses [65]. Similarly, Ref. [66] proposed a structure with high frequency isolation charging port. This system can be flexibly used both in Unipolar or Bipolar DC bus. It is made up of the front-end 3-level buck converter, which has the capability of regulating the output DC voltage and the back-end LLC resonant converter, which experiences high-frequency electrical isolation. The voltage stress and filter volume can be reduced by using this structure in the system.

Ref. [67] proposed a dual-stage power converter (AC-DC and DC-DC) which shared the same DC link as shown in Fig. 2.7. The AC-DC converter is composed of parallel structure of 2 full-bridge VSCs and allows control of grid current and of the DC link voltage. The DC-DC converter is interface between the batteries and DC link. A predictive current control algorithm is used in the study to synchronize the grid currents with the charger. It is strategy which is used to obtain sinusoidal grid currents even with distorted power grid voltages. In this paper, instead of using full power grid voltage, a signal which is proportional to fundamental component of the voltage is

used. This signal is obtained by using phase-locked-loop algorithm implemented in αβ coordinates (αβ-PLL).

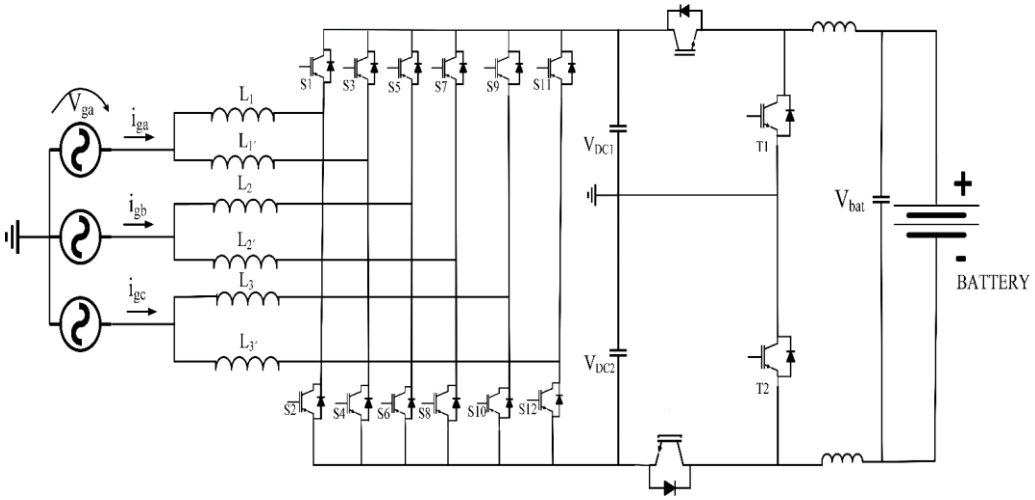

Figure 2.7. Dual Stage Power Converter [67] [23]

In Fig. 2.7, dual stage power converter is shown. It consists of 2-stages that is AC to DC and DC to DC stage. Proper control strategy is required for the smooth operation of both the stages/converters. This is an example of the system which can be employed in the FCS. VSCs can be used as first stage converter (AC to DC) in the FCS and can deliver active power and as well as reactive power requirement of the power system. Ref. [68] proposed a model of VSC based PEV for the efficient control of active and reactive power in the grid connected charging station. SoC of battery governs the active power flow and the quantity of reactive power generated depends upon the reactive power limits of the VSC and on the voltage magnitude identified at the voltage-controlled bus-bar. Authors did the computational analysis and establish the fact that big vehicular fleets behave as dispersed generators in the distribution system and helpful in active and reactive power control.

Ref. [69] explained the PEV charging model with the help of a mathematical model. Authors proposed that VSC topologies can govern active and reactive power supply of the system. Battery

storage of EV should be installed properly to board the electric charge. Charging and discharging plays an important role in the PEV charging infrastructure. In the charging mode, VSC converts the AC power to DC voltage and to the battery. In the discharging mode, VSC supplies active and reactive power into the power system in an optimal manner. This kind of arrangement can be used in peak shifting time or lessen demand responding on short time. This system can stabilize the power system.

It is evident from literature that common DC bus FCS is beneficial in many aspects if properly designed. Many operations like Grid to Vehicle (G2V), Vehicle to Grid (V2G), Vehicle to Vehicle (V2V), active and reactive EV-power system services like peak shaving, valley filling, voltage regulation, load shifting etc., are possible with the proper control and coordination of DC FCS. There are some important aspects which should be considered while designing charging stations are as follows [23] [70]:

- Proper information about the network constraints like permissible power level at the Point of Common Coupling (PCC) and nominal voltage level.
- Demand estimation of fast charging slots for a particular region.
- Number of vehicles which can be charged and area required to park those vehicles.
- Rate of allowable charging power required for concerned vehicles.

There are some important parameters like rated capacity of the charging station (S_R), DC bus voltage and size of DC capacitance which must be calculated for the design of DC FCS.

Rated capacity of DC FCS can be calculated with the help of following equation:

$$S_R = \frac{k_{load} N_{slot} P_{ev}}{Cos\Phi} \text{ VA} \quad (2.2)$$

where

N_{slot} = Number of available slots for charging of individual vehicles

CosΦ = Power factor of the system

K_{load} = Overload factor to take into account the overloading during system transients

P_{ev} = Maximum charging power rate of an EV

Second important parameter is DC bus voltage (V_{dc}) as all the EVs have to connect with common DC bus for charging.

$$V_{dc} \leq \frac{V_{min}^{bat}}{m_{min}} \tag{2.3}$$

Where

V_{min}^{bat} = Battery minimum voltage

m_{min} = Minimum modulation index of battery

Next parameter is size of DC capacitance which is important to filter the DC current ripples. In DC FCS, the number of EVs for charging may be high and the DC current ripple will increase with this number. Therefore, large value of capacitance is required to filter these ripples. Value of DC capacitance can be calculated as per following equation:

$$C_{dc} = \frac{S_R * 2nt * \Delta p * cos\emptyset}{V_{dc}^2 * \Delta V} \tag{2.4}$$

Where

S_R = rated capacity of charging station in VA

t = period of AC voltage wave

n = multiple of t

Δp = DC power range of change

$Cos\Phi$ = Power factor of the system

V_{dc} = DC bus voltage

ΔV = Allowable DC bus voltage range of change

VSC plays an important role in the FCS to connect the charging station with the grid. There are different configurations available for the VSC which can be used in FCS. In this thesis, the focus is on commonly used technology that is 2-level, 3-phase, VSC.

Detailed study of 2-level, 3-phase, VSC converter is given in chapter-3 of the thesis. These converters are grid-connected and EV batteries act as load during charging mode. So, there is presence of non-linear load (batteries) and power electronic converters which results in impact on the power quality (particularly harmonics) at grid-end. Therefore, harmonic assessment becomes the point of interest in the study. Poor power quality due to high percentage of harmonics has adverse impact on the connected equipment of the grid particularly on the distribution transformer.

2.5 Power Quality Problems associated with EV charging

The term "Power Quality" is now widely used and is defined by IEEE (IEEE 1159:2009, IEEE 1100:2005) as "The concept of powering and grounding sensitive electronic equipment in a manner that is suitable to the operation of that equipment and compatible with the supply system and other connected load". The IEC definition of power quality, as given in IEC 61000 series is "The ability of a device, equipment or system to function satisfactorily in its electromagnetic environment without introducing intolerable electromagnetic disturbances to anything in that environment." Generally, a high level of power quality is understood as low level of disturbances [71].

Power quality problems can be categorized as (i) Generation of Harmonics including; characteristic and non-characteristics harmonics, sub-harmonics, and inter-harmonics (ii) Voltage dips (iii) Voltage imbalance (iv) Voltage variations (sags and swells) (v) Frequency variations (vi) DC components in AC networks (vii) power system transients.

These events are undesirable in the power-system, and can cause short or long-term problems. These are explained as follows:

(a) Short-duration variations

These kinds of problems may be instantaneous, momentary and/or temporary in the form of interruption, sag and swell. The cause of these kind of problems may be a fault in the system, large load energization and loose connections. As per IEEE-1250,

- Instantaneous interruption - between 0.5 and 30 cycles
- Momentary interruption - between 30 cycles and 2 seconds
- Temporary interruption – between 2 seconds and 2 minutes.

Similarly, sags and swells are the short duration undesired events. Sag is the temporary reduction in the rms voltage between 0.1 and 0.9 pu, and swell is the increase in voltage magnitude between 1.1 and 1.8 which can last between 0.5 cycles and 1 pu.

(b) Long-duration variations

These problems can persist for longer than 1 minute as per IEEE-1159 and ANSI-C 84.1 standard. The reason for these variations are switching operations and load variations. These disturbances are categorized as sustained interruptions, causing over-voltages, and under-voltages.

- Sustained interruptions – as per IEEE standards, duration is more than 1 minute. These are the most serious kind of power quality problems often caused by fault incidences, incorrect relay operation, and scheduled maintenance.
- Over-voltages - increase in rms voltage from 1.1 to 1.2 pu for more than 1 minute. These over-voltages can be further classified as a lightning overvoltage, switching overvoltage, and over-voltages caused by insulation failure, ferro-resonance, tap changer transformer etc.
- Under-voltages - duration is more than 1 minute, and decrease in rms voltage from 1.1 to 1.2 pu.

The other major power quality problems are voltage imbalance and waveform distortions.

- Voltage imbalance occurs in 3-phase systems. In it, 3-phases are not the same and the phase difference in each phase is not identical i.e. 120^{o}. The reasons for this are unbalances in 1-phase loading, single-phasing, blown-out fuses in capacitor banks etc.
- Waveform distortions are termed as a steady-state nonconformity from the sinusoidal wave-shape. It may be caused by harmonics, inter-harmonics, DC offset, notching and electric noise.

  (i) Harmonics- Harmonics are a major source of distortions. Mostly, harmonics are sinusoidal in shape, but the frequency is not same as power frequency (50 or 60 Hz). These are integer multiples of the power fundamental frequency. The reason for harmonics is non-linear load, communication network frequency interference, faults, malfunctioning of control devices, resonance frequencies due to cable

capacitance and PFC capacitor. Most predominant harmonics are triplen harmonics, sub-harmonics, and inter-harmonics.

(a) Triplen harmonics are the odd multiples of the 3rd order harmonics (3,9,15,21,27, …..) which results into higher distortions. A higher proportion of the triplen harmonics is harmful to grounded-star connected system as excessive currents will flow through the neutral wire.

(b) Sub-harmonics are lower order of frequencies i.e. below the fundamental frequency. These sub-harmonics are produced in the input side and may be due to resonance between the harmonics currents/voltages and system capacitance and inductance. These sub-harmonics are generated in highly inductive or capacitive systems.

(c) Inter-harmonics appears as discrete or wide band frequencies, not as integer multiple of fundamental frequency. These harmonics occur in between the fundamental and integer multiples of frequency. In it, multiple is a non-integer number. The cause of these frequencies is modulation of current and voltage for control purposes and transient phenomenon in the system.

The other prominent harmonics that can occur are characteristic and uncharacteristic harmonics, positive, negative and zero sequence harmonics, spatial harmonics.

EV charging can have an adverse impact on the PQ of the conventional grid. In this thesis, PQ problems due to EV charging are studied in context of harmonic emissions [71] [72].

EVs are a new and dynamic load which may cause power quality-related problems having detrimental impacts on the electric grid. These effects include harmonic distortion, voltage unbalance, voltage drop, equipment overloading, phase unbalance, power system stability etc. PEV charging can be divided into coordinated and uncoordinated scenarios. Coordinated charging is preferred for the least impact on the grid and system [73]. Power quality standards set up by different organizations should be followed to examine the EV FCS. SAE, IEEE, IEC, American National Standard Institute (ANSI), British Standards (BS), Information Technology Industry Council (ITIC), Computer Business Equipment Manufacturing Association (CBEMA), and many other global societies set the standards to determine the power quality impacts.

These standards are an important tool to observe, measure and control the power quality-related problems in grid-connected EV charging stations. Some important standards are enlisted as follows [74-76]:

- IEC Standard 61000-4-7, General Guide on Harmonics and Inter-Harmonics Measurement and Instrumentation, for Power Supply Systems and Equipment Connected thereto.
- IEC Standard 61000-4-30, Power Quality Measurement Methods.
- IEC Standard 61000-4-15, Testing and Measurement Techniques—Flicker meter—Functional and Design Specifications.
- IEEE Std. 1453™, IEEE Recommended Practice—Adoption of IEC 61000-4-15:2010, Electromagnetic compatibility (EMC)—Testing and Measurement Techniques—Flicker meter—Functional and Design Specifications.
- SAE standard J2894/1_2019 defines the Power Quality requirement of PEV.

There are certain prescribed limits for voltage and current Harmonics set by IEEE 514-1992 (revised 2014) which are followed by utilities, users, manufacturers.

In Table 2.1 and 2.2, current and voltage distortion limits are listed. These limits are very important for the safe and secure operation of the FCS.

Table 2.1 IEEE Standard 519-1992: Current distortion limits for general distribution systems (129-69000 V) [77]

Maximum harmonic current distortion (in percent of I_L)						
Individual harmonic order (odd harmonics)						
I_{sc}/I_L	h<11	11≤h<17	17≤h<23	23≤h<35	35≤h	TDD(%)
<20*	4.0	2.0	1.5	0.6	0.3	5.0
20 to <50	7.0	3.5	2.5	1.0	0.5	8.0
50 to <100	10.0	4.5	4.0	1.5	0.7	12.0
100 to <1000	12.0	5.5	5.0	2.0	1.0	15.0
>1000	15.0	7.0	6.0	2.5	1.4	20.0

- Even harmonics are limited to 25% of the odd harmonics above.
- Current distortions that result in a DC offset, for example, half wave converters, are not allowed.
- I_{SC}=maximum short-circuit current at PCC and I_L= maximum demand load current (fundamental frequency component) at PCC.

Table 2.2. IEEE Standard 519-1992: Voltage distortion limits [76]

Bus Voltage at PCC	Individual voltage distortion (%)	Total Voltage distortion (%)
69 kV and below	3.0	5.0
69.001-161 kV	1.5	2.5
161.0001kV and above	1.0	1.5

Standards are formulated to regulate the extent of system harmonics such as IEEE 519-1992, IEC 61000-3-12/2-4 and EN 50160:2000 [78] [79].

With the increased use of power electronic and semiconductor-based devices, power quality (particularly harmonics) becomes a big concern for utilities and distribution companies. EVs also play a big role to escalate this problem because of use of converters in it. Equipment like Distribution Transformer (DT), switches (circuit breakers and fuses) and cables are mostly affected by the harmonics produced due to converters [80]. Refs. [81-83] showed that substantial increase

in the EV load have degrading impact on many distribution network equipment and parameters. Transformer life expectancy is affected by unplanned EV penetration. Current THD should be limited to get better transformer life expectancy. It is established that more EV loads have deteriorating impact on transformer life.

Ref. [84] investigated the effect of EV charging in the Toronto Distribution Network. This study shows that there is substantial impact of the EV charging on the system performance. The results discovered that there is overloading on the transformer secondary lead and also there is impact of ambient temperature. System sensitivity increases if the overloading due to EV charging is in the summer days. This study suggested that system upgradation is required to integrate large charging stations in the grid landscape.

In addition, unbalanced load currents generated in the FCS also produce fundamental negative sequence component in the load currents, which adversely affect the system performance of the converter. These negative sequence components produce second order ripple in the DC link voltage, which results in harmonic distortions in the grid input currents. DC link voltage ripple is an important component in the selection criteria for DC capacitor in EV charging station. As there is presence of DC impedance due to EV batteries which produces voltage ripple on the DC link [23] [85] [86]. Therefore, calculation of DC link voltage is needed. DC link voltage explains the impact of harmonics on the grid as per equation 2.5.

$$V_{dc} = \frac{3}{4c}\left(I_{dc} + \frac{I_2}{2\omega_e}\sin(2\omega_e t - \alpha_2) + \frac{I_4}{4\omega_e}\sin(4\omega_e t - \alpha_4) + \frac{I_6}{6\omega_e}\sin(6\omega_e t - \alpha_6) + \frac{I_8}{8\omega_e}\sin(8\omega_e t - \alpha_8) + \frac{I_{12}}{12\omega_e}\cos(12\omega_e t - \alpha_{12})\right) \quad (2.5)$$

The expression shows the second order harmonic component in the DC side of the converter due to negative sequence component (-α) in the converter input current. These even order harmonics

on the DC link voltage generates odd order harmonics $h = 2k + 1$ ($k = 1,2 \ldots$) on the AC side. This circulation of fundamental negative sequence currents must be entirely blocked to avoid distortions in the input grid currents [87-89]. The impacts on the power quality is major concern in case of FCS. Amendments in Control algorithm and use of bidirectional VSC can enhance the quality of input current. In this study, FCS architectures are presented to study the power quality issues related to the source-end.

2.6 Commonly used batteries in EVs, Battery Management System (BMS), Estimation of Parameter of batteries

Batteries become the very important storage device in Energy Storage Systems (ESS). Batteries store energy chemically and deliver it electrically. Rechargeable batteries are considered as secondary batteries and conversion of chemical energy to electrical energy is done by donating electrons (oxidation) or accepting electrons (reduction). These reactions are known as redox reactions and happen at both the electrodes [90].

The most expensive part of an EV is battery which covers the 25-50% part of the total vehicle cost. The exact cost of the battery depends upon various factors like technology used in the battery, availability of materials, handling and disposal cost of the battery. Cost of battery is decreasing day by day due to innovation going on in this field. At present, the cost of Li-ion (lithium-ion) batteries has decreased by over 50% from 2007 [91]. *Bloomberg New Energy Finance* predicted that there will be a decrease in the Li-ion battery price by one-fourth to the today's price and market is projected to reach USD 95.3 billion by 2030.

There are many kind of batteries which are used for various applications. Lead acid batteries are commonly used for vehicular starting, lighting and ignition roles, commercial and industrial uninterruptable power supplies (UPS) applications. Nickel Metal Hydride (NiMH) batteries are suitable for Hybrid vehicles. Li-ion batteries are used in many applications like cell-phones,

laptops, portable power tools and many more. Li-ion batteries become the popular topic and field of research and interest as they find ways in powering EVs and supporting the electric grids [92]. The reason of extensive popularity of Li-ion batteries is long life span, high energy and power density, and good charging and discharging performance. Performance and characteristics of Li-ion and other batteries is illustrated in the Table 2.3.

Table 2.3: Battery Types and their Parameters [93]

Battery Type	**Service Life (Cycle)**	**Nominal Voltage (V)**	**Energy Density ($W.h.kg^{-1}$)**	**Power Density ($W.kg^{-1}$)**	**Charging Efficiency (%)**	**Self-Discharge rate (% $month^{-1}$)**	**Charging Temperature (^oC)**	**Discharging Temperature (^oC)**
Li-ion	600-3000	3.2-3.7	100-270	250-680	80-90	3-10	0 to 45	-20 to 60
Lead acid	200-300	2.0	30-50	180	50-95	5	-20 to 50	-20 to 50
NiCd	1000	1.2	50-80	150	70-90	20	0 to 45	-20 to 65
NiMH	300-600	1.2	60-120	250-5000	65	30	0 to 45	-20 to 65

In Table 2.3, parameters of different batteries are shown. It is observed that energy density and charging efficiency of Li-ion battery is higher than other type of batteries, therefore it becomes suitable for many applications. The battery cost is also declining continuously, therefore, Li-ion becomes the choice of many EV manufacturing companies.

2.6(a) Battery Management system: Battery Management System (BMS) is very important to study the performance and parameters of batteries. Batteries are non-linear and dynamic element, so, proper management is required to handle it. BMS includes cell condition monitoring, charge and discharge control, protection and equalization, state estimation, temperature control, fault diagnosis and assessment aiming to enhancement of overall performance of the system [94]. The overview of BMS is shown in following figure:

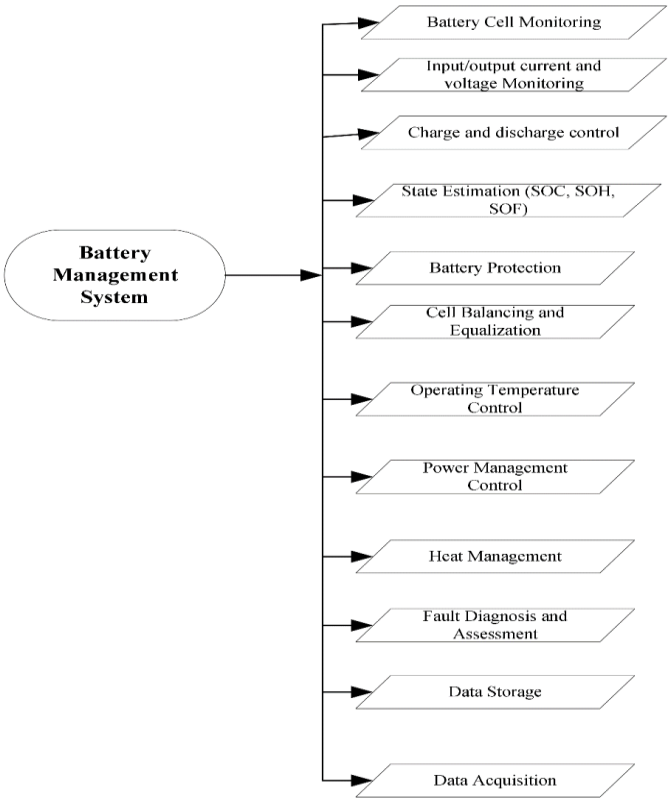

Figure 2.8. Battery Management System [94]

In Fig. 2.8, an overview of BMS is given. BMS controls the charging and discharging of battery, does the State Estimation which includes State of Charge (SoC), State of Health (SoH) and State of Function (SoF) of battery, controls the protection system of battery, store the operating data and many other related tasks for safe and reliable operation of battery. It helps in enhancing the overall performance and life of batteries.

2.6(b). Estimation of Parameters of Batteries: BMS is extremely important for batteries used in EVs and other application. Accurate SoC estimation is required to efficiently implement the BMS. The equivalent circuit model (ECM) of a battery, (Fig. 2.9) plays an important role to estimate the characteristics of the battery. There are different ECMs like RC model, Rint model, Thevenin model are available to represent electrical characteristics of EV batteries. In order to improve the polarization characteristics of a battery, a modification of Thevenin model known as DP (Dual

Polarization) model, is used to analyze the behavior of battery during charging and discharging. In this study, brief introduction to Thevenin and DP models is given as follows:

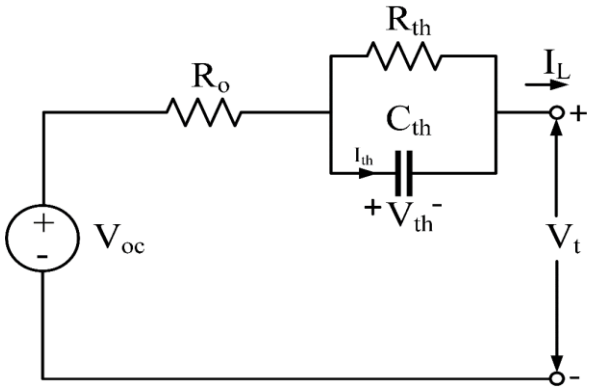

Figure 2.9 Thevenin ECM of battery

In Fig. 2.9, Thevenin model of battery consists of Open Circuit Voltage (OCV) expressed as $V_{oc,}$ internal ohmic resistance R_o, parallel connected capacitance C_{th} and polarization resistance R_{th} is shown. This model represents the transient response of battery during charging and discharging. The value of C_{th} (equivalent capacitance) defines the transient behavior of battery through charging and discharging operation. EV battery consists of thousands of RC networks which results in increase in the order of the model and, ultimately calculation becomes complicated [95]. In most of the literature, first-order and second-order ECM models are used for ease of calculation and less complexity. The expression of terminal voltage (V_t) from first-order model is in following equation (2.6):

$$V_t = V_{oc} - V_t - R_o I_L \tag{2.6}$$

Where V_{oc} is open circuit voltage, R_o is internal ohmic resistance, I_L is output current, and V_{th} is voltage of RC network.

The modification in the Thevenin model is required to understand the polarization characteristics of Li-Ion battery in detail. Polarization characteristics of battery could be simulated roughly with

the help of Thevenin model, but to study the difference between concentration and electrochemical polarization, modification is required. DP model is built to study both the polarizations separately. The ECM of DP model is as follows:

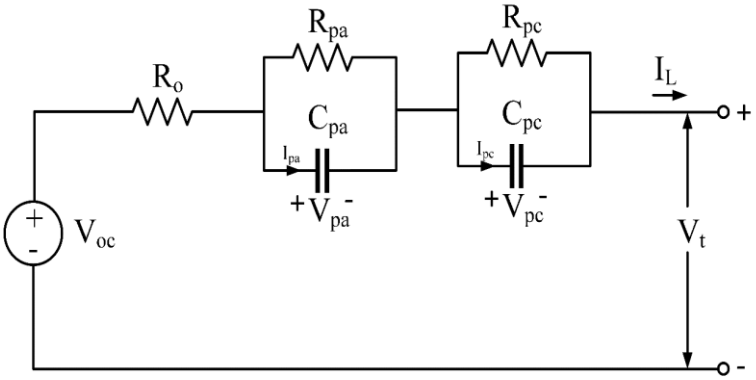

Figure 2.10 Dual Polarization (DP) ECM of battery [96] [97]

The DP consists of (i) Open circuit voltage (V_{oc}), internal ohmic resistance R_o, Polarization resistances R_{pa} (effective resistance to depict electrochemical polarization) and R_{pc} (effective resistance to depict concentration polarization), C_{pa} and C_{pc} are the effective capacitances to depict both the polarizations, V_{pa} and V_{pc} are the voltage across both the capacitors and I_{pa} and I_{pc} are the outflow current of both the capacitors [97]. The expression for terminal voltage for DP model is as follows:

$$V_t = V_{oc} - V_{pa} - V_{pc} - R_o I_L \tag{2.7}$$

SoC is one of the most important parameters for the EV battery. It is defined as the ratio of battery current capacity (Q_t) to nominal capacity (Q_n). Nominal capacity is provided by the battery manufacturer and signifies the maximum amount of charge that can be stored in the battery [98]. SoC can be expressed as follows:

$$SoC(t) = \frac{Q(t)}{Q_n} \tag{2.8}$$

Experimental method and different procedures and algorithms are proposed in the literature [97-100] to estimate the SoC and parameters of EV battery, which is not in the scope of this study.

2.7 Impact of Short Circuit Ratio (SCR) and X/R Ratio

In grid-connected EV charging system, features of AC systems have a substantial impact on the operation and working of EV FCS. The behavior of the AC-DC converter depends upon the grid strength. The relative operation of both is a vital indicator of VSC operating problems. The strength of AC system is defined by the Short Circuit Ratio (SCR) as follows:

$$SCR = \frac{MVA_{SC}}{P_{DC}} = \frac{{V_{s_{LL}}}^2}{Z_s P_{DC}} \tag{2.9}$$

where P_{DC} is the converter rated power, V_{sLL} is Line to Line voltage, Z_s is source impedance also known as equivalent Thevenin impedance, and MVA_{SC} is MVA short-circuit capacity of the system represented by the following equation:

$$MVA_{SC} = \sqrt{3} \times V_{PRE} \times I_{SC} \tag{2.10}$$

where V_{PRE} = pre-fault voltage, I_{SC} = Short-circuit current. A higher value of MVA_{SC} rating indicate stronger grid and vice-versa [101].

SCR is important to understand the strength of grid, which is classified in the Table 2.4:

Table 2.4: Classification of SCR Rating

SCR	Classification	Operating problems
SCR>10	Strong System	Lesser operating problems
2<SCR<10	Average System	Few operating difficulties and special controls are required
SCR <2	Weak system	Serious operating problems may occur in the system

The source impedance Z_s can be calculated by the following equation:

$$Z_s = \sqrt{R_s^2 + X_s^2} \tag{2.11}$$

Where R_s and X_s (AC system parameters) can be calculated by the following equations:

$$R_s = \frac{{V_{s_{LL}}}^2}{SCR * P_{DC}} \frac{1}{\sqrt{1 + {X_{ratio}}^2}} \tag{2.12}$$

$$X_s = \frac{{V_{s_{LL}}}^2}{SCR * P_{DC}} \frac{X_{ratio}}{\sqrt{1 + {X_{ratio}}^2}} \tag{2.13}$$

Where X_{ratio} is X/R ratio of the system.

From these equations, it is clear that SCR has great impact on the operating characteristics of the grid. AC system strength (Table 2.4) is measured by SCR and electric grid termed as weak or strong [102] [103]. SCR defines the fault level of the system, which is required to select the protective equipment to be installed in the grid.

The second important ratio is X/R ratio of the system. It can also be defined as tangent of an angle created by X and R of the system.

X/R ratio provides the information about damping of the system that how the system transiently recovers after a fault. Two extreme states can be considered, as follows:

State I: If X = 0 then $Z_s = R$, meaning that there is excessive damping in the system. There will be more power losses in the system.

State II: If R = 0 then $Z_s = jX$, means there is no damping in the system and transient response will be pronounced and excessively long.

So, a critically damped system is required for the desired operation of grid-connected FCS. The value of X/R ratio depend upon the factors like rating of the grid, diameter of conductors, length of conductors, spacing between conductors etc. Table 2.5 shows the typical values of X/R ratios

for different operating voltage levels of transmission/distribution systems. Table 2.6 shows the operating impact of different X/R ratios for a typical medium/low voltage distribution system.

Table 2.5: Line Voltage v/s X/R ratio [104]

Operating Voltage (kV)	X/R ratio
400	16
275	10
132	6
33	2
11	1.5

Table 2.6: Classification of X/R Ratio (For a medium/low voltage distribution system application) [104]

X/R ratio	Classification	Operating problems
X/R >10	Overdamped	Serious operating problems
0.5<X/R<10	Critically Damped	Few operating problems
X/R <0.5	Underdamped	Serious problems may occur in the system

A weak-grid contributes more towards losses in the system and a poor transient-state response. On the other hand, a strong-grid contributed towards fewer losses in the system and a better transient-state response, but at the expense of a higher cost infrastructure. Hence, a compromise is needed to provide flexibility in the case of micro-grids [102].

In Fig. 2.11, the envelope of short-circuit current waveform is shown. This transient behavior during the fault and post-fault depends upon the X/R ratio. If the X/R ratio is high, then this waveform will become overdamped and it becomes underdamped if the X/R ratio is low.

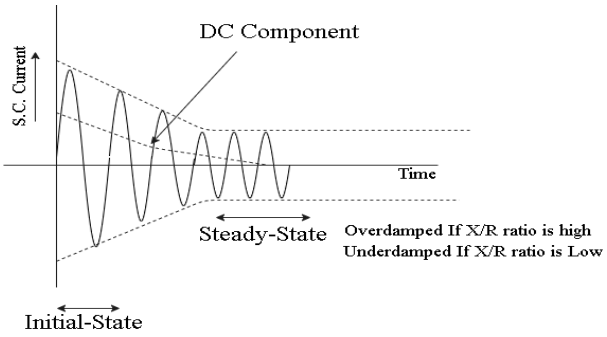

Fig. 2.11 Short-circuit behavior during and after fault

The impact of X/R ratio and MVA_{SC} could be studied by creating a 3-phase fault in a grid-connected FCS. Following is the single line diagram of 3-phase fault sequence.

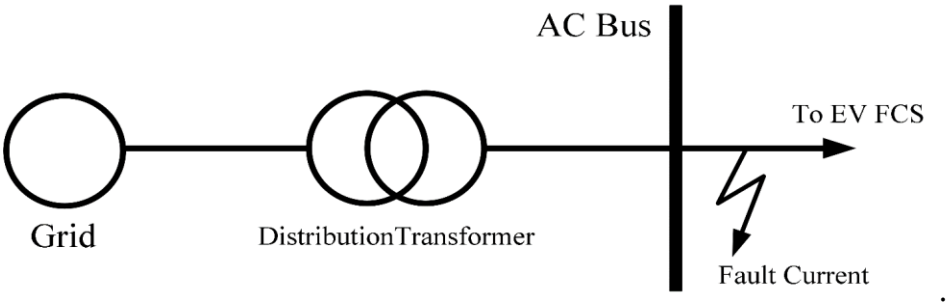

Fig. 2.12 Short-circuit fault at the Bus

The behavior of power system during the fault, and regaining capability depends upon the grid-strength, SCR and X/R ratio. The X/R ratio and SCR of the grid is important in the state of fault. In Table 2.1, I_{SC}/I_L is termed as SCR. I_{SC} is short-circuit current or fault-current, I_L is maximum demand load current. Both of these values (I_{SC} and I_L) are required to find out the SCR, and these values depends upon the X/R ratio. Harmonic emission assessment is done by using SCR value (Table 2.1) which is further used to select the rating of protective devices.

2.8 Voltage Source Converter (AC-DC Converter)

Converters are the core of EV charging infrastructure to convert infeed AC from the grid to DC via various converter arrangements [105-109] such as (i) Diode rectifiers (ii) 2-level VSC (iii) 3-level Neutral Point Clamped (NPC) VSC, and (iv) Vienna Rectifier etc. to connect DC FCS with either a 1-phase or 3-phase grid supply. Diode rectifiers are a simple and economical technology as compared to other more expensive alternatives, but a 2-level VSC using Insulated-Gate Bipolar Transistors (IGBTs) is proposed in this study [110-112] since it offers higher efficiency, low

harmonic generation, ability to have bi-directional operation with flexible gate control, snubber-less operation, higher voltage regulation and possibility for energy recuperation.

VSC works as either rectifier in charging mode or as an inverter in discharging or standalone mode to supply the load, or as an Active Power Filter (APF) for grid-connected mode etc. It can work in all the four quadrants, as shown (Fig. 2.3) and gives robust, effective and faster dynamic response [113] [114].

2.8.1 Two-level VSC

In Fig. 2.13 [114], a 2-level VSC is shown, which consists of 3 similar half-bridge converters. Each half-bridge converter is connected with one phase of the 3-phase AC side through a series R-L branch. The DC side of the half-bridge converters is connected to the DC-DC converter or with a common DC voltage source.

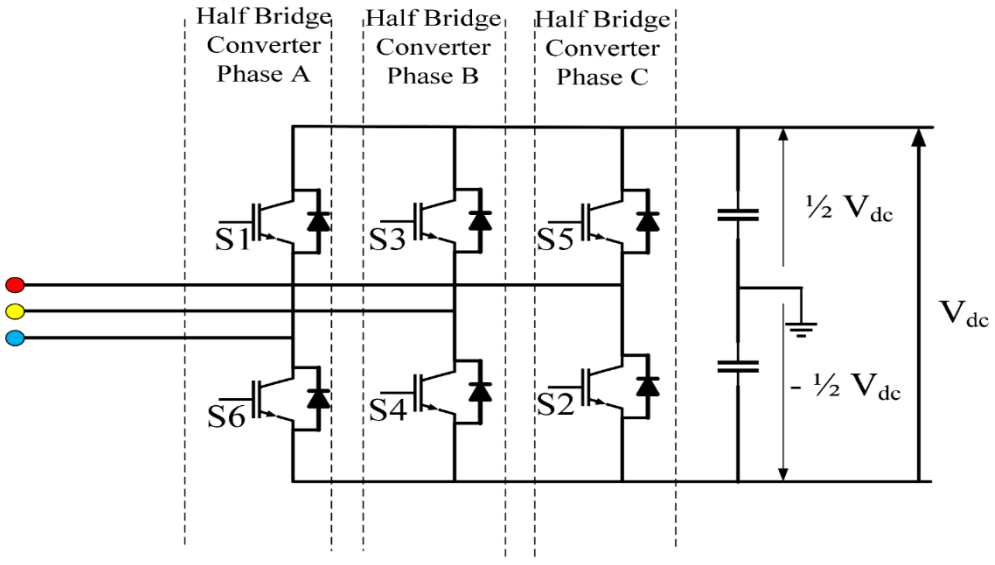

Fig. 2.13 Two-level, 3-phase VSC [114]

This VSC can be operated, with suitable control algorithms, in either uni-polar or bi-polar modes. AC-side terminal voltages can be deduced for each phase as

$$V'_{TR}(t) = m_R(t)\frac{V_{dc}}{2} - r_{on}i_R(t) \quad (2.14)$$

$$V'_{TB}(t) = m_B(t)\frac{V_{dc}}{2} - r_{on}i_B(t) \quad (2.15)$$

$$V'_{TY}(t) = m_Y(t)\frac{V_{dc}}{2} - r_{on}i_Y(t) \quad (2.16)$$

Where V'_{TR} , V'_{TB} , V'_{TY} are terminal voltages of phase R, B and Y respectively, $m_R(t)$, $m_B(t)$, and $m_Y(t)$ are the modulating signals for the respective phases. Similarly, $r_{on}i_R(t)$, $r_{on}i_B(t)$, and $r_{on}i_Y(t)$ are ohmic voltage drops of the respective phases.

2.9 Control Schemes for VSC

The grid-connected 2-level VSC (Fig. 2.13) is tied to the grid-frequency. These 3-phase variables are having a frequency which is enforced by the connected utility grid. The VSC needs a control method which are broadly classified as either frequency-domain or time-domain control schemes. Frequency-domain algorithms are mostly used for power quality monitoring and provide a sluggish control for converters. Therefore, only time-domain schemes are considered here in this study, the following three time-domain control schemes are studied.

(a) Instantaneous Reactive Power Theory (IRPT) / αβ- Theory or PQ Theory

(b) Synchronous Reference Frame Theory (SRFT)/ dq- Theory

(c) Unit Template Control (UTC) Theory or PI controller-based theory

2.9.1 αβ- Theory or PQ Theory

The advantage of αβ- frame theory (Fig. 2.14) is that independent control of real power (P) or reactive power (Q) is possible.

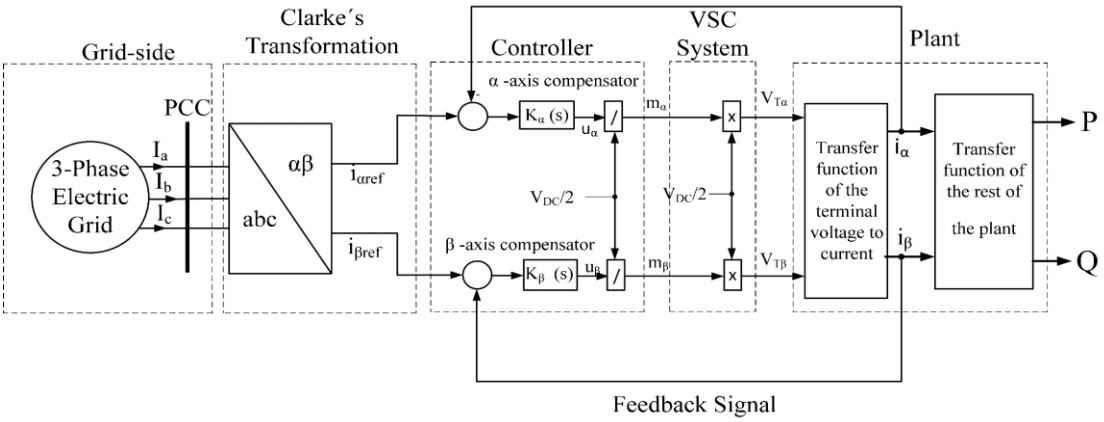

Fig. 2.14 Control block diagram of a VSC system based on the αβ-frame control [114] [115]

The scheme works on the basis of Instantaneous Reactive Power Theory (IRPT) which is also known as PQ theory. It is based on Clarke's transformations. These transformations are applied to the 3-phase voltage and current coordinates in the abc-frame, and transfers these coordinates into the 0αβ frame (also known as αβ-frame).

The control block diagram shown in Fig. 2.14 can be sub-divided into five blocks which are (a) Grid-side (b) Clarke´s Transformation (c) Controller (d) VSC system, and (e) Plant.

(a) Grid-side: VSC is connected to the PCC. The utility grid supplies the system with the 3-phase voltage (V_a, V_b and V_c) and current coordinates (are termed as I_a, I_b and I_c) in the abc-frame.

(b) Clarke´s Transformations: In this block, the sensed grid currents (I_a, I_b, I_c) are converted to reference current values ($i_{\alpha ref}$ and $i_{\beta ref}$) by using Clarke´s transformation using the generalized equation (2.17).

$$\begin{bmatrix} f_\alpha(t) \\ f_\beta(t) \end{bmatrix} = \frac{2}{3} C \begin{bmatrix} f_a(t) \\ f_b(t) \\ f_c(t) \end{bmatrix} \qquad \text{where} \qquad C = \begin{bmatrix} 1 & -\frac{1}{2} & -\frac{1}{2} \\ 0 & \frac{\sqrt{3}}{2} & -\frac{\sqrt{3}}{2} \end{bmatrix} \tag{2.17}$$

In this equation, $f_a(t), f_b(t), f_c(t)$ are the input values, which may be current or voltage. This generalized equation can be used for either current or voltage control strategy. The strategy used in the Fig. 2.14 is current control strategy.

The voltage control strategy is normally used in high-voltage and high-power applications like in industrial operations, FACTS controllers etc. It is a simple strategy and has fewer control loops, but there is not committed control-loop for the VSC line current which makes the VSC vulnerable to over-currents in low-voltage distribution systems [116] [117].

(c) Controller Block: In the controller block, there are two compensators, one for the α-axis, and the other for the β-axis. These compensators are fed from the AC input-side and feedback signals from the output-side. The inputs to these compensators are $i_{\alpha ref}$ and $i_{\beta ref}$, which are reference current values for αβ- frame respectively.

As per equation (2.17), the reference values are used to generate control signals u_α and u_β with the help of feedback signals and compensators (α- axis and β- axis compensators). The output of compensators (u_α and u_β) are scaled down by a factor $V_{dc}/2$ to generate modulating components (m_α and m_β) of both the α and β sub-systems respectively.

(d) VSC-System: The components of the modulating signals (m_α and m_β) which are generated from the controller, and further fed to VSC-system. VSC-system is connected with plant which is responsible to produce feedback signals and output active power (P) and reactive power (Q) in αβ-frame.

In the VSC-system, AC-side terminal voltage is described with the help of equations (2.18) and (2.19).

$$V_{T\alpha}(t) = \frac{V_{DC}}{2} m_{\alpha}(t) \quad (2.18)$$

$$V_{T\beta}(t) = \frac{V_{DC}}{2} m_{\beta}(t) \quad (2.19)$$

where m_{α} and m_{β} = components of the modulating signals, $\frac{V_{DC}}{2}$ = proportionality constant.

These two equations (2.18) and (2.19) gives the relationship between AC-side terminal voltage and modulating signal in αβ-frame.

(e) Plant: Outputs of the VSC-system are the terminal voltages $V_{T\alpha}$ (α-axis component of the converter AC side terminal voltage) and $V_{T\beta}$ (β-axis component of the converter AC side terminal voltage) which are fed to the plant. The plant consists of 2-cascaded sub-plants.

In the first sub-plant, $V_{T\alpha}$ and $V_{T\beta}$ are the inputs, and it gives i_{α} and i_{β} as the outputs. It makes the control strategy as current-controlled based on αβ-frame. These currents (i_{α} and i_{β}) act as input to the second cascaded sub-plant, and produces P (real-power) and Q (reactive-power) in αβ-frame as final output [114] [115]. P and Q are further used as feedback to produce reference values for the controller as shown in Fig. 2.15. These quantities (P and Q) can be expressed as real and reactive power outputs in the αβ- frame as follows:

$$P(t) = \frac{3}{2}[V_{t\alpha}(t) i_{\alpha}(t) + V_{t\beta}(t) i_{\beta}(t)] \quad (2.20)$$

$$Q(t) = \frac{3}{2}[-V_{t\alpha}(t) i_{\alpha}(t) + V_{t\beta}(t) i_{\beta}(t)] \quad (2.21)$$

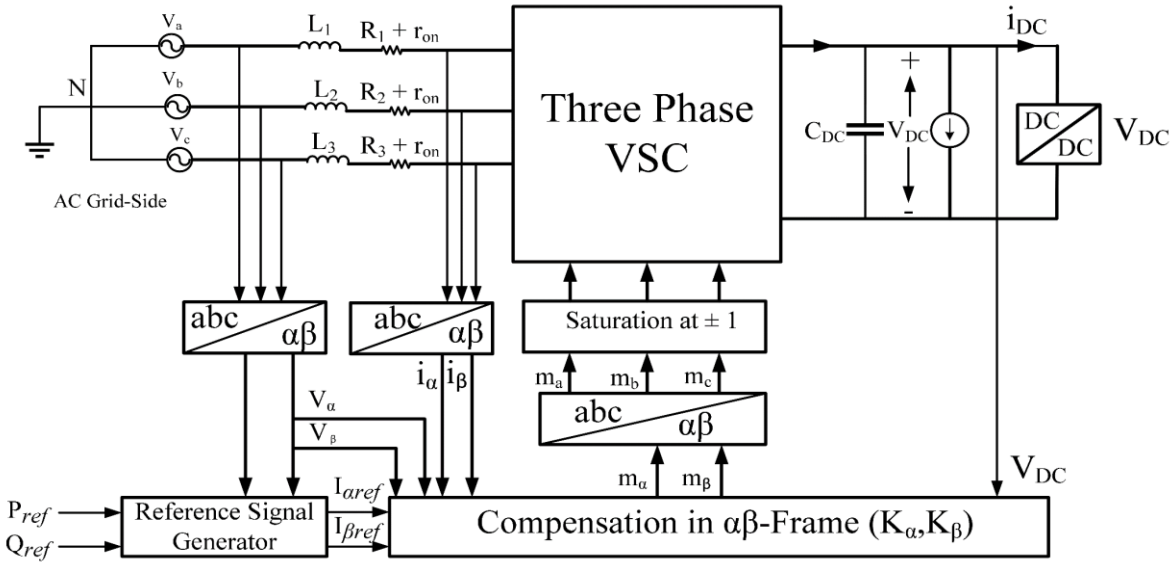

Fig. 2.15 Schematic diagram of a current-controlled VSC system based on the αβ- frame control [114]

In the Fig. 2.15, schematic diagram αβ- frame of current-controlled VSC system is shown. The reference values of active power (P_{ref}) and reactive power (Q_{ref}) are used to generate reference current commands $I_{\alpha ref}$ and $I_{\beta ref}$ respectively which are further processed in compensators to yield control signals m_α and m_β. These control signals (m_α and m_β) are further fed to abc-frame (Inverse Clarke´s transformation) to produce 3 control signals (m_a, m_b, and m_c) which are limited by a saturation block. Finally, these signals are supplied to VSC with the help of PWM controller or HCC to provide gating pulses. All the feed-forward and feedback signals are transformed for these operations with the help of αβ- frame.

The control system is based on the inner and outer control loops. The inner and outer control loop is shown in Fig. 2.15 and it controls the power between the DC bus or link and the electric-grid, while the outer loop delivers the reference current to the inner loop [117] [118].

2.9.2 The dq-SRF Control Strategy

In the dq-SRF (Synchronous Reference Frame) control strategy, alternating quantities (voltage or current) are converted into equivalent DC quantities. A 3-phase frame (d-q-0) that is rotating at

synchronous speed is considered as the reference frame. This frame consists of a 2-phase axis, namely d- (Direct axis) and q- (Quadrature axis). As the speed of this frame is the same as system frequency or stationary frame, so the dq-frame is assumed as the DC quantity under steady-state conditions. The implementation of the dq-SRF method can be understood from equations (2.22) and (2.23) for real (P) and reactive power (Q) [114].

$$P(t) = \frac{3}{2}\left[v_d(t)i_d(t) + v_q(t)i_q(t)\right] \quad (2.22)$$

$$Q(t) = \frac{3}{2}\left[-v_d(t)i_d(t) + v_q(t)i_q(t)\right] \quad (2.23)$$

In equations (2.22) and (2.23), if v_q (q- axis voltage) = 0, then, the real and reactive power components P(t) and Q(t) are proportional to i_d and i_q, respectively. Due to this simplification, the dq-SRF strategy is widely used for controlling the VSC.

Equation (2.22) can be rewritten in power balance as

$$V_{DC}(\mathrm{t})i_{DC}(\mathrm{t}) = \frac{3}{2}\left[V_{td}(t)i_d(t) + V_{tq}(t)i_q(t)\right] \quad (2.24)$$

The block diagram of the dq-SRF strategy is shown in Fig. 2.16 and implemented in five blocks.

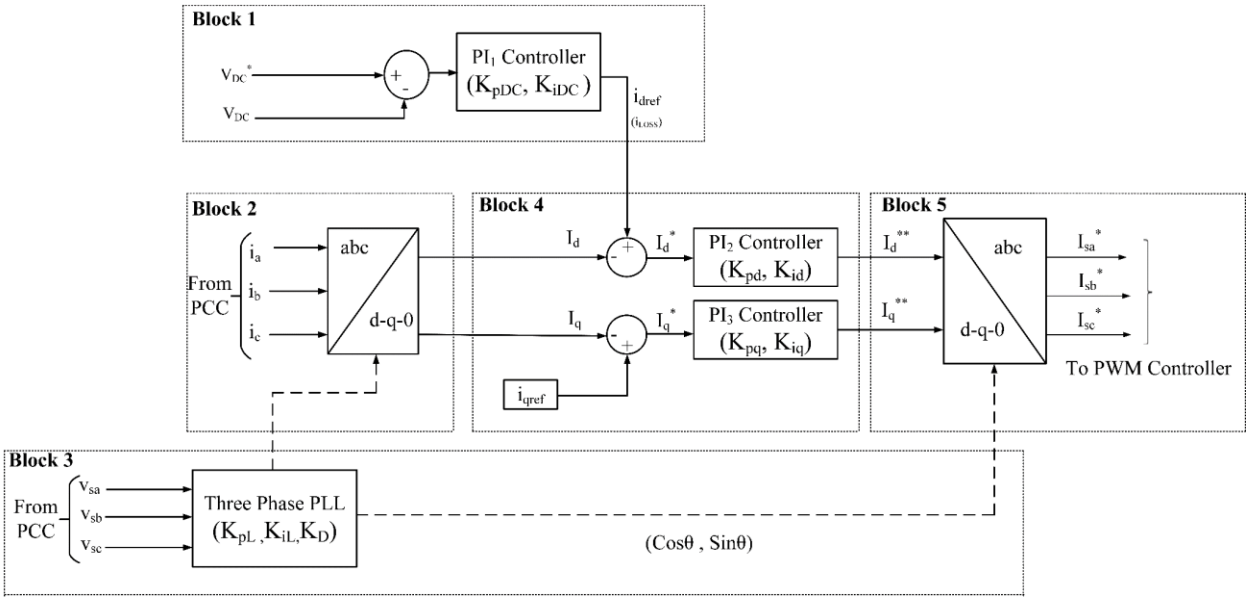

Fig. 2.16 Block diagram of dq-SRF control strategy [118]

Block 1: The DC bus voltage (V_{DC}) of the converter-side is sensed and compared with the reference DC voltage (V_{DC}^{*}) to obtain reference signal (i_{dref}) for the direct-quadrature component.

Block 2: In this block, the three grid currents (i_a, i_b, i_c) which are sensed at the PCC are transformed into the dq0 frame by using Park´s transformation as per equation (2.25):

$$\begin{bmatrix} i_d \\ i_q \\ i_o \end{bmatrix} = \frac{2}{3}\begin{bmatrix} cos\theta & -sin\theta & \frac{1}{2} \\ \cos(\theta - \frac{2\pi}{3}) & -\sin(\theta - \frac{2\pi}{3}) & \frac{1}{2} \\ \cos(\theta + \frac{2\pi}{3}) & \sin(\theta + \frac{2\pi}{3}) & \frac{1}{2} \end{bmatrix}\begin{bmatrix} i_a \\ i_b \\ i_c \end{bmatrix} \quad (2.25)$$

Block 3: Line voltages (V_{sa}, V_{sb}, V_{sc}) are sensed at the PCC. These PCC voltages are fed to three-phase PLL which work as a synchronizer for converter side signals and PCC voltages. It estimates the frequency and phase of the input PCC voltages. The outputs of the SRF-PLL are cosine and sine signals (Cosθ, Sinθ) which are obtained by estimating the phase of the input voltages.

Block 4: Two PI controllers are used in this block. A PI_2 controller (with gains K_{pd} and K_{id}) is used to extract the DC quantity (i_d'') from DC bus, and therefore non-DC quantities are separated

from the reference values. The direct current component (I_d) is compared with the reference value (I_{dref}) from PI_1 and fed into controller PI_2.

Since, Unity Power Factor (UPF) operation is desired for control operation, I_{qref} is set to zero. Again, a PI_3 controller (with gains K_{pq} and K_{iq}) is used to obtain the DC quantity (i_q'') . The proportional and integral values of the PI_2 and PI_3 controllers are set to obtain stable output values.

Block 5: Further, reference currents ($i_{sa}^*, i_{sb}^*, i_{sc}^*$) are obtained by using the inverse Park's transformation as per equation (2.26):

$$\begin{bmatrix} i_{sa}^* \\ i_{sb}^* \\ i_{sc}^* \end{bmatrix} = \begin{bmatrix} cos\theta & sin\theta & 1 \\ \cos(\theta - \frac{2\pi}{3}) & \sin(\theta - \frac{2\pi}{3}) & 1 \\ \cos(\theta + \frac{2\pi}{3}) & \sin(\theta + \frac{2\pi}{3}) & 1 \end{bmatrix} \begin{bmatrix} i_d^* \\ i_q^* \\ i_0^* \end{bmatrix} \quad (2.26)$$

In the dq-SRF control strategy, the extraction of synchronizing components (Sin θ, Cos θ) is done by using Park and Inverse Park transformations. These reference supply currents ($i_{sa}', i_{sb}', i_{sc}'$) are supplied to the PWM controller to generate the gate signals for VSC.

2.9.3 Unit Template Control (UTC) Strategy

Unit Template Control (UTC) is a simple method for the generation of reference source currents and control of VSC. UTC is an efficient control strategy based on Synchronous Reference Frame Theory (SRFT) and supports grid-connected VSC. It is used as switching control of the converter and reactive power control of the grid [118] [119]. These applications are described in Fig. 2.17.

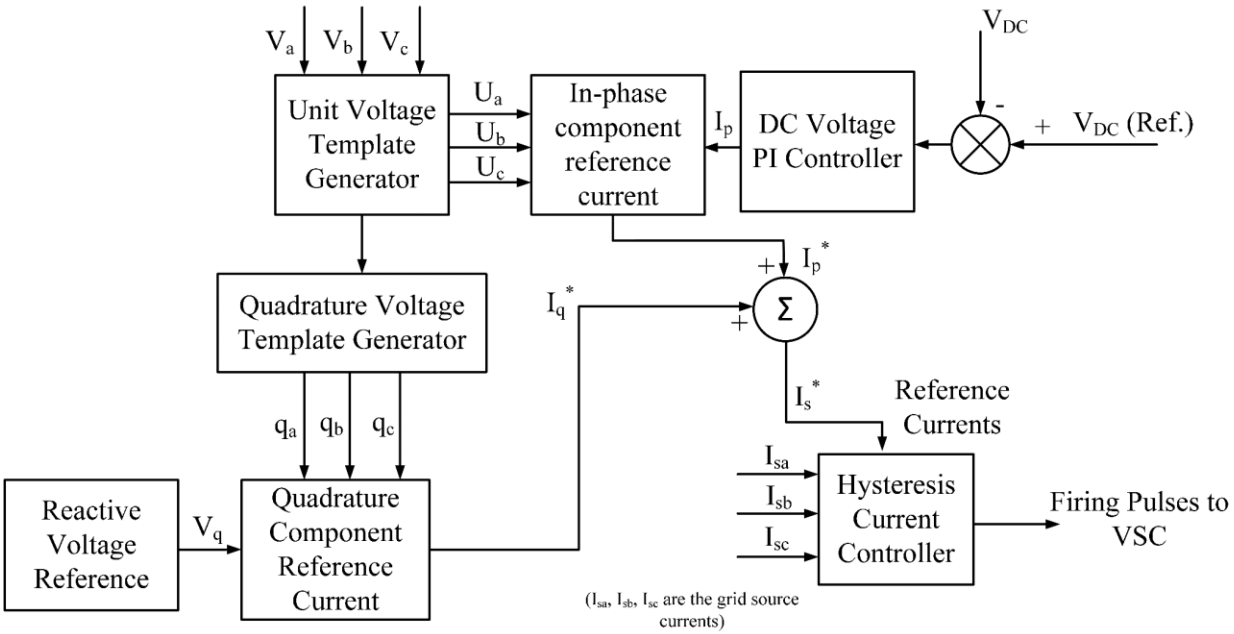

Fig. 2.17 Block diagram of UTC strategy [119] [120]

An indirect current control method is used to obtain reference signals (I_s^*) for HCC switching of the VSC. The reactive power is controlled by obtaining quadrature unit templates (q_a, q_b, q_c) and by comparing it with the desired value. Similarly, active power is controlled through direct unit templates (U_a, U_b, U_c) and addition ($I_q^* + I_p^*$) of these serve as reference signals to obtain switching pulses. The implementation of the control strategy is shown in four block Fig. 2.18.

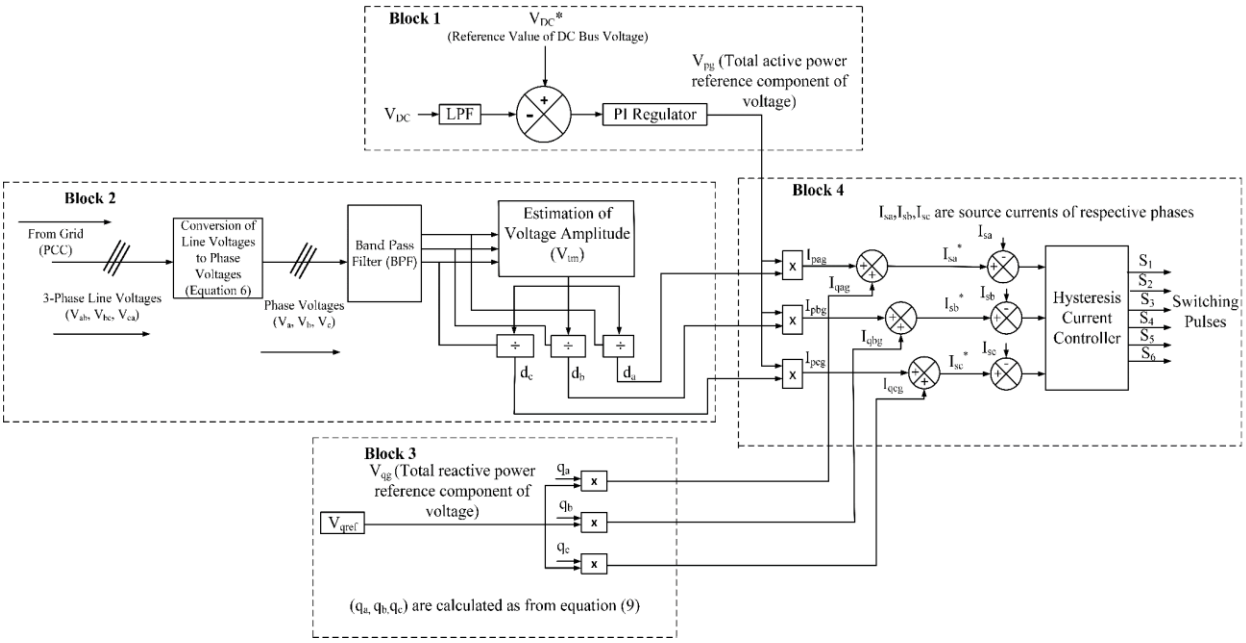

Fig. 2.18 Control Implementation of UTC Strategy [23] [121]

Block 1: The sensed DC Voltage V_{DC} is filtered through a low-pass filter (LPF). It is then compared with a desired reference DC voltage V_{DC}^*, to generate an error signal which is fed through a PI Regulator to generate V_{pg} which is the total active power reference component of voltage.

Block 2: The 3-line voltages (V_{ab}, V_{bc}, V_{ca}) are sensed from the PCC and the 3-phase voltages (V_a, V_b, V_c) are generated, as per equation (2.27). These are filtered with a Band Pass Filter (BPF) to remove any noises, and then fed to the voltage estimator block to produce V_{tm}, as per equation (2.28). The in-phase unit templates of phase voltages (d_a, d_b, d_c) are obtained as per equation (2.29). Similarly, three quadrature unit templates (q_a, q_b, q_c) of the phase voltages are derived as per equation (2.30).

$$V_a = \frac{2}{3} V_{ab} + \frac{1}{3} V_{bc}\ ,\ V_b = -\frac{1}{3} V_{ab} + \frac{1}{3} V_{bc}\ ,\ V_c = -\frac{1}{3} V_{ab} - \frac{2}{3} V_{bc} \quad (2.27)$$

$$V_{tm} = \sqrt{\left(\frac{2}{3}\right)(V_a^2 + V_b^2 + V_c^2)} \quad (2.28)$$

$$d_a = \frac{V_a}{V_{tm}}\ ,\ d_b = \frac{V_b}{V_{tm}}\ ,\ d_c = \frac{V_c}{V_{tm}} \quad (2.29)$$

$$q_a = -\frac{d_a}{\sqrt{3}} + \frac{d_c}{\sqrt{3}}, q_b = \sqrt{3}\frac{d_a}{2} + \frac{(d_b - d_c)}{2\sqrt{3}}, q_c = -\sqrt{3}\frac{d_a}{2} + \frac{(d_b - d_c)}{2\sqrt{3}} \quad (2.30)$$

Block 3: In this block, the desired reactive power V_{qref} or V_{qg} (total reactive power reference component) is multiplied with 3 quadrature unit templates (q_a, q_b, q_c) to generate 3 quadrature current reference values (I_{qag}, I_{qbg}, I_{qcg}) as per equation (2.31).

$$V_{qg} * q_a = I_{qag}, V_{qg} * q_b = I_{qbg}, V_{qg} * q_c = I_{qcg} \quad (2.31)$$

Block 4: The in-phase unit templates (d_a, d_b, d_c) which are computed in block 2 are used to generate the direct reference values for the gating pulses of the VSC by multiplying with the total active component of voltage (V_{pg}) as per equation (2.32):

$$V_{pg} * d_a = I_{pag}, \; V_{pg} * d_b = I_{pbg}, V_{pg} * d_c = I_{pcg} \quad (2.32)$$

Afterward, direct and quadrature values are used to obtain reference grid currents ($I_{sa}^*, I_{sb,}^* I_{sc}^*$) as per equation (2.33):

$$I_{sa}^* = I_{pag} + I_{qag}, I_{sb}^* = I_{pbg} + I_{qbg}, I_{sc}^* = I_{pcg} + I_{qcg} \quad (2.33)$$

A comparison of these reference values ($I_{sa}^*, I_{sb}^*, I_{sc}^*$) is made with the sensed grid currents (I_{sa}, I_{sb}, I_{sc}), and Hysteresis Current Controller (HCC) produces the gate pulses (S_1 to S_6) for VSC. HCC is one of the control techniques suitable for grid-connected applications. In this, an instantaneous current is regulated to stay within a tolerance band known as the Hysteresis band [23] [122].

2.10 Hysteresis Current Controller (HCC)

HCC is an accurate and easy technique that is suitable for grid-connected applications. In this technique, an instantaneous current is regulated to stay within a narrow tolerance band known as

the Hysteresis band. It is a robust control method and provides good dynamics and is less affected by the disturbances in the system.

In HCC, pre-set upper and lower hysteresis tolerance limits are compared with the extraction error signal. This hysteresis tolerance bandwidth is usually twice the error signal [122]. Variable switching frequency is the drawback of this technique. HCC uses varying instantaneous currents to generate the gate pulses as compared to the fixed frequency in other methods, as shown in Fig. 2.19 [123]. This technique is different from other methods which employ fixed frequency switching.

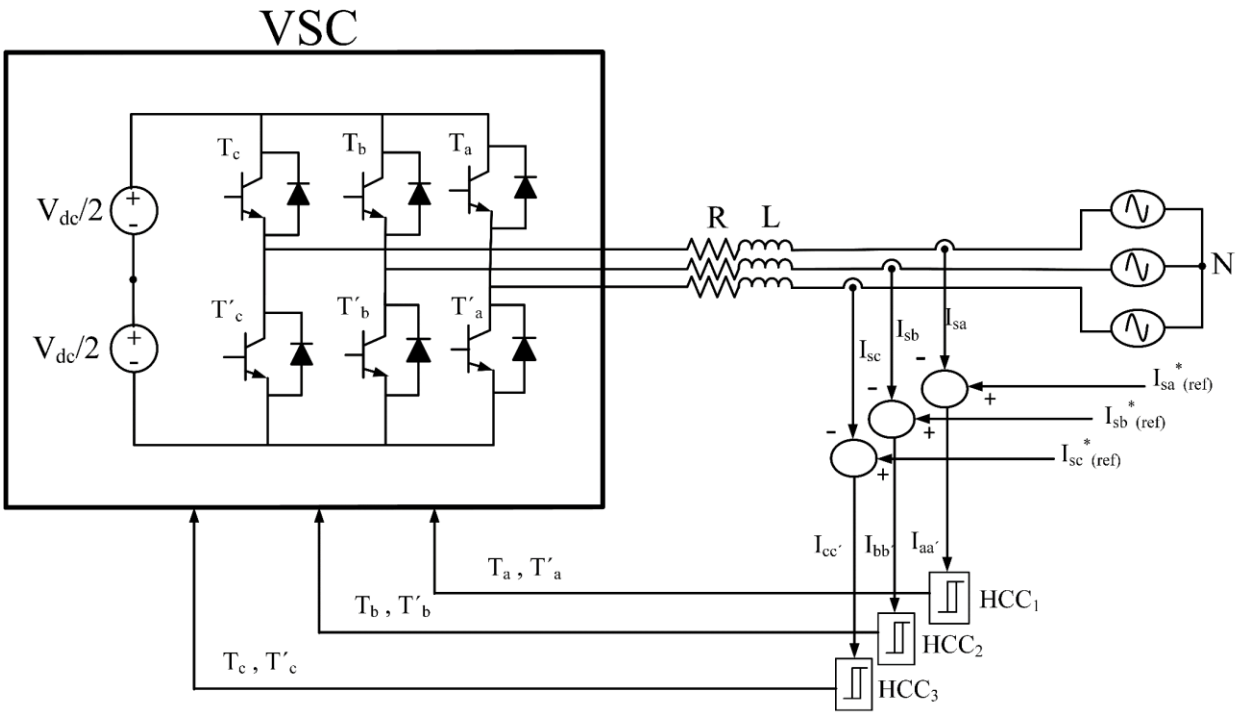

Fig. 2.19 Hysteresis Current Controller [123]

In Fig. 2.19, the basic operation of HCC is shown; each phase in the VSC has a separate HCC. These controllers generate gate signals for the IGBTs based on the input current errors. The output of individual HCC is supplied to the separate legs of the VSC. Different switches are shown in the Fig. 2.19 as T_a and $T_{a'}$ for leg 1, T_b and $T_{b'}$ for leg 2 and T_c and $T_{c'}$ for leg 3. Similarly, current in each leg is controlled by input gate signals which form a separate HCC. The switching in the HCC

is complementary and depends on the position of the input current in the hysteresis band (Fig. 2.20).

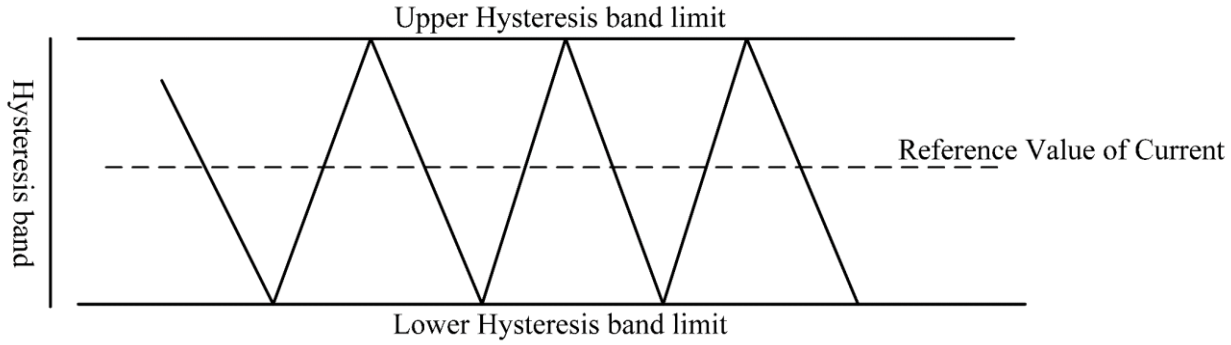

Fig. 2.20 Instantaneous Current trajectory and hysteresis band limits [123] [124]

There are limits for instantaneous currents (I_{aa}´, I_{bb}´, I_{cc}´) in hysteresis controller mentioned as upper hysteresis band limit and lower hysteresis band limit as shown in Fig. 2.20. The upper switches (T_a, T_b, T_c) are turned off when the instantaneous value of current reaches upper hysteresis band limit and these switches turned on again when this current reaches the lower hysteresis band limit. The switches (T_a´, T_b´, T_c´) in the lower leg turned on when upper switches are off.

There may be a problem in this HCC that current errors may reach twice the hysteresis limit band with a system of isolated neutrals. This problem can be corrected by employing the controller in dq- or αβ- frame or by using compensators. This is a basic HCC technique, and more advanced methods like Space Vector Modulation (SVM) HCC can also be used. In SVM, the hysteresis tolerance band is made smaller, which results in a better output. But with this method, simulation is more time-consuming.

The above-mentioned techniques are used for the AC grid-side control. On the DC side, however, there is a requirement for EV battery charge control where, Constant-Current Constant-Voltage (CC-CV) is used.

2.11 EV Charge Control (DC-DC Converter)

A DC-DC converter is required for the EV´s State of Charge (SoC) control of the battery. In this work, the charging operation is implemented with the help of the Constant Current-Constant Voltage (CC-CV) method which is an amalgamation of two modes of operation. First, the battery is charged with a pre-set constant current value until the battery voltage reaches a pre-set voltage level. When the battery voltage reaches this pre-set value, the current starts decreasing. Now, the constant voltage is maintained at this pre-defined value, and battery current is allowed to decrease till the battery gets fully charged. This method is suitable for fast charging, and there are fewer chances of overcharging and causing damage to the battery [125] [126].

These converters allow bi-directional power flow to/from the EV battery and to support in absorbing the regenerative braking energy during the driving operation. The operation of the converter can be divided into buck and boost operations. It works as in buck-mode during discharging and acceleration periods, and as in boost-operation during charging and regenerative braking periods [127-130].

The buck-boost converter operation is shown in Fig. 2.21.

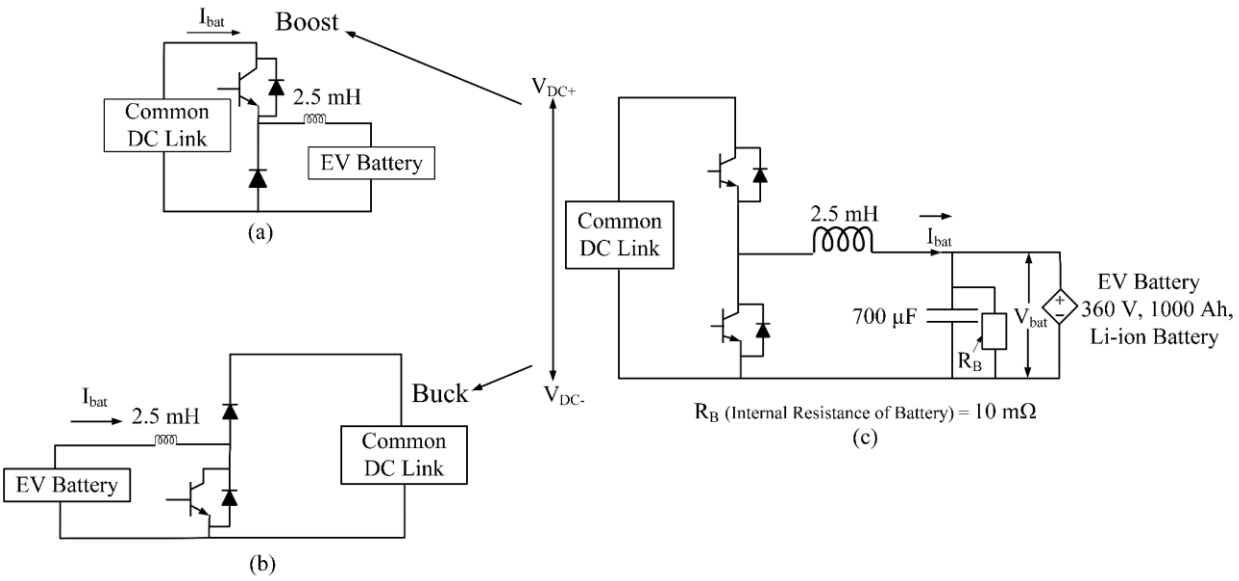

Fig. 2.21 Buck-Boost DC-DC Converter

In Fig. 2.21 (a), the boost converter operation is shown, which works when there is charging of EV battery termed as Grid to Vehicle (G2V) mode or regenerative braking mode during the driving cycle of the vehicle. In it, the upper IGBT and lower parallel diode operate consecutively. This operation charges the battery during either the fast charging operation or when there is braking of the vehicle. It saves energy during the driving cycle and improves the system efficiency.

Similarly, In Fig. 2.21 (b), the buck converter operation is shown, which works during battery discharging i.e., Vehicle to Grid (V2G) operation and acceleration mode of driving cycle [23] [130]. In it, the lower IGBT and upper diode conduct consecutively. This bi-directional operation makes the system efficient and economical.

In the further chapters, two system of architectures, Inclusion of PV-panel into the architecture, results and discussion and finally conclusions have been made.

CHAPTER 3

COMMON AC AND DC SYSTEM OF ARCHITECTURES

3.1 Common AC and DC System of Architectures

Two architectures (Common DC Bus and Common AC Bus) for the EV FCS are compared in this dissertation. The two EV FCS architectures are assumed to be fed from the grid and feed into an assumed charging load on the basis of 10 bays having a typical EV (e.g. Nissan Leaf S Plus 2020 with a 62 kWh battery, 214-hp, 160 kW motor) in each bay. The vehicles are assumed to attain up to 80% of their charge within 25 minutes. The criteria used to calculate the rating of the station is P = E/t where P = charging power in watts, E = Battery Energy in Wh, t = charging time in hours [131], a charging station with a rating of 118 *10 kW, i.e. 1.18 MW is required. Assuming some contingency and allowances for different types of vehicles to be charged, the FCS power rating is, therefore, estimated to be about 2 MVA. Therefore, there are certain conditions required to maintain the seamless operation of the charging from the grid. These conditions as shown in Table 3.1 to achieve efficient operation of the system.: -

Table 3.1 Required conditions on Grid and charger [23]

Grid Side	**Charger Side**
UPF operation is required for the grid-connected operation. Appropriate control algorithm must be used to achieve this.	Controller should be capable of maintaining Sufficient Voltage level ($V \pm \Delta V$) at DC link in common DC bus to charge the EVs with lesser ripples. (In this model battery voltage is 360 V and $\Delta V = 10\%$). In common AC bus, individual rectifier stage is required for each bay and afterwards voltage level is maintained.
As per IEEE 519-1992 (revised in 2014), 5% voltage harmonic distortion limit and 8% THD limit should be maintained at PCC. In case of current harmonics, IEEE and IEC standards should also be maintained and it depends upon the ratio of I_{sc} (Short-circuit current) and I_L (Load current). If I_{sc}/I_L is 20 to < 50, then allowed TDD is less than 8% [132] [133]. THD is the ratio of sum of powers of all harmonic components to the power of fundamental frequency. TDD is calculated harmonic current distortion against the full demand level of the electrical system. At full load, THD(I) = TDD(I).	Charger side converter and controls are responsible to maintain the voltage and current harmonic limits as per International standards (IEEE 519-1992 and IEC 61000-3-12/2-4). CC-CV method is used at the charger end as DC-DC converter for regulation. It saves the battery from overcharging and increase the life of battery.

In these conditions, power factor is an important parameter. Complex power in an electrical system is defined as:

$$S = VI^{*} \tag{3.1}$$

Definition of PF is as follows:

"Power Factor (PF) is the ratio of working power, measured in kilowatts (kW), to apparent power, measured in kilovolt amperes (kVA)." Mathematically, PF can be expressed as in equation (3.2).

$$P.F. = \frac{P}{S} = \frac{P}{VI_S} = \text{Cos}\Phi \tag{3.2}$$

In (3.2), P is working power, S is apparent power, I_S is rms value of current.

$$S = V_S I_S \tag{3.3}$$

In ideal case, PF should be 1. It means reactive power should be zero.

Another important factor for electrical distribution system is Displacement Power Factor (DPF). DPF is defined as follows:

"DPF is the power factor due to the phase shift between voltage and current at the fundamental line frequency."

DPF is a power factor which is equal to PF in linear circuits with sinusoidal voltages and currents.

DPF is used to measure when there is phase-shift in the system, and PF is used to determine the overall system effectiveness in the presence of harmonics. It means when there is difference between DPF and PF, then harmonics are present in the system, and further investigation is required. Relation between both PF and DPF can be defined as equation (3.4).

$$PF = \frac{1}{\sqrt{1+ THD_I^2}} \text{DPF} \tag{3.4}$$

From equation (3.4), PF is comprising of DPF and THD_I. If the content of harmonics increases in the system, then PF becomes poor.

There is requirement to maintain constant DC link voltage at the charger side. Further, allowed harmonic distortions at PCC (grid-side) are mentioned in Table 3.1.

In this study, the charging/discharging operation of EVs and its impact on the harmonics is the focus. The system components such as DT, filters, 2-level VSC, common DC bus rating, common DC capacitor rating, DC-DC converter, Battery-side capacitors and inductors are integrated in the EV FCS model. Some of these ratings also depends upon the type of DC FCS that is either common AC bus or common DC bus.

The required equations used to do important calculations of rated capacity of the FCS (S_R), common DC bus voltage (V_{DC}), Capacitor rating (C_{DC}) are given next. Demand estimation of charging slots,

location and area of the charging station, rate of allowable charging power for each vehicle, nominal voltage level and permissible power levels at the point of common coupling are the important aspects that should be considered while designing a charging station [23].

Rated capacity of charging station S_R can be analyzed by the equation (3.5):

$$S_R = \frac{K_{load} N_{slot} P_{ev}}{cos\Phi} \tag{3.5}$$

Where K_{load} = 1.1 (Overload factor which takes into account the overload due to transients)

N_{slot} = Number of available charging slots (taken as ten for fully loaded case)

P_{ev} = Maximum charging power rate of an EV

$cos\Phi$ = Power factor of the system (0.95)

DC bus voltage is another important factor of the DC fast charging station. If the FCS is connected to the grid through the DT, then bus voltage depends upon minimum battery voltage V_{min}^{bat} and minimum modulation index m_{min}. The relationship can be represented by equation (3.6):

$$V_{DC} \leq \frac{V_{min}^{bat}}{m_{min}} \tag{3.6}$$

DC bus stability should be maintained, as it is a very significant factor for the reliable operation of the FCS. It directly depends upon the size of the DC capacitance. The value of capacitance is calculated by using the equation (3.7) and by considering transients and ripple current.

$$C_{DC} = \frac{S_R * 2nt * \Delta p * cos\Phi}{v_{DC}^2 * \Delta V} \tag{3.7}$$

Where t = period of AC voltage wave

n = multiple of t

Δp = DC power range of change

ΔV = allowable DC bus voltage range of change in percentage

These ratings are important to design both the architectures for common DC bus and common AC bus. In this study, maximum ten EV slots are considered and varied to five for certain comparisons. The grid circuit for the two architectures is modeled as Thevenin equivalent of distribution electric grid, which is considered without any electric load except EVs. The design of two FCS are shown and explained next.

The two FCS architectures are (a) DC bus architecture (Fig. 3.1) and (b) AC bus architecture (Fig. 3.2).

3.1.1 The DC bus architecture

The DC bus architecture is a well-established architecture (Fig. 3.1) [134-137] and contains two power conversion stages. First is the common (central) AC-DC rectifier stage, which is followed by the DC-DC conversion stage for regulation purposes. The proposed load consists of 10 bays.

The grid connection is at 12 kV, 2 MVA, 60 Hz, which feeds into the main FCS 2 MVA, star (Y)-delta (Δ) (or Δ-Y, Δ-Δ, Y-Y, DT connection configurations), 1200/600 V, 60 Hz, DT. The secondary of the DT has an AC filter (60 kVA, 5 Ω, 20 µF) and 4 mH smoothing reactor for filtering purposes and feeds into the 2-level, 3-phase, active AC-DC, 6-switch, VSC (IGBT/diode). The DC-link capacitor is 3300 µF at the common DC bus voltage of 400 V_{DC}. Ten EV bays (EV1 to EV10) are connected to the common DC bus. Each EV bay consists of a DC-DC converter with a DC capacitor filter of 700 µF. The EVs can then be connected to this stage. In between each bay, an inductive link with 0.3 µH is assumed (this is assumed to be part of the leakage/parasitic inductance between bays). The battery is rated at 360 V, 1000 Ah Li-ion battery.

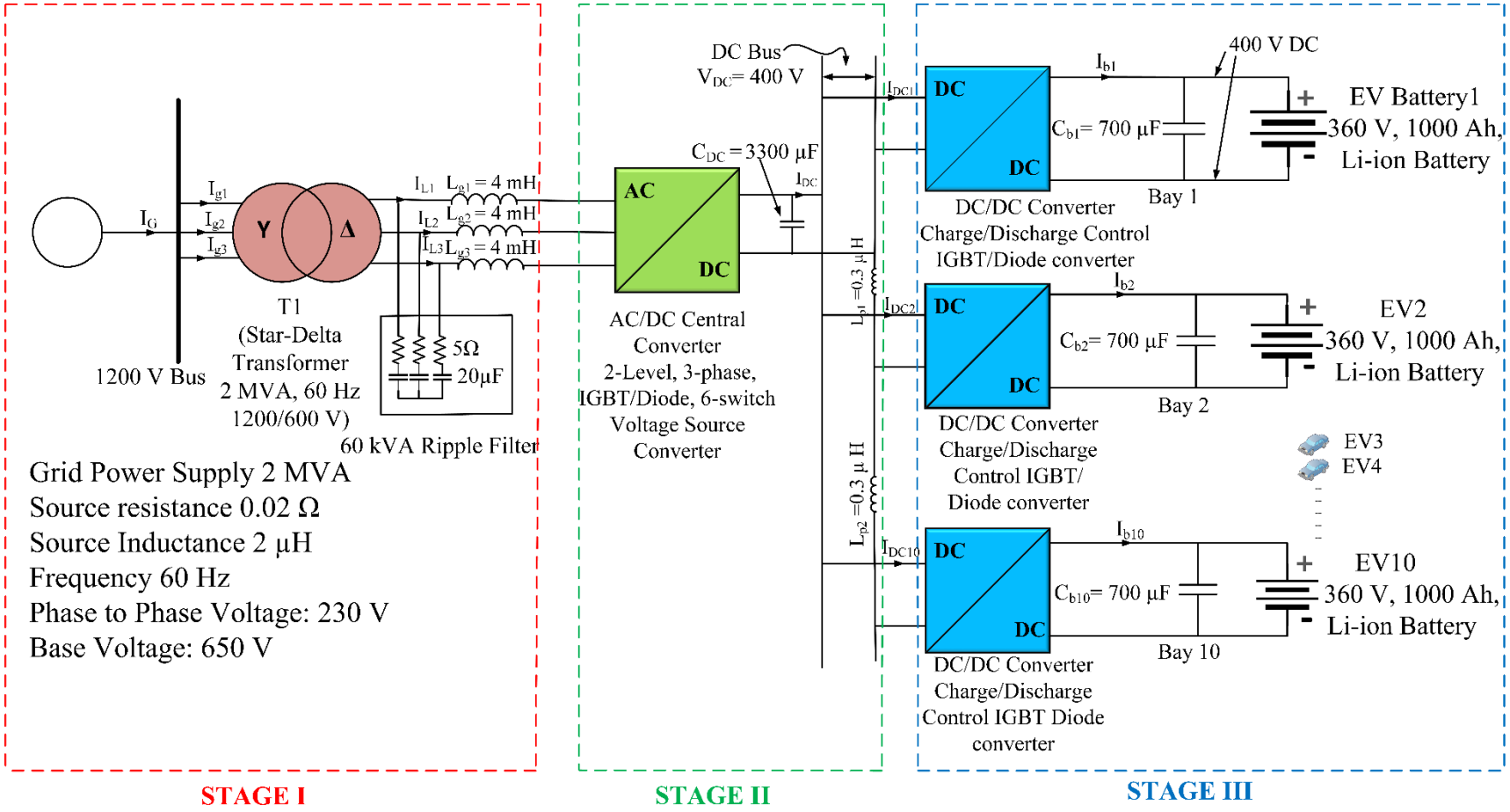

Fig. 3.1 Common DC Bus FCS

DC FCS is a flexible DC grid structure in which the inclusion of distributed energy resources is possible at DC bus. The system becomes more efficient as fewer number of conversion stages are required.

EVs need efficient charging infrastructure which can deliver higher range in minimum time to the batteries. The use of super-capacitors or energy efficient storage devices is one another option for this purpose. They can provide long durability, higher power density, less maintenance and temperature-independent system. Super-capacitors act as a buffer between the FCS and grid-side which results in least disturbances on the grid-side.

There are certain drawbacks in this system. The rating of the central converter is higher, so there are more stern requirements for THD as per grid code. The level of fault current might become dangerous due to non-existence of natural zero-crossing point [138]. AC systems have natural zero-crossing current point which is helpful in interrupting the short-circuit current, while the absence of natural zero-crossing current point in DC circuits requires the protection system to artificially create one in order to interrupt the current. This is both expensive and more difficult to implement. Therefore, a DC system requires more complex and expensive protection devices. However, in spite of this, the proper designing and inclusion of energy efficient devices, use of renewable energy sources can still make common DC charging stations a sustainable solution [139].

3.1.2 The AC bus architecture

AC bus architecture is a common architecture [23] [131] [137], which can be used to connect the charging bays in FCS to the electric grid (Fig. 3.2). There are also two conversion stages in this structure. First is an AC-DC conversion stage for each bay (decentralized) and then followed by a

DC-DC conversion for regulation. A separate firing, control and filtering system for each stage is needed. Hence, it makes the system more complex and expensive.

The grid connection of AC bus Architecture is also taken at 12 kV, 2 MVA, 60 Hz which feeds into the main FCS 2 MVA, star (Y)-delta (Δ) (or Δ-Y, Δ-Δ, Y-Y DT connection configurations), 1200/600 V, 60 Hz, DT. The secondary of the DT has an AC filter (60 kVA, 5 Ω, 20 μF) and 4 mH smoothing reactors for filtering purposes, which is connected to the 600 V AC bus. Afterwards, there is a tapping on the AC bus, which feeds into the separate (10 bays in proposed architecture from EV1 to EV10) 2-level, 3-phase, active AC-DC, 6-switch, VSCs (IGBT/diode). These VSCs are further connected to the DC-DC converter for regulating the voltage with a DC capacitor filter. Subsequently, these chopper converters are feeding EV batteries. In between the VSC and converter, a parasitic inductive link of 0.3 μH is assumed as in the case of the Common AC bus.

Three-phase AC bus is used to tap the connections for each and every charging point, and every point can work independently. But, due to the use of several rectifiers and different stages, there are chances for inter-actions and of the production of unwanted harmonics at the utility grid [140]. It is an expensive option as there is a need for several rectifiers with as many filters and sensors.

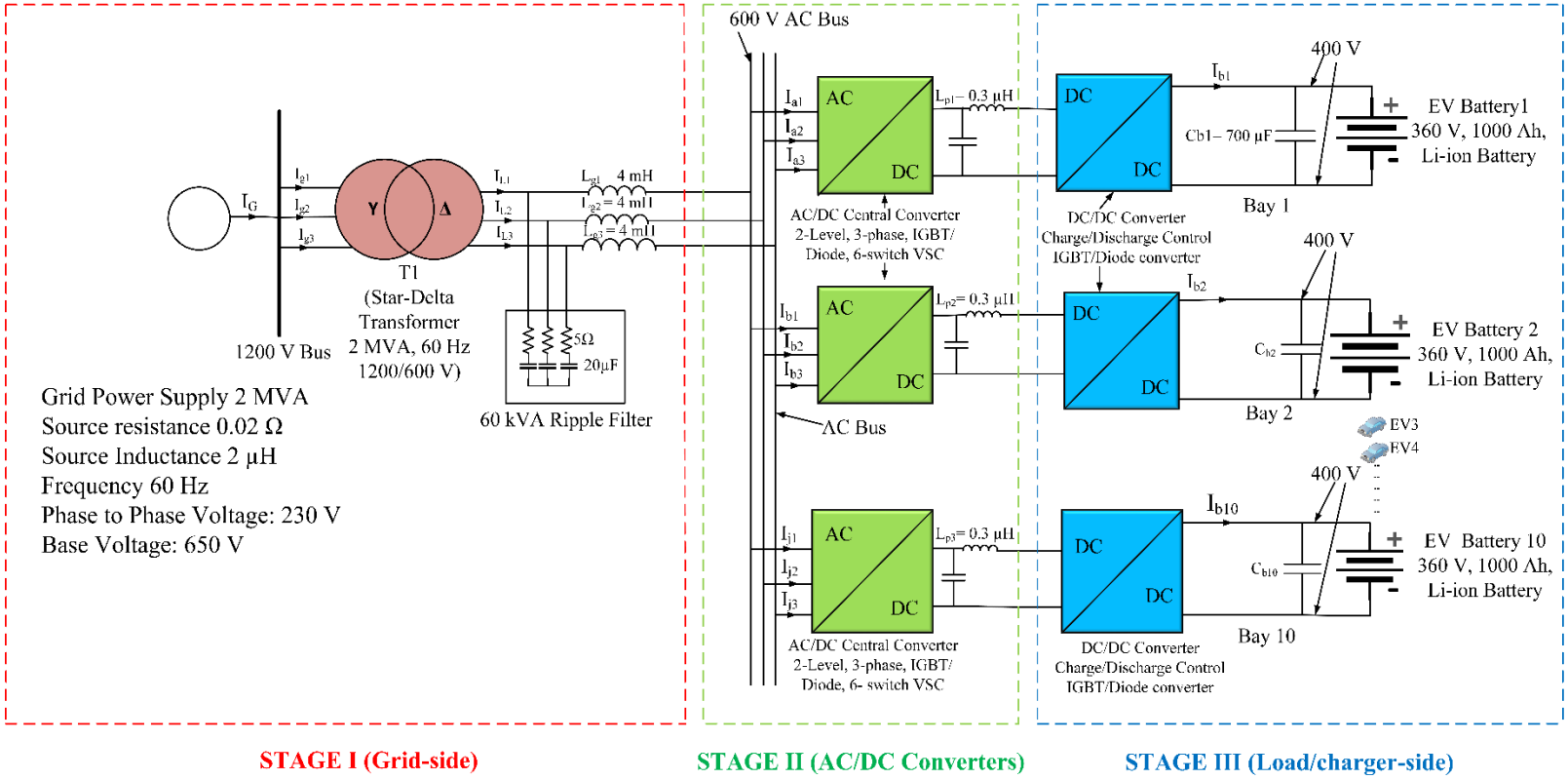

Fig. 3.2 Common AC Bus FCS

EVs have a detrimental impact on the electric grid due to their dynamic nature and many charging rates. These effects include harmonics in line currents, voltage deviations, DC offset, stray fluxes and phantom loading. Power electronic converters are non-linear by nature, and due to that they inject higher-order harmonics in the line current drawn by them [141] [142]. These problems arise in both the FCS and are unavoidable, but can be minimized. It can deteriorate the performance and efficiency of the electric distribution network. These harmonics add to the I^2R losses in the winding of DT and are damaging for its age.

VSC is main interfacing equipment between the FCS and grid. Therefore, control strategy for the VSC is helpful in reducing the impacts on the power quality of the distribution system. Some important control strategies for the VSC are discussed in chapter-3. In this study, UTC control method is employed on both the architectures. It produces balanced and sinusoidal reference values for the smooth and efficient operation of FCS. It is found to be less complex than the popular PLL techniques [143-146]. The above-said reasons made the UTC strategy a suitable candidate for FCS.

A comparison of both the architectures is made in Table 3.2.

Table 3.2 Comparison of Common AC Bus and DC bus Architectures

AC Bus Architecture	**DC Bus Architecture**
Needs individual controllers for each and every AC to DC converter.	Only one centralized converter is required and one controller for the main converter.
It is more reliable system than the common DC bus architecture due to interleaved converters.	There is only one main converter and failure of it make the system unreliable.
Due to more converters, cost of the system is high.	It is more economical as there is only one main converter as compared to number of converters in AC Bus Architecture.
More flexible as there are individual controller for each EV.	Less flexible as failure of main converter can result into catastrophic effects.
This system is not suitable for distributed energy generation as it is a complex system.	This is appropriate for distributed generation as it is easy to control single converter and it makes the system reliable and simple.
AC Protective devices can be used.	DC protective devices are required as there is no natural zero crossing point in the DC system, so, these devices are expensive.
Conversion losses are high (typically about 32%)	Conversion losses are less than the AC Bus architecture (typically less than 10%).
More filters are required to reduce the THD in the system.	Main LCL filter can be designed to reduce the THD in the system.

It has been concluded from Table 3.2 that Common AC bus architecture (CACB) requires more conversion stages which increases the losses in the system. Interleaved converters are used in CACB, which results in reliable system as compared to common DC bus (CDCB), but also make it more expensive than CDCB. The more stages in the AC bus architecture results in increase in the conversion losses. CDCB requires only one main VSC and failure of which results into a complete loss situation. Protective devices (DC circuit breaker) are required to avoid this situation in DC bus architecture, which is a costly proposition. The complex system of CACB architecture made it hard for the combined operation with the renewable energy sources, despite CDCB architecture can run easily with different kind of renewable sources which makes it suitable choice for smart-grid operation.

Common DC bus FCS are coming as suitable solution to meet the charging needs of consumers in urban centres as well as isolated rural areas where Islanded-operation (with the help of renewable energy resources) is possible.

3.2 Inclusion of PV-panel into the FCS, impact of grid-strength and varying X/R ratio

A grid-connected EV FCS can increase the grid instability. The increase in number of EVs results in rise in grid losses. So, inclusion of Photo-Voltaic (PV) system or any other renewable energy source into the FCS can make it more efficient and reliable. The PV system can be a part of the grid-connected FCS (Fig. 3.3) or can supply it on a standalone basis. The PV system adds to the total load handling capacity of the system, which is helpful to a typically weak distribution grid (having low MVA_{SC}).

PV system can supply the FCS in standalone mode too. There is no need of an AC-DC converter in this system and it is easy to maintain. EV batteries can act as storage devices which is beneficial for a Vehicle to Everything (V2E) operation. V2E operation includes Vehicle to Grid (V2G), Vehicle to Vehicle (V2V), Vehicle to Home (V2H), and Vehicle to Building (V2B) etc. These standalone PV based charging stations are emerging as a possible charging solution for the parking lots, apartment buildings, office buildings and commercial complexes. It encourages the consumers for “charging while parking” concept and beneficial when abundance of solar energy is available.

Both weak and strong electric grids with and without PV systems, are compared in this study. The effect of varying the X/R ratio on the damping of the system, and the impacts on the power quality at the PCC is also performed.

X/R ratio is an important parameter to decide damping of the system, and is explained in detail in chapter-2. But, X/R ratio is also vital in short-circuit analysis of the system. The fault current consists of an AC component which is also known as the symmetrical current, DC component which is directly proportional to X/R ratio of the system i.e. if X/R ratio is higher, then the DC component takes time to decay and results in an increase in the asymmetrical current [147]. This can be seen in equation (3.8).

$$I_{peak} = \sqrt{2} * I_{AC(RMS)} * \langle 1 + e^{\frac{-2\pi\tau}{X/R}} \rangle \quad (3.8)$$

Where I_{peak} = Peak fault current, $I_{AC(RMS)}$ = RMS value of the current, $\tau = 0.49 - 0.1 * e^{\frac{-X/R}{3}}$

It is clear form equation (3.4) that peak current (I_{peak}) increases with an increase in value of X/R ratio. X/R ratio is directly proportional to DC component in case of fault current which results in slow decay of fault current in the system. Therefore, it is essential to consider X/R ratio for the selection of protection equipment in case of grid-connected FCS.

3.2.1 DC FCS Architecture with PV system

The five EV bays are used to study the DC FCS with PV system. The boost converter is placed with the PV-panel to harvest the maximum energy. The schematic figure of the proposed infrastructure with PV-panel built in Simulink® is shown in Fig. 3.3:

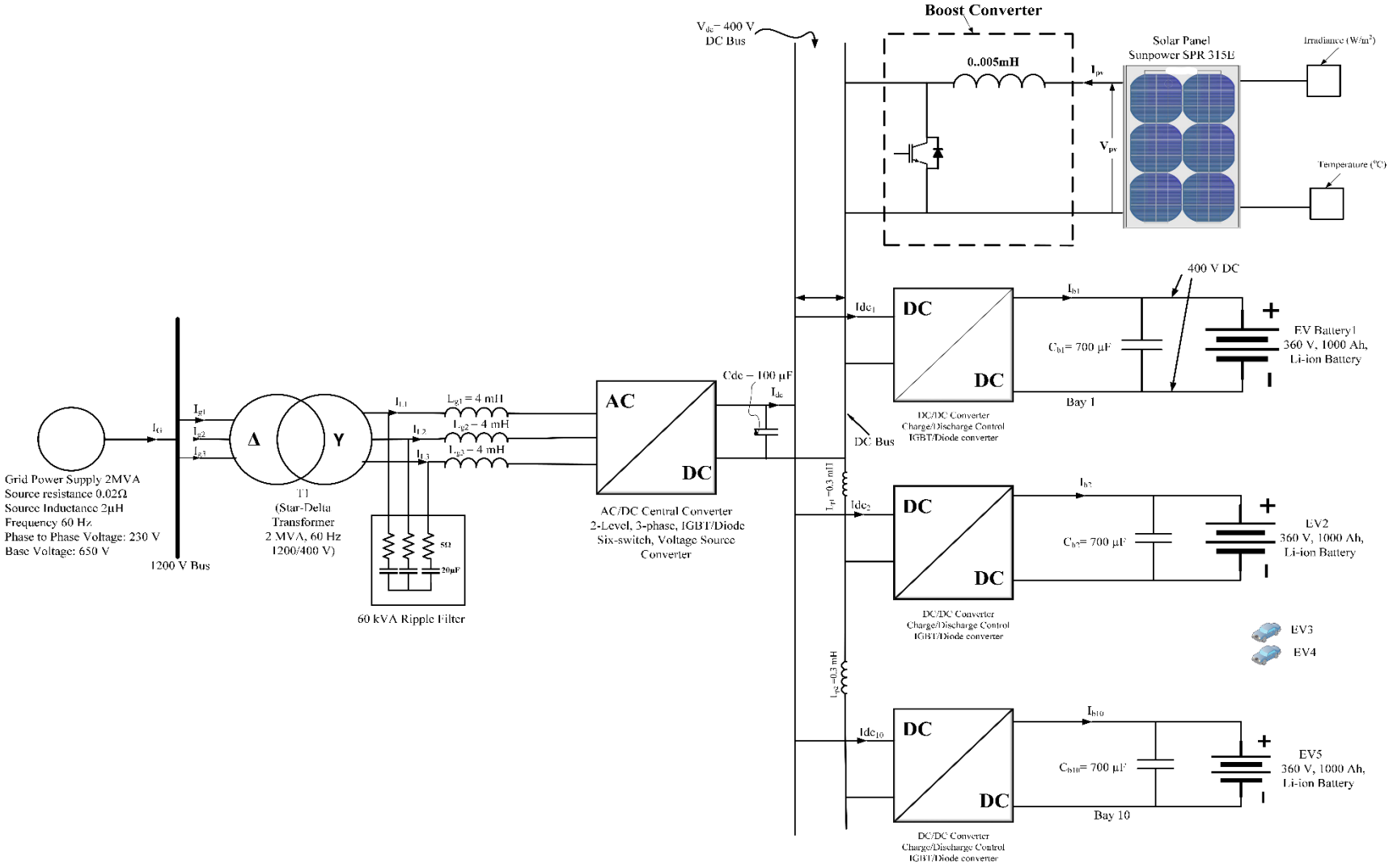

Fig. 3.3 EV FCS connected with Electric Grid and PV-panel

EV FCS architecture with PV system (Fig. 3.3) consists of four different stages: (1) Grid connection using a Distribution Transformer (DT) (2) AC-DC conversion with 2-level VSC and Common DC Bus (CDCB) (3) PV-panel with boost converter, and (4) DC-DC conversion stage for connection to the EV. These stages are described next.

3.2.1.1 Stage 1 (Grid to Distribution Transformer)

In stage I (Fig. 3.3), the host utility grid is connected to a 2 MVA, 1200/600 V, 60 Hz, DT and low pass filters. The assumed electric grid rating is 2 MVA, 230 V (Phase-to-Phase), 60 Hz on the basis of feeding 5 bays FCS. The rating of grid is varied from weak to strong systems and the impact is assessed. An AC low-pass filter of rating 60 kVA, (comprised of a 5 Ω resistor and 20 μF capacitor in parallel, and with a 4 mH series smoothing reactor) is used for filtering purposes. The filter is important to remove distortions from the supply waveform as the load is non-linear in nature. This filter consists of capacitors C_{r1} to C_{r3}, small damping resistors R_{d1} to R_{d3}, and smoothing series inductors L_{g1}-L_{g3}.

In the grid-connected EV charging system, features of AC systems have a substantial impact on the operation and working of EV FCS. The AC-DC converter operation depends upon the grid strength. The relative operation of both is a vital indicator of VSC operating problems.

3.2.1.2 Stage 2 (AC to DC conversion with 2-level VSC and CDCB)

A 2-level, 3-phase, 6-switch VSC is used as the main AC-DC converter. This DC supply is fed to the common DC bus voltage of 400 V_{DC} with the support of a DC link capacitor. This capacitor might be an electrolyte capacitor or a super capacitor; an assessment of the capacitor duty will be made based on transient requirements. This system load is designed for charging a maximum of 5

EVs at a time. There are many advantages of the common DC bus as it increases the flexibility of the system.

The control strategy is required to maintain Unity Power Factor (UPF) at the source side. Reference source currents are generated by the Unit Template Control (UTC) method which are compared with sensed grid currents to generate switching pulses for the VSC.

3.2.1.3 Stage 3 (PV as energy source with boost converter)

The inclusion of a PV source in this integrated system makes the overall system more flexible and green. The PV source is connected with the common DC bus through a boost converter. Fig. 3.4 shows a basic step-up boost converter. This converter contains the DC source voltage V_P from the PV-panel, inductor L, switch S, diode D, capacitor C, load resistance R. V_L is voltage across load, i_S is current through switch, i_C is capacitor current, V_o is voltage across load. The operation of boost converter is explained by the following modes.

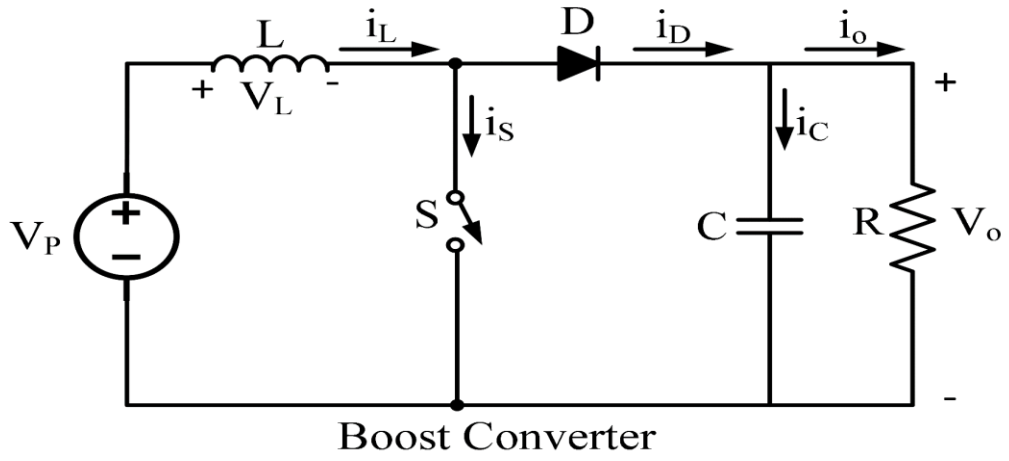

Fig. 3.4 Boost Converter [148]

Mode I: In this mode, switch S is OFF, diode D is turned-on, then input voltage (V_P) appears across the load and inductor releases its energy to boost the load and charge the capacitor. In this period, the current flowing in the diode is given by equation (3.9):

$$i_D = i_C + i_o \tag{3.9}$$

Mode II: In this mode, switch S is ON, and the input supply charges the inductor. The capacitor starts discharging through the load. Continuous Conduction Mode (CCM) of the converter depends upon the values of inductor and capacitor. The voltage ripple of boost converter is affected by the choice of these components.

In this study, the boost converter is controlled by P & O (Perturb and Observation) algorithm. The two inputs to the PV array are Sun Irradiance (W/m^2) and Temperature (^oC). Both of these are fluctuating quantities. Maximum Power Point Tracking (MPPT) system using the P & O algorithm (Fig. 3.5) is used to maximize the power obtained from the PV source. The duty cycle (D) of the boost converter is varied to adjust the power and voltage as per received inputs from the PV array. This duty cycle D = T_{ON}/T, where T_{ON} = on period for the converter, and T = total time period. The algorithm measures PV-panel voltage (V) and current (I) first, which is further used to calculate the power (P=V*I). Afterward, dV = V - V_{old} and dP = P - P_{old} are calculated. Then, the duty cycle is obtained as shown in the flow chart.

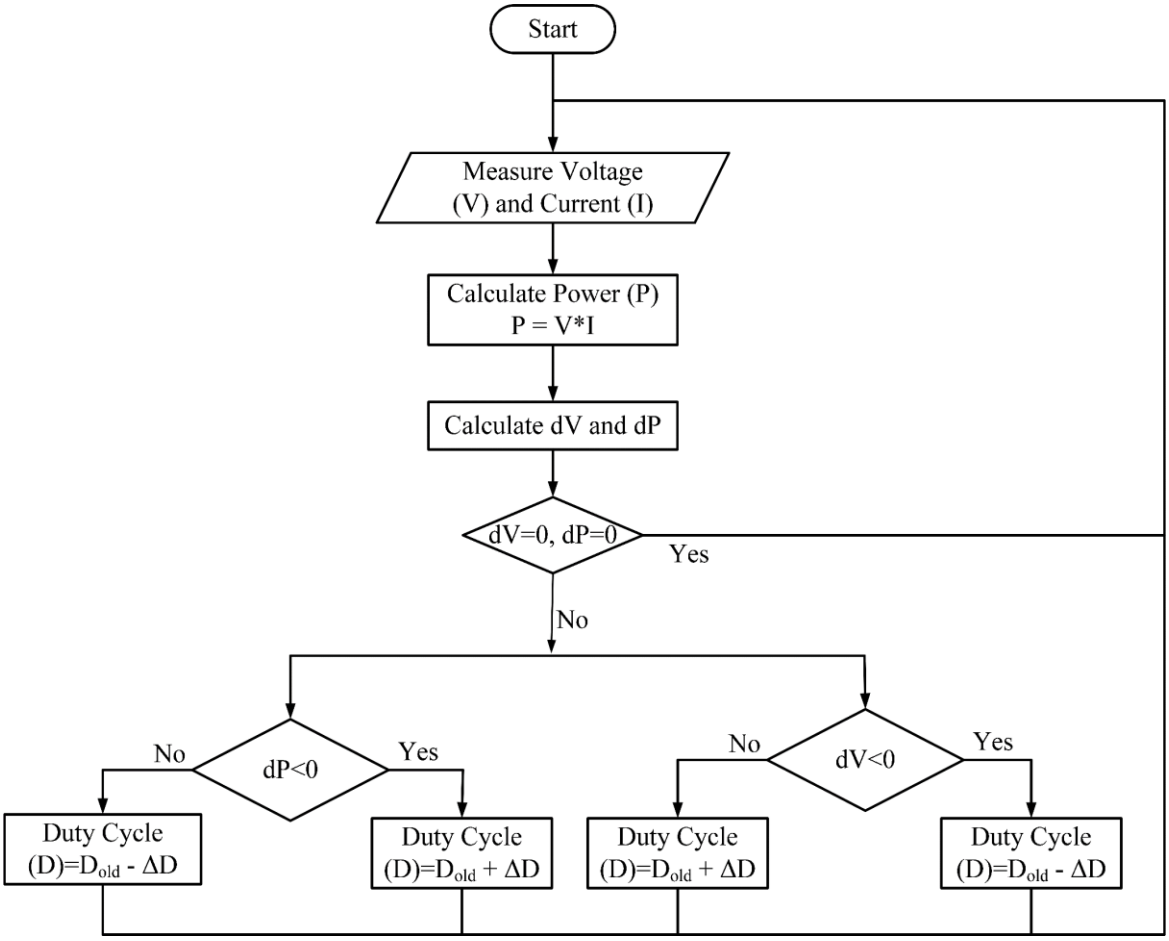

Fig. 3.5 P & O Algorithm Flow Chart for Boost Converter [148]

The inclusion of PV system into the grid-connected FCS (Fig. 3.3) made the complete system more flexible and environment friendly. There are different types of PV/solar-panels available in the market. The output power of the solar panels depends upon solar irradiance, module temperature and characteristics of solar-panel. In this Simulink model, a Sunpower SPR-315E-WHT-U PV-panel is used whose important parameters are shown in Table 3.3.

Table 3.3 Parameters of Sun-power SPR-315E-WHT U PV-panel [149]

Parameter	Rating
Standard Test Conditions (STC) Power Rating	315 W
PVUSA Test Conditions (PTC) Power Rating *Photovoltaics for Utility Systems Applications (PVUSA)	290 W
STC Power per unit area	192.9 W/m^2 (17.9 W/ft^2)
Peak efficiency	19.3 %
Power Tolerances	-5%/+5%
Number of Cells	96
I_{mp} (Current at maximum power point)	5.76 A
V_{mp} (Voltage at maximum power point)	54.7 V
I_{sc}	6.14 A
V_{oc}	64.6 V
Nominal Open Circuit Temperature (NOCT)	45^o C
Maximum System Voltage	600 V

3.2.1.4 Stage 4 (DC to DC conversion with EV Batteries)

Each EV bay consists of a DC-DC converter with a DC filter capacitor of 700 µF. A 0.3 µH inductance is assumed to be part of the leakage/parasitic inductance between bays. The battery is a 300 V, 1000 Ah Li-Ion battery which is based on a Nissan Leaf S Plus 2020 with a 62 kWh battery, 214-hp, 160 kW motor) similar to previous cases of CDCB and CACB architectures.

In the charging mode, this bidirectional converter acts as a boost converter, and during the discharging mode, it works as a buck converter. In this work, the charging stage is operated with the help of the Constant Current-Constant Voltage (CC-CV) control method.

A DC-DC converter is required to control the charging/discharging of the battery. This converter may be either on-board or off-board. These converters permit bi-directional power flow from the EV battery and help in absorbing the regenerative braking energy during driving. In the charging mode, this bidirectional converter acts as a boost converter, and during the discharging/braking mode, it works as a buck converter [23]. In this work, the buck-boost converter operation can be understood from Fig. 3.6.

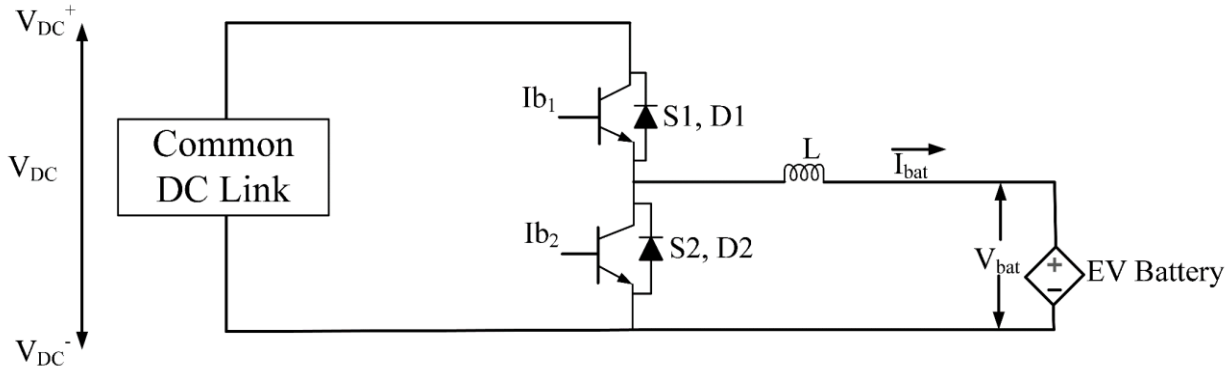

Fig. 3.6 DC-DC Converter (Buck-Boost Converter)

The boost converter operation works when there is charging of EV battery termed as Grid to Vehicle (G2V) mode in active or regenerative braking during the driving cycle of the vehicle. In it, the upper IGBT S1 and lower diode D2 and is working. This operation charges the battery during either the fast charging operation or when there is braking of the vehicle. It saves energy during the driving cycle, making the system more efficient. Similarly, buck-mode of operation works during battery discharging, i.e., when Vehicle to Grid (V2G) operation is active and acceleration mode of driving cycle. The operation is explained with the help of the following modes:

I. Mode 1 (Charging): In the charging or boost mode, there is flow of constant charging current from the common DC link to the EV battery (when $V_{bat} < V_{DC}$) until the battery

reaches up to a desired voltage level. It initially implies constant current operation, and when the battery reaches to its desired voltage level, the current starts decreasing and there is constant voltage operation. In this operation, initially the RHS of inductor has positive polarity and the switch S1 (IGBT part) is controlled by gating current Ib_1. Then flow of current is from V_{DC}+- S_1-L-Bat-V_{DC}-. When battery get completely charged, then polarity of inductor reverses. Due to this, the diode D2 gets forward biased and inductor discharges (L+ –Bat-D2-L-) through it to make the polarity of inductor same as initial state. The voltage loop is used to control the battery voltage and inhibits the battery from being overcharged. The reference voltage is set to prevent the battery from overcharging. This reference voltage is usually 10% more than the nominal voltage. When the voltage is less than this set voltage, then CC mode starts working and charging of battery is initiated [149].

II. Mode 2 (Discharging): In the discharging or buck mode, Switch S2 (IGBT part) is ON and controlled by Ib_2 and inductor polarity reverses by using that loop. When the inductor polarity reverses and V_{bat} is higher than the $V_{DC+,}$ diode D1 gets forward biased and discharging of battery (V2G) is initiated.

In mode I, the current remains constant, and the voltage rises up to a pre-set value. In mode II, a constant voltage is delivered by the charging circuit, and the current starts decreasing slowly as shown in Fig. 3.7.

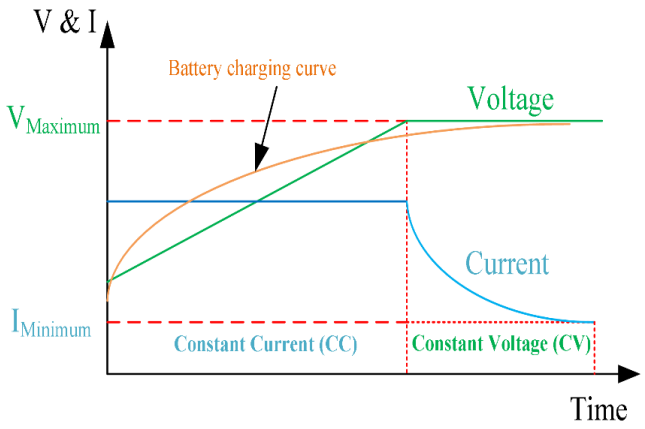

Fig. 3.7 CC-CV operation

In Fig. 3.7, CC-CV has been shown. It shows that current remains constant until battery voltage reaches a pre-set value, afterward current starts decreasing and voltage remain constant.

This bi-directional operation makes the system more efficient. In this work, charging/discharging operation of the EV battery is studied and converter works both in buck-boost mode. The buck-mode is required in the case of Vehicle to Grid (V2G) operation which is explained in next section.

3.3 Vehicle to Grid (V2G) Mode

In previous sections, impact of charging of grid connected EVs was discussed for both the common AC and DC bus architectures. Bidirectional VSC is used in both the architectures.

In this section, few changes have been made to study the Vehicle to Grid (V2G) mode in both the architectures which can be seen in Fig. 3.8 and Fig. 3.9. V2G mode is beneficial for the smart grid in following ways [150] [151]:

- Voltage support
- Power factor regulation
- Reactive power compensation

- Load balancing
- Peak shaving
- Islanding operation during emergency shut-down of grid

In view of these advantages, V2G is a promising technology for EV owners and utility operators. The concept of virtual power plant/virtual synchronous machine and use of EVs as backup source of energy is becoming reality in many parts of the world. It looks like win-win situation for both the EV owners and utility operators. EV owners can earn revenue whenever EVs are standstill (non-commercial EVs remain standstill for more than 95% time) and utility operators can solve problems which are listed above. But, it is still a topic of debate and interest because of following issues:

- Possible impact on the life of Li-ion batteries due to continuous charging-discharging cycles.
- Possible threat to cyber security as EVs will be attached to the smart grids and can used as probable entry point for malware and viruses.
- It needs uniformity in the design of standards and connectors for EV charging station. There are many types and makes of connectors right now which needs collaboration for implementation of V2G technology.
- Link between the energy, communication and EV manufacturing industry is required for effective implementation of V2G technology.
- Impacts on the power quality of grid connected EVs during V2G operation.

In this study, the focus is on harmonic emission assessment during discharging operation too. Both the AC/DC architectures have been used by including a small load in it to study the harmonic problems as shown in Fig. 3.8 and Fig. 3.9.

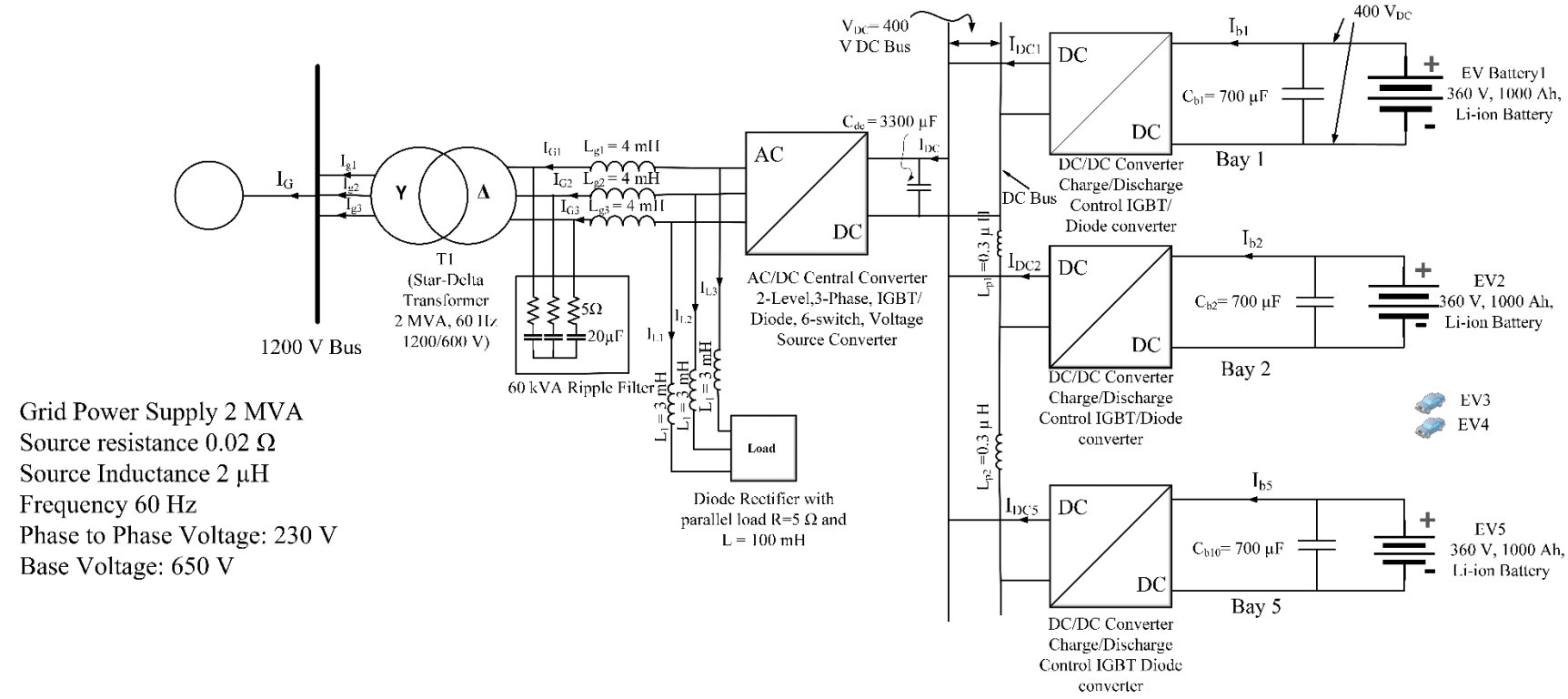

Fig. 3.8 DC Bus Architecture with 5 EVs (with load) for V2G operation

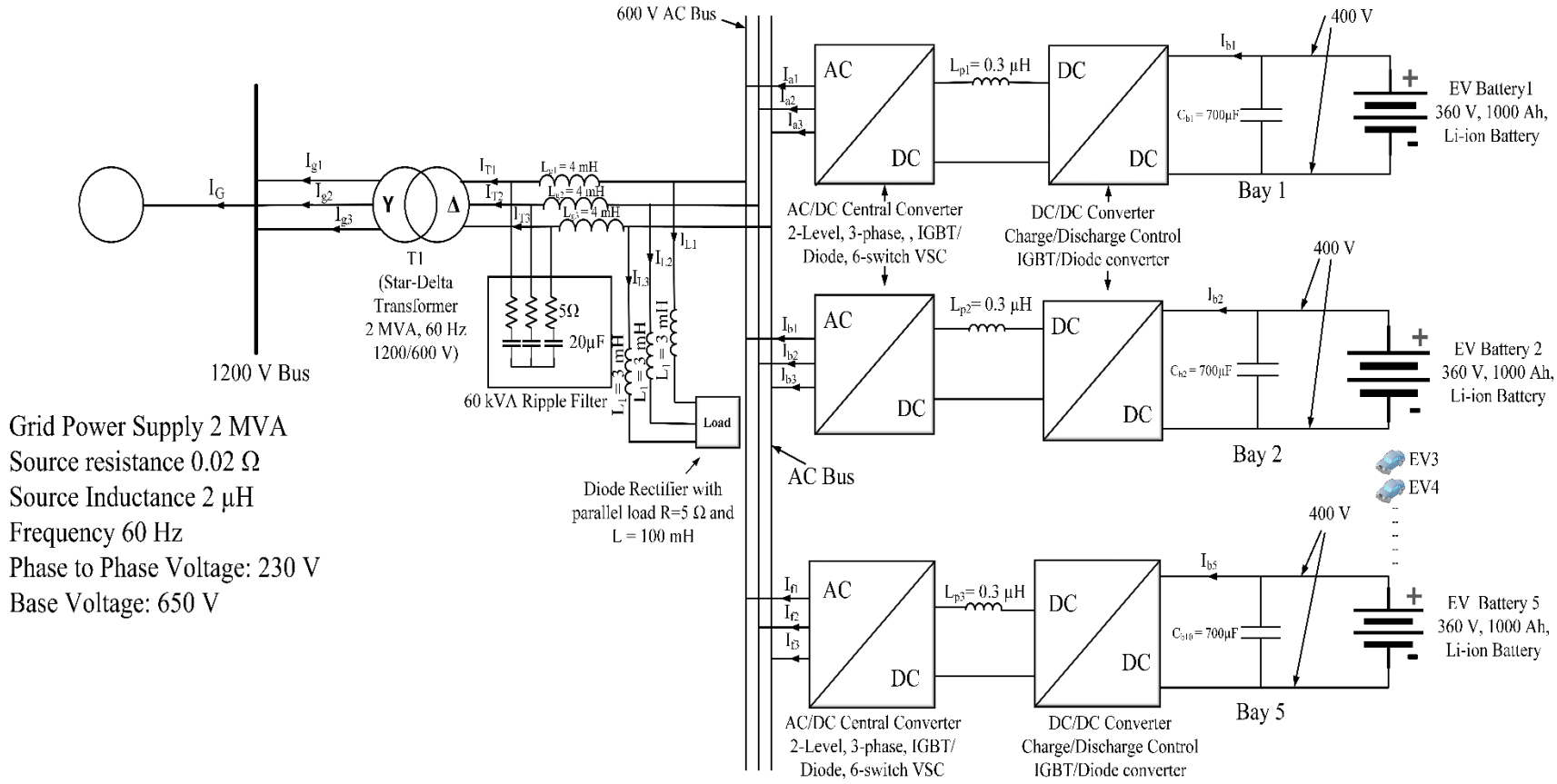

Fig. 3.9 AC Bus Architecture with 5 EVs (with load) for V2G operation

In above-shown figures, V2G operation is explained. Both the systems are based on five EV bays. The AC-DC converter works in inversion mode, and DC-DC converter works in buck mode. A non-linear R-L load is introduced in both the models to do the harmonic assessment while the system is working as V2G.

3.4 Test Cases

Both the AC and DC bus architectures are simulated in MATLAB/Simulink® environment to study the impact on the power quality (particularly harmonic emission assessment) due to the EV charging Infrastructure. A Distribution Transformer (DT) is used as an interface between the grid supply system and non-linear loads (power electronic converters), which are further connected to the EV batteries. DT is an important but expensive equipment for these two architectures and, therefore, different transformer configurations are studied to propose a suitable option. The magnitude of the third harmonic component depends upon the transformer configuration as it is important after the fundamental component [152]. The higher value of the 3rd harmonics produce more distortions in the system, and suitable configuration of DT can minimize it to some extent.

The two AC and DC architectures with 10 bays are shown in Figs. 3.1 and 3.2, respectively. The architecture with the inclusion of PV array into the DCFCS is shown in Fig. 3.3 and architectures in V2G mode shown in Fig. 3.8 and 3.9. The following test cases are studied by using both systems:

(a) Comparison of Fully Loaded common DC and AC bus FCS in Charging Mode (with 10 EVs) by considering following cases:

(i) Comparison of State of Charge (SoC) of EV battery, PCC Voltages, PCC Currents, Reference Voltages.

(ii) Comparative harmonic emission assessment (THD_V and THD_I) analysis (during charging).

(iii) Analysis during a fault on the bus (dynamic-state).

(b) Comparison of UTC and dq-SRF control strategy (in case of DC FCS only).

(c) Impact of varying X/R ratio and MVA_{SC} on the performance of grid-connected DC FCS.

(d) Comparison of grid-connected DC FCS with and without PV-panel.

(e) Comparison of grid-connected DC FCS by using Super-capacitors.

(f) Comparative harmonic emission assessment (THD_V and THD_I) of common DC and AC Bus FCS (V2G Mode).

In these cases, the behavior of FCS during steady-state and dynamic-state is examined. The PCC voltage and current waveforms are studied to evaluate the harmonic emissions. In the common DC bus architecture, the DC bus link voltage is an important factor during charging. UTC strategy is used to maintain the grid-connected operation at nearly UPF in the case of both the architectures for cases (a) to (f). The dq-SRF strategy is employed in case (b) to compare it with the UTC strategy and also there is no requirement of AC to DC converter in case of Islanded-mode of operation (only with PV-panel). The CC-CV method is used to control the charging current at the battery end, and used in EVs as (EV Charge Control) which is explained in chapter-2 and section 3.2.1.4.

CHAPTER 4

RESULTS AND DISCUSSION

4.1 System Results and Comparisons

Both the AC and DC bus architectures are simulated in MATLAB/Simulink ® environment to study the impacts on the power quality (particularly harmonic emissions) due to the EV charging infrastructure. The simulations were run for 10 times (approx.) to verify the computational and process correctness.

Different cases are considered to study the FCS as mentioned in the Test-cases (Section 3.4). Results of different cases are presented next.

4.1.1 Case I-Comparison of Fully Loaded common DC and AC bus FCS

The performance of two architectures, CDCB and CACB (Fig. 3.1 and Fig. 3.2), with full load operation (i.e. 10 EVs being charged) is compared in Grid to Vehicle (G2V) mode. The following result waveforms are presented for comparison purposes:

(a) State of Charge (SoC) percentage (%age) of battery during charging,

(b) DC bus voltage,

(c) PCC Voltages and THD_V (with Uniform battery charge),

(d) PCC Currents and THD_I (with Unifrom battery charge),

(e) THD_V and THD_I (with divesified battery charge), and

(f) Reference Voltages generated by UTC strategy for CDCB and CACB architecture.

(a) State of Charge (SoC) percentage of battery during charging

In Fig. 4.1, SoC of battery graph w.r.t. time is given for both the architectures. SoC is one of the most important parameters for an EV battery. It is defined as the ratio of battery current capacity (Q_t) to nominal capacity (Q_n). Nominal capacity is provided by the battery manufacturer and signifies the maximum amount of charge that can be stored in the battery [93]. SoC for battery is expressed as follows:

$$SoC(t) = \frac{Q_t}{Q_n} \tag{4.1}$$

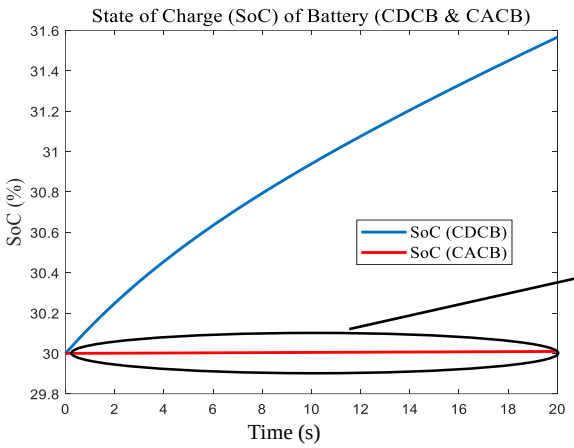

Fig. 4.1 (a) SoC of EV Battery (CDCB & CACB Arch.)

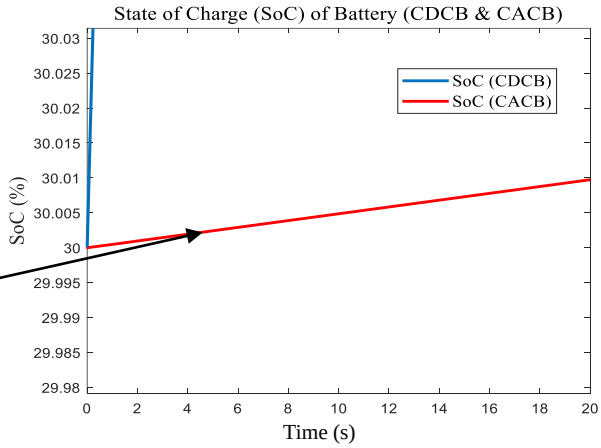

Fig. 4.1 (b) Zoomed view of SoC of EV Battery

In Fig. 4.1 (a), SoC of battery during charging in CDCB and CACB architectures is given. In case of CDCB, battery SoC is at 30% initially and charges up to 31.6% (blue line in Fig. 4.1 (a)) in 20 seconds i.e. the battery charges about 1.6% in 20 seconds. If this constant rate is maintained, the battery will get fully charged from 0% to 100% in approximately 21 minutes. In a FCS, this time can be further improved by increasing the charging current. In most practical cases, battery charging is recommended when its SoC is at a low value of around 30%. The battery should be charged to a high value of about 90% SoC for maximumizing the life of the battery. Thus, it takes approximately 13 minutes to charge the battery from 30% to 90% SoC by using the CDCB Architecture.

Similarly, SoC profile of EV battery during charging with the CACB architecture is shown (red line in Fig. 4.1 (a)) and a zoomed view of it is shown in Fig. 4.1 (b). Battery charges from 30% to approx. 30.01% in 20 seconds i.e. it would take approximately 33 hours to charge the battery from 30% to 90% in CACB architecture. Hence, a higher grid rating is required to increase the charging rate in the case of CACB architecture which is a serious concern.

(b) DC bus voltage

In Fig. 4.2, a comparison of DC bus link voltage for both the architectures is shown. In case of CDCB architecture, a common DC bus link is a convenient way to connect all of the 10 EV batteries to the grid. In this, only one conversion stage is needed to provide a common DC bus for all the connected EVs. It is important to maintain this voltage constant with a control strategy for smooth charging of the batteries. A fluctuating voltage can adversely affect battery life.

In CACB architecture, there is a separate VSC for each EV and therefore, DC bus voltage is measured at the output of the individual VSCs. This voltage is supplied to DC/DC converters for voltage regulation which are further connected with the EV batteries.

In this study, UTC strategy is used for both the architectures. The input-side grid rating and load (10 EVs) is same for both the architectures. The reference DC bus voltage is maintained at 400 V for both the architectures. It can be changed as per the requirements and load of the FCS.

DC bus voltage depends upon the reference voltage and battery voltage. The sensed DC bus voltage is filtered through a low pass filter and then compared with the reference voltage. Afterward, an error signal is generated through a PI regulator which serve as total active power reference component of voltage (V_{pg}). This reference signal plays an important role to generate gate signals for the VSC.

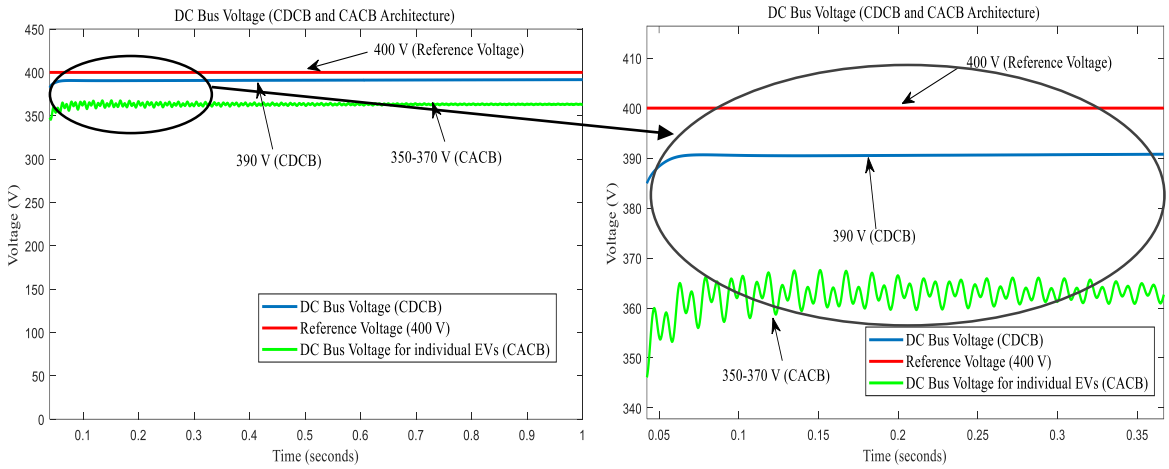

(a) Normal view (b) Zoomed view of initial-state

Fig. 4.2 Common DC Bus Voltage (CDCB)/ Bus Voltage of single EV (CACB) v/s reference voltage

In Fig. 4.2, comparison of DC bus voltages for both the architectures is shown. The result shows that common DC bus voltage is 390 V in case of CDCB architecture and varies between 350-370 V for CACB architecture. In case of CACB, attained DC bus voltage is flucutuating in nature. There is around 20-40 V difference in the achieved bus voltage in case of both the architectures while control strategy is entirely same. This difference and fluctuating voltage in case of CACB results in very slow charging and higher losses. The variations in CACB architecutre can be seen clearly in zoomed view (Fig. 4.2 (b)). The reason for the sluggish response in case of CACB is more number of stages, use of individual VSCs for each EV bay, and a more complex strucutre.

(c) PCC Voltages and THDv

An analysis of the PCC voltages is important to observe the impacts on harmonics of the grid-connected FCS. Fig. 4.3 (a) and Fig. 4.3 (b) shows the PCC voltages (Phase-to-Phase) of the CDCB and CACB architectures with uniform battery voltage, respectively. Both the architectures are with a DT having a star-delta (Y-Δ) configuration. A comparative examination of the PCC voltages for the two architectures shows that the 3-phase voltage harmonics are higher in the case of CACB FCS as compared to CDCB FCS. A closer analysis of the harmonic content in the two

configurations is made with FFT analysis as shown in Figs. 4.4 (a) and 4.4 (b) for CDCB and CACB architectures, respectively.

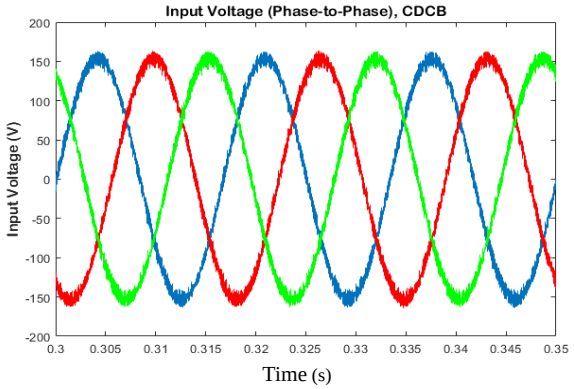

Fig. 4.3 (a) PCC Voltages (Phase-to-Phase) CDCB

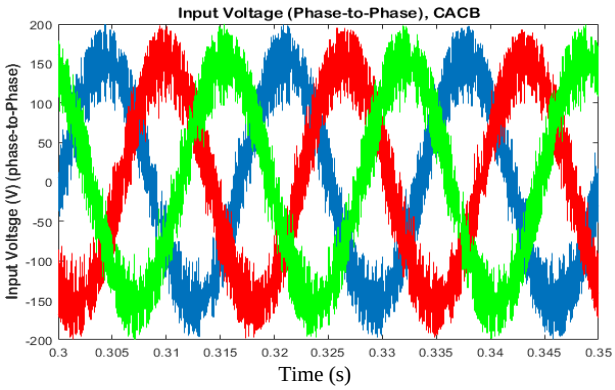

Fig. 4.3 (b) PCC Voltages (Phase-to-Phase) CACB

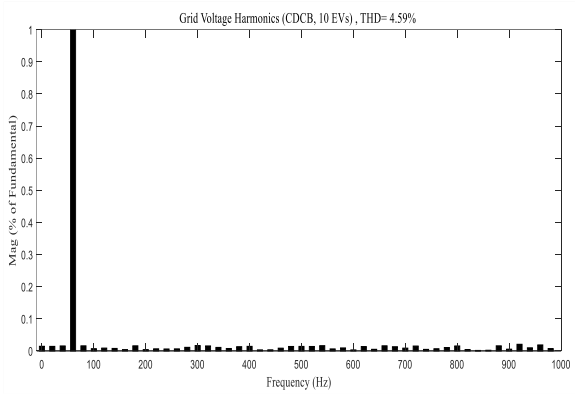

Fig. 4.4 (a)

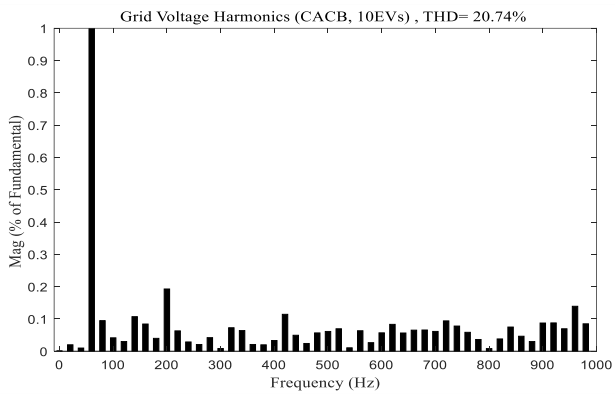

Fig. 4.4 (b)

Fig. 4.4 (a) Grid Voltage Harmonics CDCB (THD_V = 4.59%, DC component= 0.021) and Fig. 4.4 (b) CACB (THD_V = 20.74%, DC component= 0.006)

It is observed from the comparative analysis of both of these waveforms (Fig. 4.3) and FFT analysis (Fig. 4.4) that voltage harmonics are 15 to 16% higher (also depends upon the DT connection configuration) in case of CACB FCS as compared to the CDCB FCS. Fig. 4.4 (a) indicates a THD_V of 4.59% for CDCB architecture, and THD_V of 20.74% for CACB architecture. From this analysis, it is seen that the THD_V is higher than the recommended value in IEEE-519 standard for CACB configuration. This kind of higher value (20.74%) in case of CACB architecture is unacceptable for a grid-connected system and may result in increased losses, lower efficiency and reduced life of the connected equipment.

(d) PCC Currents and THD_I

An analysis of the PCC currents is significant to see the impacts on harmonics of grid-connected FCS. Fig. 4.5 (a) and Fig. 4.5 (b) show the comparative analysis of PCC currents for CDCB and CACB architectures with uniform battery voltage, respectively. A comparative examination of the PCC currents for the two architectures shows that the 3-phase current harmonics are higher in the case of CACB FCS as compared to CDCB FCS. A closer analysis of the harmonic content in the two configurations is made with a FFT analysis shown in Figs. 4.6 (a) and 4.6 (b) for CDCB and CACB architectures, respectively.

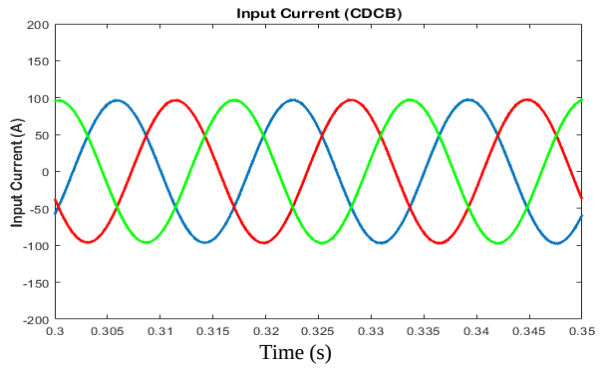

Fig. 4.5 (a) PCC Currents (CDCB)

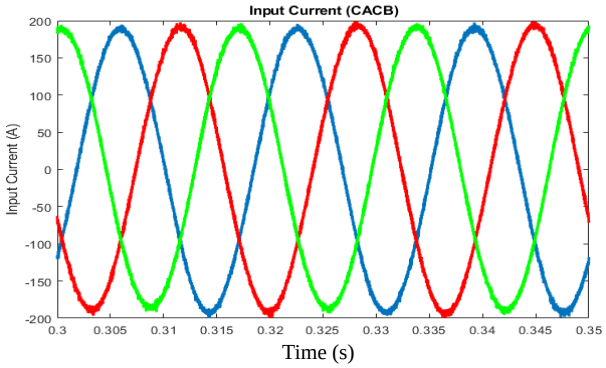

Fig. 4.5 (b) PCC Currents (CACB)

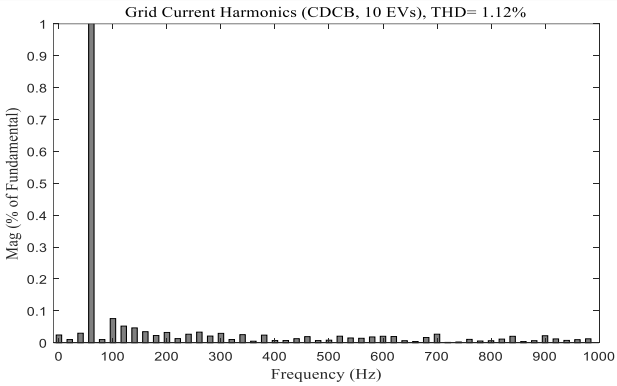

Fig. 4.6 (a)

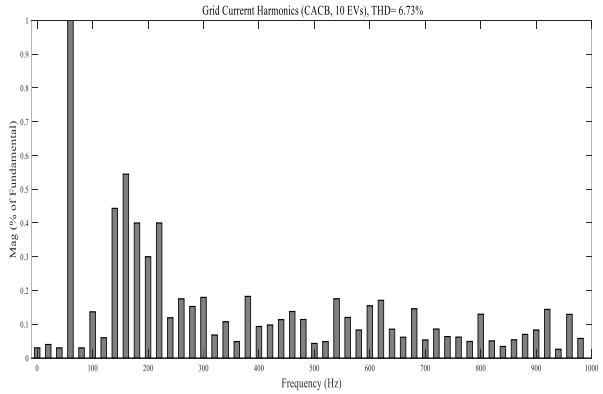

Fig. 4.6 (b)

Fig. 4.6 (a) Grid Current Harmonics CDCB (THD_I = 1.12%, DC component = 0.024) and Fig. 4.6 (b) CACB (THD_I = 6.73%, DC component = 0.062)

It is observed that in CACB architecture (Fig. 5.5 and Fig. 5.6), approximately 40-50% more currents are drawn by 10 EVs and THD_I (6.73%) is higher than the THD_I (1.12%) of CDCB architecture. It has been seen that current harmonics are under the limits for CDCB architecture as

per IEEE-519 standards, but are higher (6.73%) in case of CACB architecture. Higher value of current harmonics may cause problems in protection and grid-synchronizing systems. These harmonics should be minimized to protect the expensive grid equipment.

In the detailed harmonic analysis, 2^{nd}, 3^{rd}, 5^{th} and 7^{th} harmonics are predominant in Total Harmonic Distortions (THD). Therefore, analysis of these harmonics is important for comparison of both the architectures. Table 4.1 shows the comparison of 2^{nd}, 3^{rd}, 5^{th} and 7^{th} harmonics in case of star-delta (Y-Δ) DT configuration for both the architectures.

Table 4.1 Comparison of harmonic order (2^{nd}, 3^{rd},5^{th}, 7^{th}) for CDCB and CACB architecture

2^{nd} , 3^{rd} , 5^{th} and 7^{th} order harmonics (during battery charging), %age ,star-delta (Y-Δ) DT configuration					
Harmonic order → / **Type of Architecture ↓**	**Harmonic Type**	**2^{nd}**	**3^{rd}**	**5^{th}**	**7^{th}**
CDCB Architecture	**Voltage Harmonics**	0.01%	0.01%	0.03%	0.03%
	Current Harmonics	0.05%	0.01%	0.03%	0.02%
CACB Architecture	**Voltage Harmonics**	0.24%	0.29%	0.07%	0.09%
	Current Harmonics	1.23%	1.22%	0.06%	0.03%

It is observed from Table 4.1 that values of 2^{nd}, 3^{rd}, 5^{th} and 7^{th} are higher in case of CACB architecture as compared to CDCB. These values add up and results in overall higher value of THD_V and THD_I in case of CACB.

(e) THD_V and THD_I (with divesified battery charge)

In the real situation, EVs come to FCS with different charging profiles. In following results, both the architectures are compared by varying battery residual charge capacity. The residual charging capacities (in % age) of 10 EV batteries (for both the CACB and CDCB FCS) are assumed as per Table 4.2.

Table 4.2 EV number v/s Residual Charge

EV Number	Residual Charge (% age)
EV1	70%
EV2	50%
EV3	30%
EV4	75%
EV5	60%
EV6	50%
EV7	75%
EV8	45%
EV9	90%
EV10	25%

The simulation is run for both the architectures by setting residual charge value of EV batteries as per Table 4.2. The results of THD_V and THD_I for both the architectures is shown in Fig. 4.7 and Fig. 4.8.

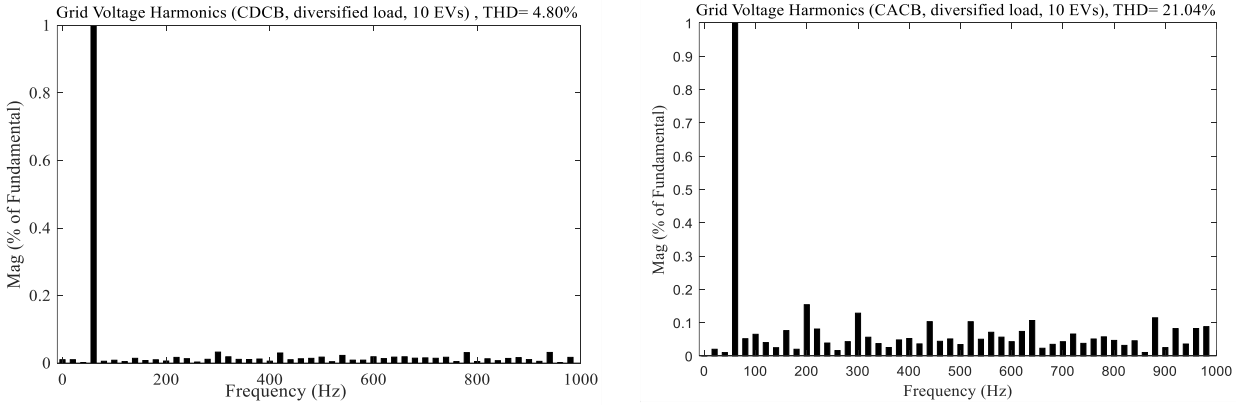

Fig. 4.7 (a) Grid Voltage Harmonics CDCB, (THD_V = 4.80%) and Fig. 4.7 (b) CACB (THD_V = 21.04%), with diversified load

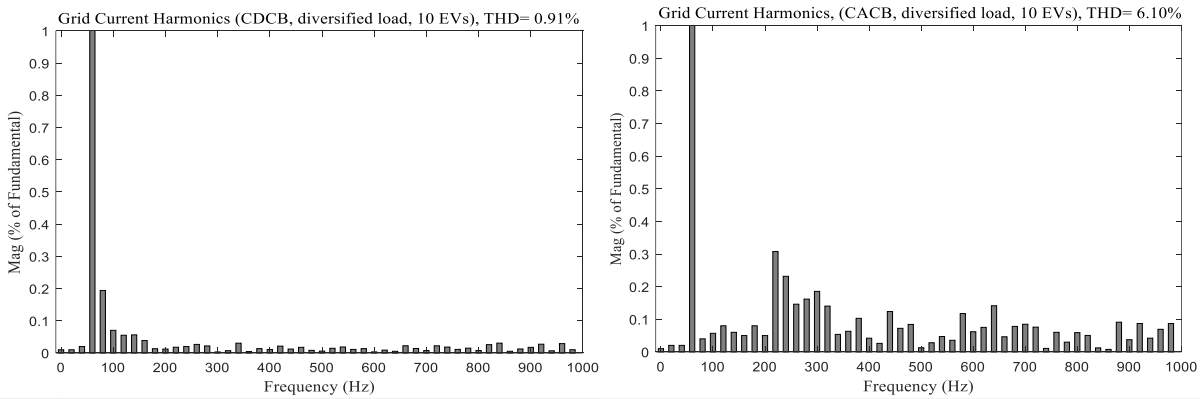

Fig. 4.8 (a) Grid Voltage Harmonics CDCB, diversified load (THD_I = 0.91%) and Fig. 4.7 (b) CACB (THD_I = 6.10%), with diversified load

It is observed from THD_V and THD_I analysis (divesified load, 10 EVs) that there is slight increase (0.20 to 0.30%) in THD_V, and slight decrease in (0.20 to 0.60%) in THD_I due to divesified load. The reason for decrease in THD_I is cancellation of harmonics due to divesified load.

(e) Reference Voltages generated by UTC strategy for CDCB and CACB architecture

Reference voltages are generated for both the architectures by UTC strategy and was explained in detail in chapter-3. These voltages are derived by using following equations in control strategy:

$$V_a = \frac{2}{3} V_{ab} + \frac{1}{3} V_{bc}\ ,\ V_b = -\frac{1}{3} V_{ab} + \frac{1}{3} V_{bc}\ ,\ V_c = -\frac{1}{3} V_{ab} - \frac{2}{3} V_{bc} \quad (4.2)$$

Where V_a, V_b, V_c are phase voltages, V_{ab}, V_{bc} are line voltages.

These reference voltages are further used to generate direct and quadrature unit templates. The comparison of these voltages for CDCB and CACB architecture is made in Fig. 4.9.

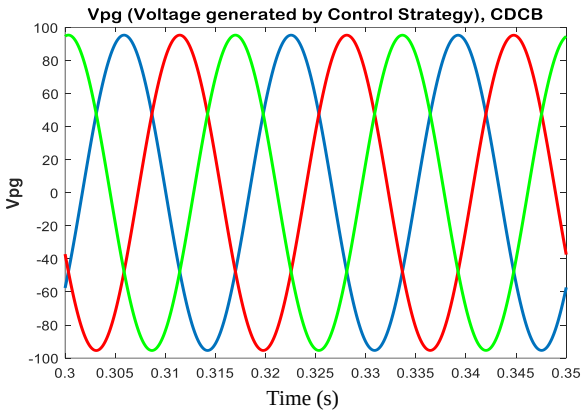

Fig. 4.9 (a)

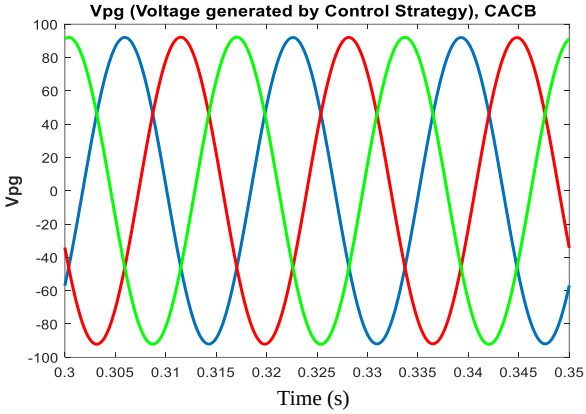

Fig. 4.9 (b)

Fig. 4.9 (a) Voltage generated by Control Strategy (CDCB) Fig. 4.9 (b) Voltage generated by Control Strategy (CACB)

Fig. 4.9 (a) and Fig. 4.9 (b) shows the reference voltage for CDCB and CACB architectures, respectively. Comparison shows that reference voltage waveforms are similar for both the architectures. It reveals that the UTC strategy produces similar reference grid voltages in both the architectures, so there is no indication of any issues resulting from this for either control systems.

4.1.2 Case II-Comparative Power Quality (PQ) analysis by varying Distribution Transformer (DT) configurations

In this section, a comparative harmonic emissions analysis of both the architectures (CDCB and CACB) with different DT configurations (Y-Δ, Δ-Y, Y-Y, and Δ-Δ) is presented. Different DT configurations were used to select the best suitable configuration with the least harmonic components for both the voltage (THD_V) and current (THD_I) profiles, as suggested by IEEE-519 standards.

Comparison of both the architectures (CDCB and CACB) in case of different DT configurations is shown in Table 4.3 and Table 4.4 for THD_V and THD_I, respectively.

In the harmonic spectrum, 3^{rd}, 5^{th}, and 7^{th} order harmonics have a major impact on the THD_V and THD_I. In Table 4.3, these harmonics orders are compared for both the architectures and with two different loading conditions, i.e. fully (i.e. with 10 EVs) and lightly loaded (i.e. with 5 EVs) buses.

Table 4.3 Comparison table for 3rd, 5th and 7th order Harmonics for Different Transformer Configurations (fully loaded buses and lightly loaded buses)

3rd, 5th and 7th order harmonics during Battery Charging (G2V)								
Fully/Lightly Loaded Arch. →			**Fully Loaded Bus (10 EVs)**			**Lightly Loaded Bus (5 EVs)**		
Architecture	**Transformer Connection Configuration**	**Harmonics Type**	**3rd Order**	**5th Order**	**7th Order**	**3rd Order**	**5th Order**	**7th Order**
Unipolar Common DC Bus (CDCB) Charging	Star-Delta	Voltage	0.01%	0.03%	0.03%	0.00%	0.01%	0.01%
		Current	0.01%	0.03%	0.02%	0.06%	0.04%	0.02%
	Delta-Delta	Voltage	0.01%	0.03%	0.01%	0.01%	0.00%	0.00%
		Current	0.01%	0.01%	0.04%	0.04%	0.02%	0.03%
	Star-Star	Voltage	0.01%	0.03%	0.01%	0.01%	0.01%	0.00%
		Current	0.01%	0.01%	0.04%	0.04%	0.02%	0.03%
	Delta-Star	Voltage	0.01%	0.03%	0.01%	0.00%	0.02%	0.01%
		Current	0.02%	0.02%	0.04%	0.02%	0.06%	0.05%
Unipolar Common AC Bus (CACB) Charging	Star-Delta	Voltage	0.29%	0.07%	0.09%	0.80%	0.04%	0.02%
		Current	1.22%	0.06%	0.03%	0.10%	0.01%	0.01%
	Delta-Delta	Voltage	0.34%	0.02%	0.05%	0.77%	0.03%	0.02%
		Current	1.44%	0.10%	0.02%	3.61%	0.06%	0.06%
	Star-Star	Voltage	0.34%	0.02%	0.05%	0.77%	0.03%	0.02%
		Current	1.44%	0.10%	0.02%	3.61%	0.06%	0.06%
	Delta-Star	Voltage	0.23%	0.07%	0.05%	0.73%	0.09%	0.04%
		Current	1.34%	0.08%	0.02%	3.55%	0.11%	0.05%

In Table 4.4, readings of THD_V, THD_I, and DC offset component are compiled for both fully loaded (10 EVs) and lightly loaded (5 EVs) conditions with different transformer configurations.

Table 4.4 Comparison table of THD for different Transformer Configurations (Fully Loaded Buses and Lightly Loaded Buses)

Harmonics during Battery Charging (G2V)						
			Fully Loaded Bus (10 EVs)		**Lightly Loaded Bus (5 EVs)**	
Architecture	**Transformer Connection Configuration**	**Harmonics Type**	**Percentage Harmonics (THD)**	**Off-set component**	**Percentage Harmonics (THD)**	**Off-set component**
Unipolar Common DC Bus (CDCB) Charging	Star-Delta	Voltage	4.59	0.005	2.50	0.010
		Current	1.12	0.032	0.83	0.030
	Delta-Delta	Voltage	4.89	0.008	2.49	0.008
		Current	1.13	0.039	0.83	0.034
	Star-Star	Voltage	4.93	0.008	2.48	0.007
		Current	1.13	0.039	0.83	0.034
	Delta-Star	Voltage	4.88	0.007	2.49	0.006
		Current	1.12	0.030	0.82	0.055
Unipolar Common AC Bus (CACB) Charging	Star-Delta	Voltage	20.74	0.006	11.66	0.063
		Current	6.73	0.062	4.66	0.696
	Delta-Delta	Voltage	20.64	0.127	11.62	0.032
		Current	6.87	0.259	4.81	0.575
	Star-Star	Voltage	20.64	0.127	11.62	0.032
		Current	6.87	0.259	4.81	0.575
	Delta-Star	Voltage	21.07	0.120	11.76	0.071
		Current	6.85	1.045	4.83	0.320

It is evident from Table 4.3 and Table 4.4 that the CDCB architecture gives better results in case of harmonic emissions (voltage and current) than the CACB architecture. Star-delta (Y-Δ)

configuration of DT is with fewer harmonics and minimal value of DC offset for both the CACB and CDCB configurations. As per FFT analysis, the current harmonic percentage is very high in common AC bus charging infrastructure as compared to common DC bus architecture. In terms of load, there is a considerable impact in the case of CACB architecture. Substantial increase in voltage harmonics in case of a common AC bus structure has been observed, and it is unacceptable as per IEEE-519 standards. Large and expensive filters would be needed as a possible solution to mitigate these harmonics. The large amounts of harmonics make the Common AC bus charging stations a more expensive solution for the FCS.

4.1.3 Case III-Analysis during a 3-phase fault on the bus

Dynamic-analysis is important to analyze the impacts of fault conditions in the grid-connected FCS. EV integration in to the electric-grid is not an usual occurrence for most utilities. Therefore, a fault is created in the simulation, and transient behavior is recorded for both the architectures.

The dynamic-state of both the architectures (CDCB and CACB) in fully-loaded state (i.e. 10 EVs) is studied and compared. A 3-phase fault state for 3-cycles duration (0.083 s to 0.133 s) for both the architectures (CDCB & CACB) is studied. The following results are presented:

(a) PCC Voltages,

(b) PCC Currents,

(c) Reference voltage generated during both the architectures (CDCB and CACB).

(a) PCC Voltages

An analysis of PCC voltages during and after dynamic-state is important to observe the impacts on the harmonics of the grid-connected FCS.

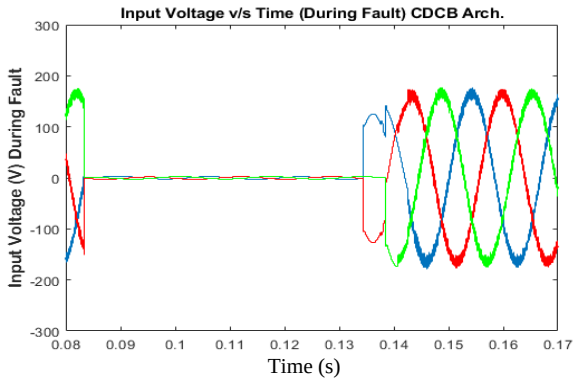

Fig. 4.10 (a) PCC Voltages (CDCB) during Fault

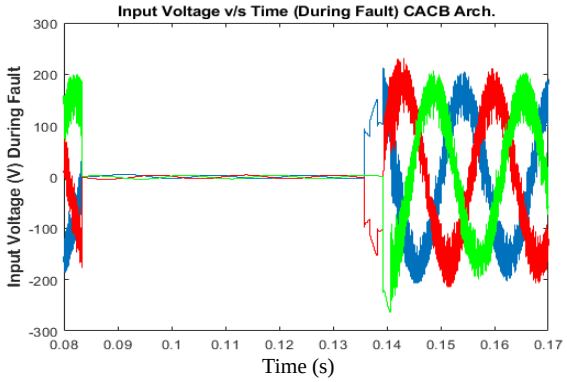

Fig. 4.10 (b) PCC Voltages (CACB) during Fault

It is observed from comparative analysis that PCC voltages get stable slightly faster (at 0.14 s) in CDCB architecture (Fig. 4.10 (a)) as compared to CACB architecture (at 0.145 s).

(b) PCC Currents

As excessive higher currents in fault condition may damage the expensive equipment like DT, this analysis is also important to select the short-circuit rating of protective equipment for the grid-connected FCS.

Fig. 4.11 (a) and Fig. 4.11 (b) shows the comparison of PCC currents during dynamic-state analysis.

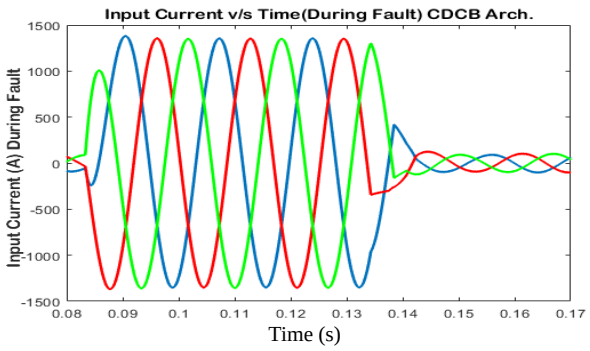

Fig. 4.11 (a) PCC Currents (CDCB) during Fault

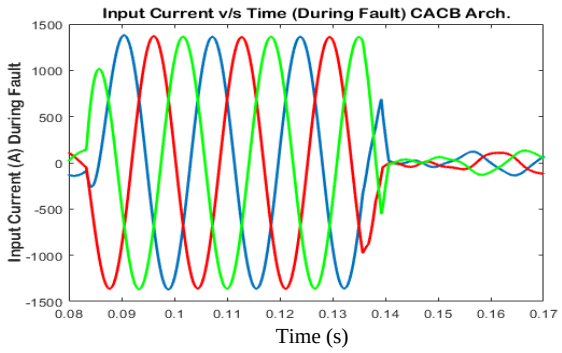

Fig. 4.11 (b) PCC Currents (CACB) during Fault

In Fig. 4.11, comparison of PCC currents during dynamic-state is made. It has been observed that PCC currents get stable faster in case of CDCB architecture (at 0.14 s) than the CACB architecture (at 0.16 s) after the fault has been cleared.

(c) Reference voltage generated during both the architectures (CDCB and CACB)

In the Fig. 4.12, reference voltage generated by UTC strategy in case of both the architectures is shown.

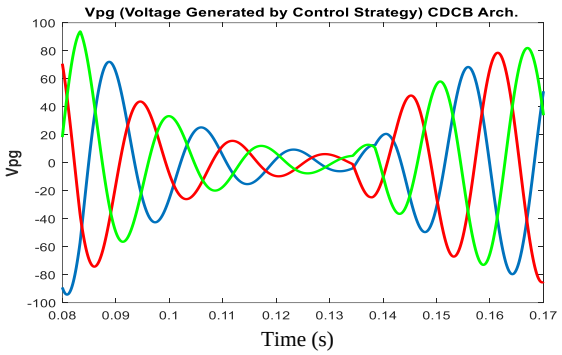

Fig. 4.12 (a) V_{pg} (CDCB) during Fault

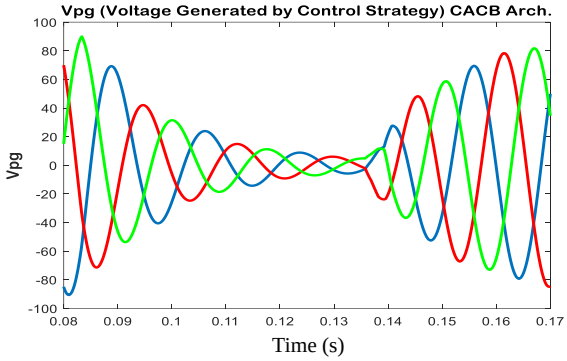

Fig. 4.12 (b) V_{pg} (CACB) during Fault

It is observed from these results that reference voltage (V_{pg}) generated by UTC strategy is similar in both the architectures during the dynamic-state too. The impact of 3-phase fault is visible in reference voltage waveforms and is for the same duration as in PCC voltages and PCC currents.

It is clear from fault-analysis that excessive currents are damaging for connected equipment if fault condition persists for a longer duration. Proper protective devices are needed to safeguard the expensive infrastructure. Circuit breakers should be employed at key locations to protect the costly structure associated with the FCS.

4.1.4 Case IV-Comparison of UTC and dq-SRF control strategy (CDCB Arch.)

The dq-SRF (Synchronous Reference Frame) is a popular control method for power electronic converters due to its simple implementation. Unit Template Control (UTC) strategy is proposed in this dissertation for the FCS. The details of both the control strategies is given in Chapter-2.

In case IV, both of these control strategies are employed to the CDCB architecture of FCS with different DT configurations in the MATLAB/Simulink® environment. The analysis is done for (a) Steady-state and, (b) Dynamic-state. The following result waveforms are studied and compared for both the control strategies:

(a) SoC of EV battery,

(b) PCC Voltages,

(c) PCC Currents,

(d) Closed-loop stability analysis,

(e) Dynamic-state analysis.

The following results are presented.

(a) SoC of EV battery

Faster charging rate is key requirement for the FCS and State of Charge (SoC) is very important parameter to measure this rate. Control strategy for VSC plays a vital role in accelerating the SoC. Therefore, SoC of EV battery is measured and compared for dq-SRF control and UTC strategies.

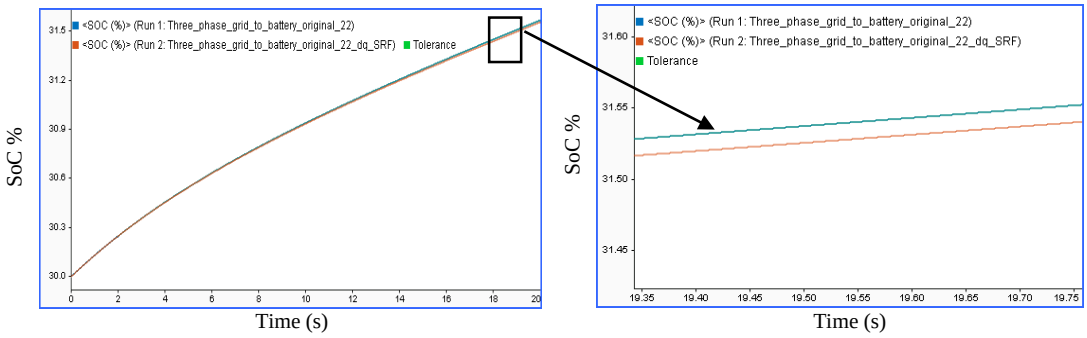

Fig. 4.13 (a) Fig. 4.13 (b)

Fig.4.13 Comparison of SoC of dq-SRF Control Strategy and UTC Strategy (Blue line)

In Fig. 4.13 (a), State of Charge (SoC) of EV battery is compared by using both the control strategies. The zoomed Fig. 5.13 (b) shows that battery charges faster in case of UTC than the dq-SRF control strategy. The difference between the charging speed and performance between two methods is because dq-SRF strategy requires extraction of Sinθ and Cosθ (synchronizing components) by using standard PLL method. The execution of this process takes more time which ultimately delays the generation of reference currents. While UTC strategy is having simple

process which takes less execution time. The faster generation of reference currents makes the fast switching which results into an efficient control system.

(b) PCC Voltages

A comparison of PCC voltages by using dq-SRF control and UTC strategy is done in Fig. 4.14. This comparison is important to propose more efficient control strategy from both of these.

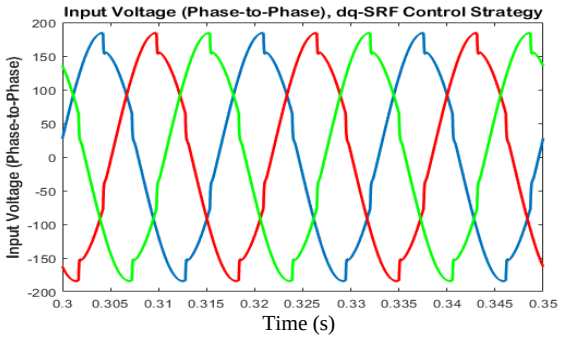

Fig. 4.14 (a)

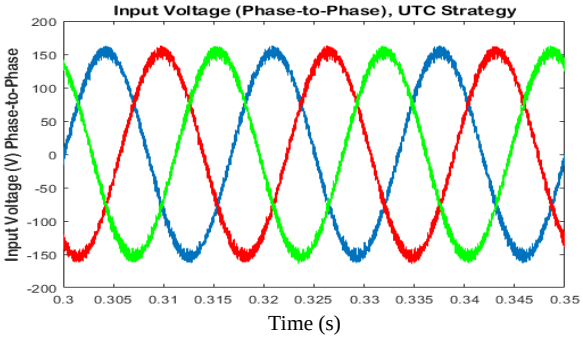

Fig. 4.14 (b)

Fig. 4.14 Comparison of PCC Voltages with (a) dq-SRF control strategy (b) UTC strategy

Results shows that voltage waveforms during UTC strategy are more balanced and sinusoidal as compared to the dq-SRF strategy. There are notches in the case of dq-SRF voltage waveforms which results in more losses, unbalance and harmonics in the system. The harmonic spectra for both the control strategies by using star-delta (Y-Δ) DT configuration is shown in Fig. 4.15.

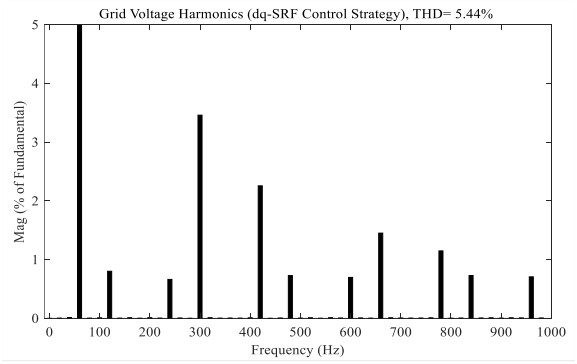

Fig. 4.15 (a)

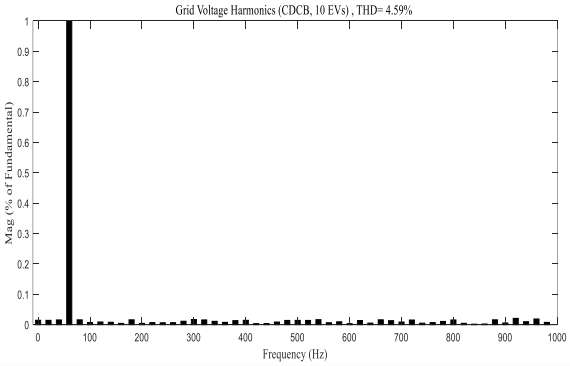

Fig. 4.15 (b)

Fig. 4.15 Comparison of THD_V (Voltage Harmonics) for control strategies (a) dq-SRF control strategy, THD_V = 5.44% and (b) UTC, THD_V = 4.59% with Fully-Loaded (10 EVs) common DC Bus in Star-Delta (Y-Δ) DT Configuration

The FFT analysis in Fig. 4.15 shows that THD_V is higher (5.44%) in case of dq-SRF strategy as compared to the UTC strategy (4.59%). The harmonics are 0.7% higher in case of the dq-SRF control strategy. These higher THD_V in case of the dq-SRF control strategy increase the losses and results in less-efficient system. The reason of higher harmonics is more execution time in dq-SRF control strategy due to standard PLL and three PI controllers in comparison to only one PI controller required in the UTC strategy. Due to it, there is lag in the voltage and current waveforms in the dq-SRF control strategy. These drawbacks in the dq-SRF control strategy affect the wave-shape for both voltage and current which increases the total harmonics in the system.

(c) PCC Currents

The comparison of PCC currents is important to visualize impact of different control strategies on the current waveforms. The results of PCC currents in case of both the strategies (dq-SRF and UTC) is shown in Fig. 4.16 and harmonic spectra by using star-delta (Y-Δ) DT configuration is shown in Fig. 4.17.

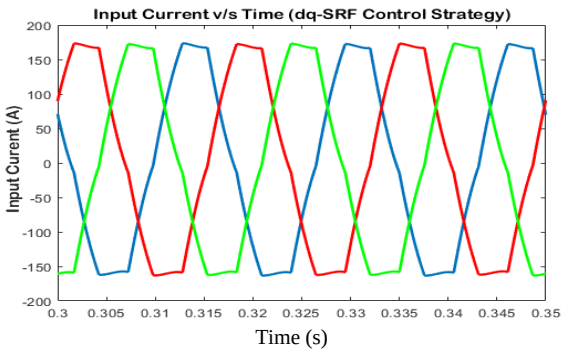

Fig. 4.16 (a)

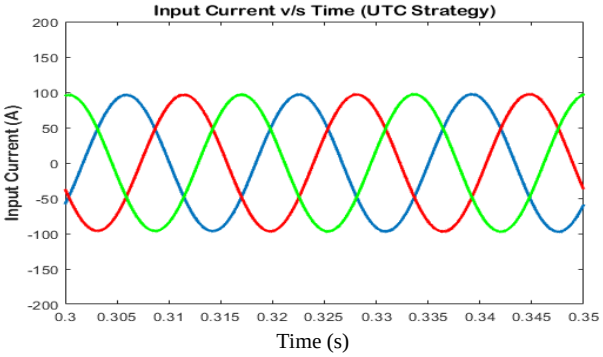

Fig. 4.16 (b)

Fig. 4.16 Comparison of PCC Currents (a) dq-SRF control strategy with (b) UTC strategy

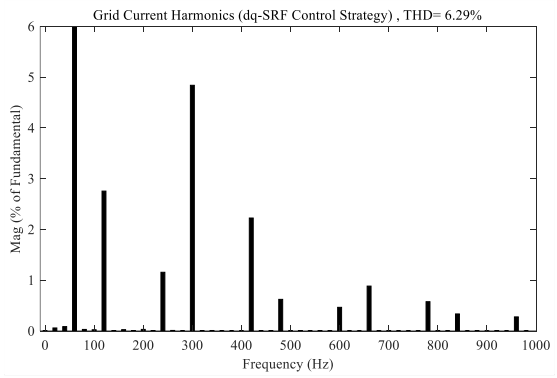

Fig. 4.17 (a)

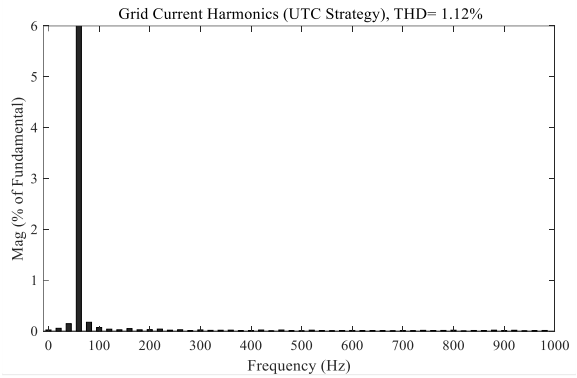

Fig. 4.17 (b)

Fig. 4.17 Comparison of THD_I (Current Harmonics) for control strategies (a) dq-SRF control strategy, THD_I = 6.29% and (b) UTC strategy, THD_I =1.12% with Fully-Loaded (10 EVs) CDCB in Star-Delta (Y-Δ) DT Configuration

In Fig. 4.16, PCC current waveforms in case of both the strategies are compared. It is observed that current waveforms using UTC strategy are more stable and balanced as compared to the dq-SRF control strategy. It shows that charging is faster in case of UTC strategy, but magnitude of current is quite higher in case of dq-SRF control strategy as compared to UTC strategy. It shows that UTC strategy is more efficient and having fewer losses than the dq-SRF strategy.

In the case of harmonic analysis (Fig. 4.17), current harmonics (THD_I) are higher (6.29%) in the dq-SRF control strategy, which is unacceptable as per IEEE-519 standards. An interesting result observed in the dq-SRF control strategy case is that even-order harmonics (2^{nd}, 4^{th} etc.) are leading, which outcomes in unbalance in the resultant waveforms.

In Table 4.5, THD_V and THD_I for both the control strategies are compared by considering different DT configurations.

Table 4.5 Comparison table for different DT Configurations (Fully-Loaded and Lightly-Loaded Buses)

Harmonics during Battery Charging (G2V), Fully Loaded Bus (10 EVs)

Control Strategies Used →			**dq-SRF Control Strategy**		**UTC Strategy**	
Type	**Transformer Connection Configuration**	**Harmonics Type (THD)**	**Percentage Harmonics (THD)**	**Off-set component**	**Percentage Harmonics (THD)**	**Off-set component**
Unipolar Common DC Bus Charging	*Star-Delta*	Voltage	5.44	Nil	4.74	0.02
		Current	6.29	Nil	1.12	0.02
	Delta-Delta	Voltage	5.44	0.01	4.89	0.01
		Current	6.20	0.07	1.13	0.03
	Star-Star	Voltage	5.44	0.07	4.89	0.08
		Current	6.20	0.07	1.13	0.03
	Delta-Star	Voltage	5.44	0.01	4.88	0.01
		Current	6.21	0.09	1.12	0.03

It has been observed that THD_I is unacceptable in the case of dq-SRF as per IEEE-519, and there is more unbalance in the waveforms due to even order harmonics (2^{nd}, 4^{th} order), as even order harmonics cancel out and THD_V magnitude is lesser.

(d) Closed-loop stability analysis

The stability of the system is an important parameter to observe the performance of both the control strategies. The stability of the closed-loop system depends upon feedback-loop and noise in the system. Excessive noise or disturbance results in increase in the bandwidth, reduces the gain and ultimately comes as poor or unstable system. Therefore, closed-loop stability analysis is required for both the strategies.

In Fig. 4.18, closed-loop stability analysis using Bode-plots for both the control strategies (dq-SRF control and UTC strategy) is presented.

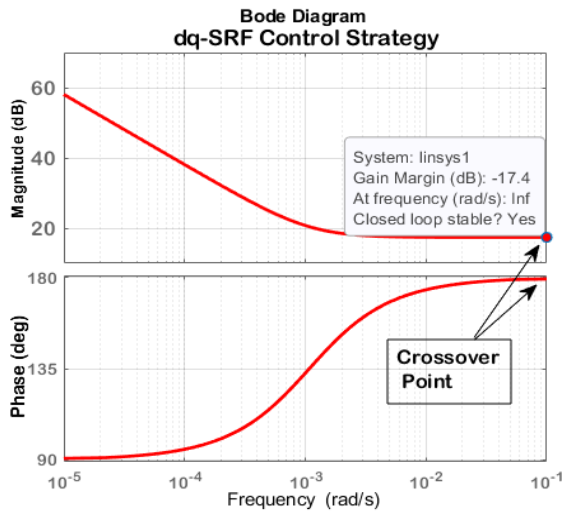

Fig. 4.18 (a)

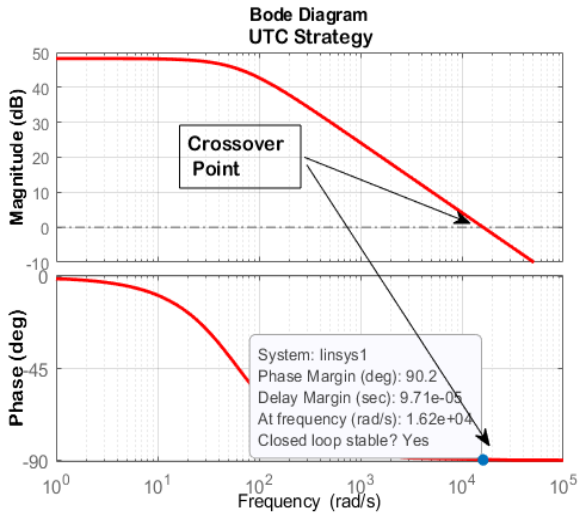

Fig. 4.18 (b)

Fig. 4.18 Comparison of Stability (a) dq-SRF control strategy with (b) UTC strategy

It can be seen from Bode-plots (Fig. 4.18) that both the control strategies are stable. The phase margin is 90.2 degrees at gain crossover-frequency in UTC strategy while gain margin is 17.4 dB during phase crossover-frequency in dq-SRF control strategy. Comparative analysis of both the values shows that UTC strategy is more stable and gives faster response in closed-loop stability analysis.

(e) Dynamic-state analysis

In the Figs. 4.19 and 4.20, results of the star-delta (Y-Δ) configuration of DT during the dynamic-state caused by three-phase (short-circuit) fault are shown. The fault state is created for a small duration of 3-cycles (0.083 s to 0.133 s), and stability of the system for both the control strategies is compared.

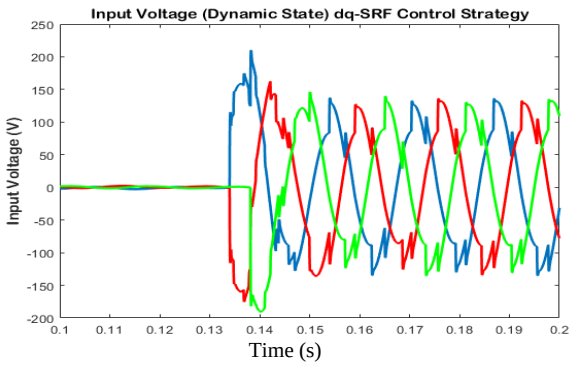

Fig. 4.19 (a)

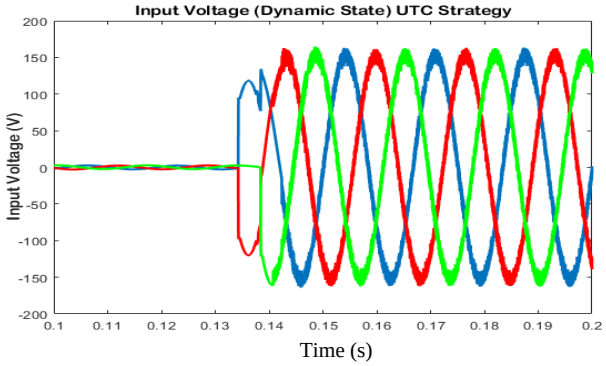

Fig. 4.19 (b)

Fig. 4.19 Comparison of PCC Voltages (Dynamic-State) with (a) dq-SRF control strategy (b) UTC strategy

In Fig. 4.19, PCC voltage waveforms for both the control strategies during the fault-state are compared. It is observed that PCC voltages of UTC gets stable in 0.015 secs. as compared to more than 0.04 secs. in dq-SRF control strategy. There are more distortions (notches and swells) in case of dq-SRF based system.

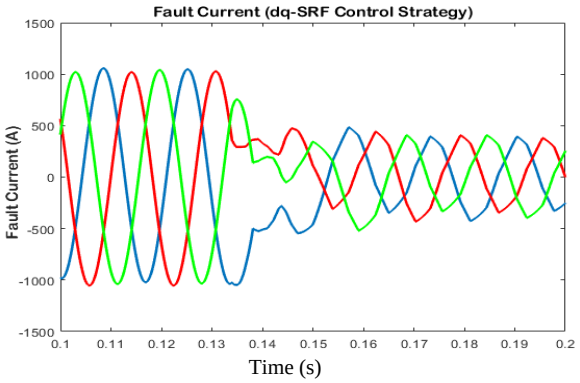

Fig. 4.20 (a)

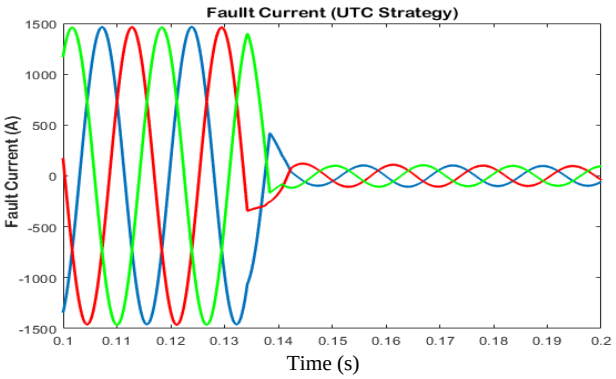

Fig. 4.20 (b)

Fig. 4.20 Comparison of PCC Currents (Dynamic-State) with (a) dq-SRF control strategy (b) UTC strategy

In Fig. 4.20, PCC Currents in case of both the strategies during the dynamic-state is compared. It can be seen that the waveforms of UTC gets stable in 0.01 secs. as compared to 0.035 secs. in the case of the dq-SRF control method. From these results, it is clear that the UTC strategy is more stable than the dq-SRF control strategy and response is faster.

4.1.5 Case V-Impact of varying X/R ratio and MVA_{SC}

In this section, the impact of the strength of the AC grid on the behavior of the FCS system is considered. The strength of AC grid is modified by varying its MVA_{SC} rating and X/R ratio. X/R ratio is significant for deriving the peak asymmetrical fault current for selection of the protective gear and to determine the damping in the system to transients. In the distribution system, the value of circuit resistance is higher as compared to a transmission system. For a typical distribution system, the value of X/R ratio varies between 0.2 to 10. Since the FCS presents a novel load to the distribution grid, so, this analysis is important to look at protection aspects of the FCS. The details of X/R ratio are given in Chapter-2. Different scenarios considered for this investigation are as follows:

Scenario I- Steady-state Analysis: This investigation is done by considering the following ratings in grid-connected CDCB FCS connected with full load (10 EV bays) for weak and strong AC grid:

(a) Weak-grid (2 MVA_{SC})

- X/R = 0.2, Phase to phase Voltage = 230 V, Base Voltage = 650 V, 1200/600 V Xer, Y/D
- X/R = 10, Phase to phase Voltage = 230 V, Base Voltage = 650 V, 1200/600 V Xer, Y/D

(b) Strong-grid (8 MVA_{SC})

- X/R = 0.2, Phase to phase Voltage = 230 V, Base Voltage = 650 V, 1200/600 V Xer, Y/D
- X/R = 10, Phase to phase Voltage = 230 V, Base Voltage = 650 V, 1200/600 V Xer, Y/D

In this investigation, following signals are captured for analysis:

1. SoC,

2. PCC voltages and THD_V,

3. PCC currents and THD_I.

(a) Comparison by assuming rating of 2 MVA_{SC} (weak-grid), X/R = 0.2 and 10

(i) Comparison of State of Charge (SoC)

SoC is very important parameter to measure the speed of EV charging. In Fig. 4.21, SoC of grid-connected DC FCS with a weak-grid (2 MVA_{SC}), and with X/R = 0.2 and X/R =10 is compared.

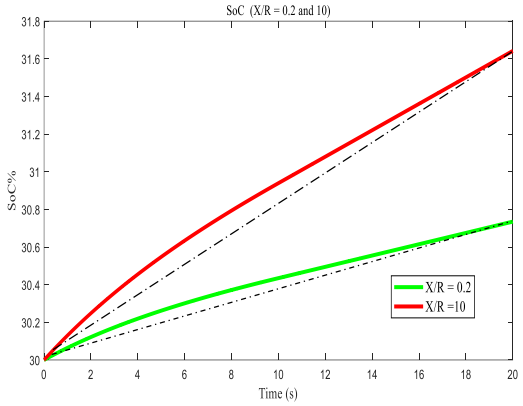

Fig. 4.21 Comparison of SoC for 2 MVA_{SC} grid-rating with X/R =0.2 and X/R = 10

The waveform shows that battery is initially at 30% and charges up to approx. 31.6% (red line in Fig. 4.21) in case of X/R = 10 while it reaches up to approx. 30.7% (green line in Fig. 4.21) in case of X/R = 0.2 in 20 seconds. The growth in both the curves is exponential and not straight line as shown by dotted lines in the Fig. 4.21. If this approximate constant rate is maintained, the battery will get charged from 30% to 90% in about 12 minutes for X/R = 10 and takes about 26 minutes for X/R = 0.2. Representative simulation is done by taking 20 seconds time-window due to the

computational limitations and time of simulation. Otherwise, a full simulation will take quite a long time and also there is memory limitation of computer used for this work.

Results shows that there is visible impact of X/R ratio on charging speed in case of weak-grid. The lower value of X/R ratio (0.2) makes the EV battery charging speed slow.

(ii) PCC Voltages and voltage harmonics (THDv)

A comparative analysis of PCC voltages by using X/R = 0.2 and 10 is presented in Fig. 5.24. The comparison is to show the impact of low and high X/R ratio on the PCC voltages in case of weak-grid (2 MVA_{SC}).

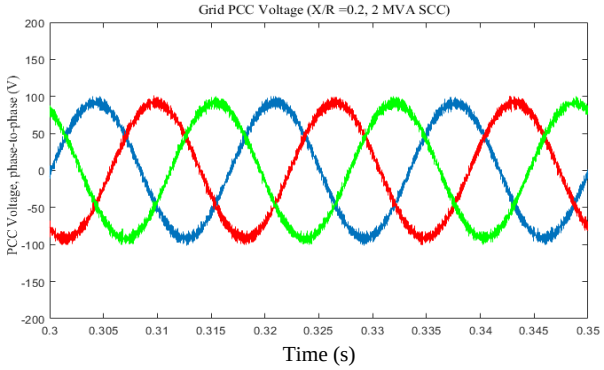

Fig. 4.22 (a)

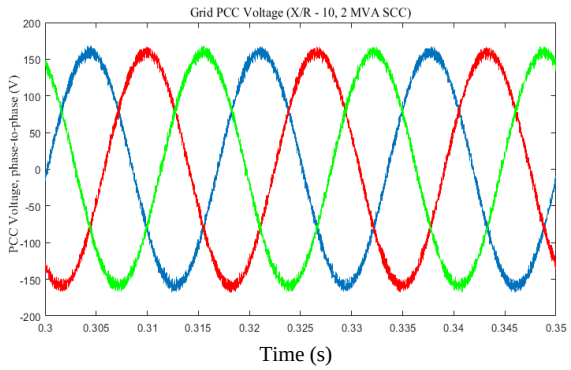

Fig. 4.22 (b)

Fig. 4.22 Comparison of PCC Voltages (Phase-to-Phase) for 2 MVA_{SC} grid-rating (a) X/R = 0.2 and (b) X/R = 10

The comparison shows that the magnitude of PCC voltages is higher in case of X/R = 10 as compared to X/R = 0.2. PCC voltages are about 60 V higher in case of X/R = 10.

There are more harmonics in case of lower X/R ratio. Harmonic content of the PCC voltages is shown in Fig. 4.23.

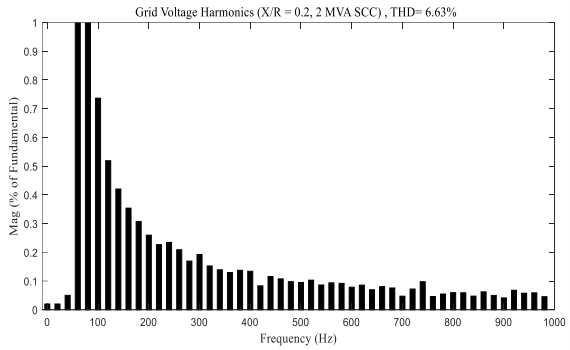

Fig. 4.23 (a)

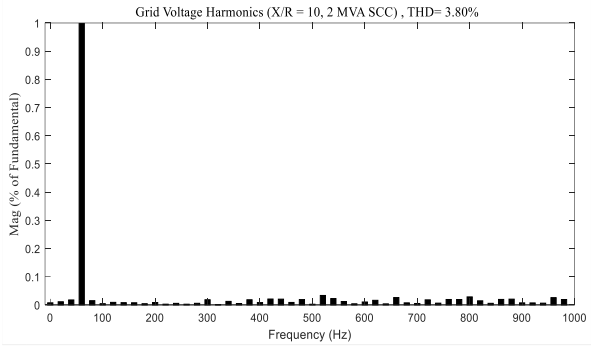

Fig. 4.23 (b)

Fig. 4.23 Comparison of THD_V (a) THD_V = 6.63% with X/R = 0.2 (b) THD_V = 3.80% with X/R =10

It is observed from the comparisons in Fig. 4.22 and Fig. 4.23 that magnitude of PCC voltages is higher in case of X/R =10, but THD_V is lower. The THD_V is 2.83% higher in case of X/R = 0.2 than the X/R =10 with a 2 MVA_{SC} weak-grid. Also, the range of characteristic and non-characteristic harmonics present is much higher with X/R = 0.2 as very little damping is present. The magnitude of harmonics rises due to low damping and results in increase in voltage non-symmetry.

(iii) PCC Currents and current harmonics (THD_I)

The comparison of PCC currents is shown in Fig. 4.24 for X/R = 0.2 and 10.

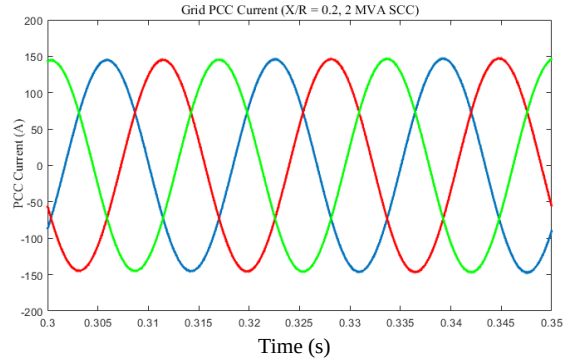

Fig. 4.24 (a)

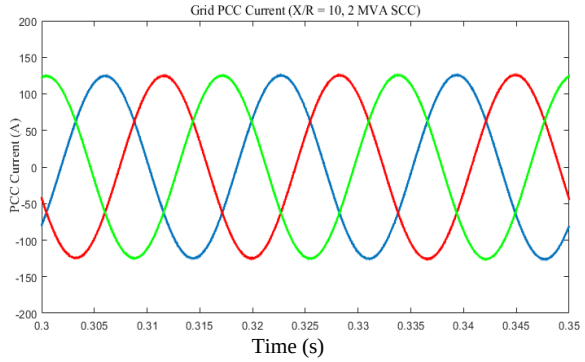

Fig. 4.24 (b)

Fig. 4.24 Comparison of PCC Currents for 2 MVA_{SC} grid-rating (a) X/R = 0.2 and (b) X/R = 10

This comparison of PCC currents shows that there is higher magnitude of current in case of X/R = 0.2. It is observed that PCC current magnitude is approx. 25 A higher in case of X/R = 0.2, but,

the charging speed is lower (Fig. 4.21). It means these higher currents adds up in more losses in the system. Grid current harmonics (THD_I) are shown next.

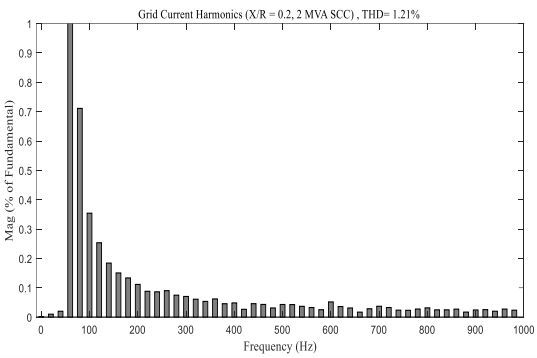

Fig. 4.25 (a)

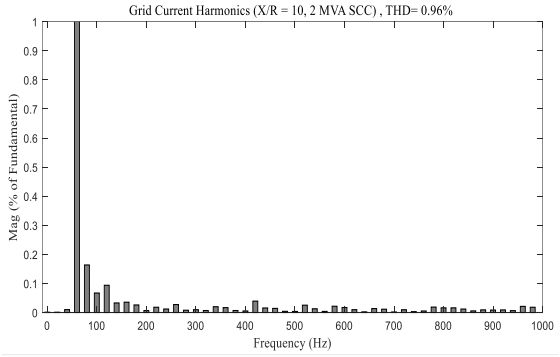

Fig. 4.25 (b)

Fig. 4.25 Comparison of THD_I (a), THD_I = 1.21% with X/R =0.2 and (b) THD_I = 0.96% with X/R = 10

Fig. 4.25 shows that there are higher current harmonics (THD_I) in case of X/R = 0.2. The magnitude of current harmonics is 0.25% higher in case of X/R =0.2 as compared to X/R = 10. It results in more time in charging and increase in losses.

It is observed from the above-shown results that higher X/R ratio makes the system more efficient even in case of weak-grid (2 MVA_{SC}). Also, the range of characteristic and non-characteristic harmonics present is much higher with X/R = 0.2 as very little damping is present. There is more impact of non-linear load on the harmonics in case of low X/R ratio.

(b) Comparison by assuming rating of 8 MVA_{SC}, X/R = 0.2 and, X/R = 10

In this case, results are taken by assuming grid-rating as 8 MVA_{SC} (strong-grid) and varying the X/R ratio from 0.2 to 10 (same as previous case of weak-grid). The results for PCC voltages, PCC currents, THD_V and THD_I are presented next.

(i) PCC voltages and voltage harmonics (THD_V)

The PCC voltages and associated THD_V is shown in Fig. 4.26 and Fig. 4.27, respectively.

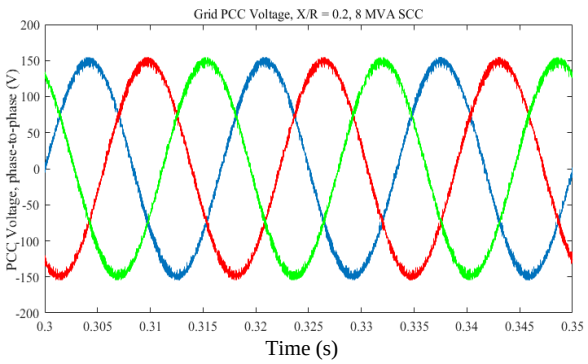

Fig. 4.26 (a)

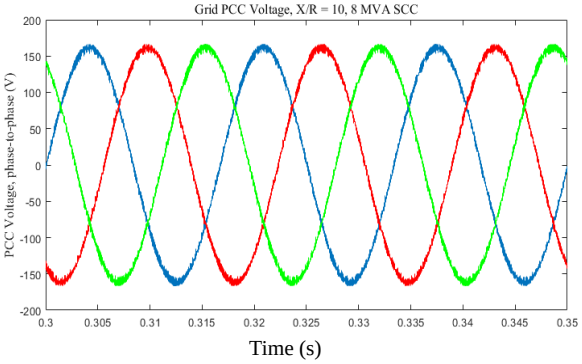

Fig. 4.26 (b)

Fig. 4.26 Comparison of PCC Voltages (Phase-to-Phase), 8 MVA_{SC} for (a) X/R =0.2 and (b) X/R =10

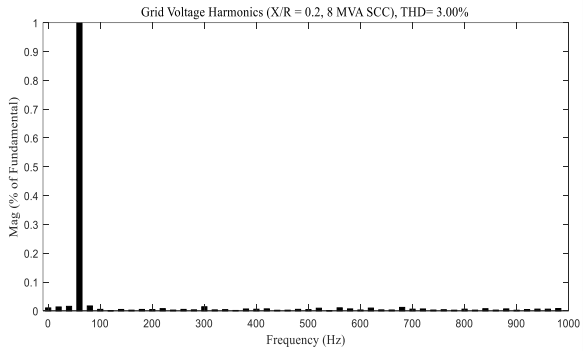

Figure 4.27 (a)

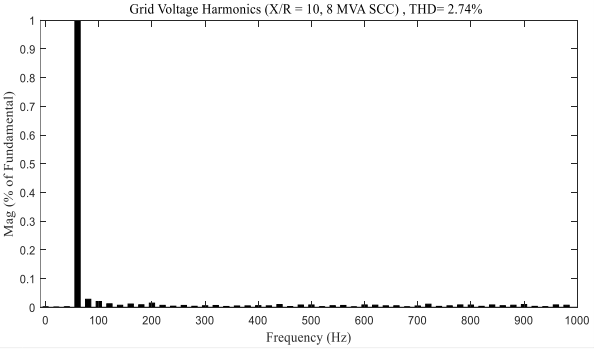

Figure 4.27 (b)

Fig. 4.27 Comparison of THD_V (a) THD_V = 3.00% with X/R =0.2 and 8 MVA_{SC} (b) THD_V = 2.74% with X/R =10 and 8 MVA_{SC}

Fig. 4.26 and Fig. 4.27 shows that there is minor difference in PCC voltages and THD_V in case of X/R = 0.2 and 10 with 8 MVA_{SC} (strong-grid) grid-rating. The range of characteristics and non-characteristics harmonics are much lower in strong-grid as compared to weak-grid as shown in Fig. 4.27. It confirms that grid-strength cancels out the impact of low X/R ratio up to a large extent.

(ii) PCC currents and current harmonics (THD_I)

The comparison of PCC current waveforms and current harmonics (THD_I) for X/R = 0.2 and 10 with a strong-grid (8 MVA_{SC}) is shown in Fig. 4.28 and Fig. 4.29, respectively.

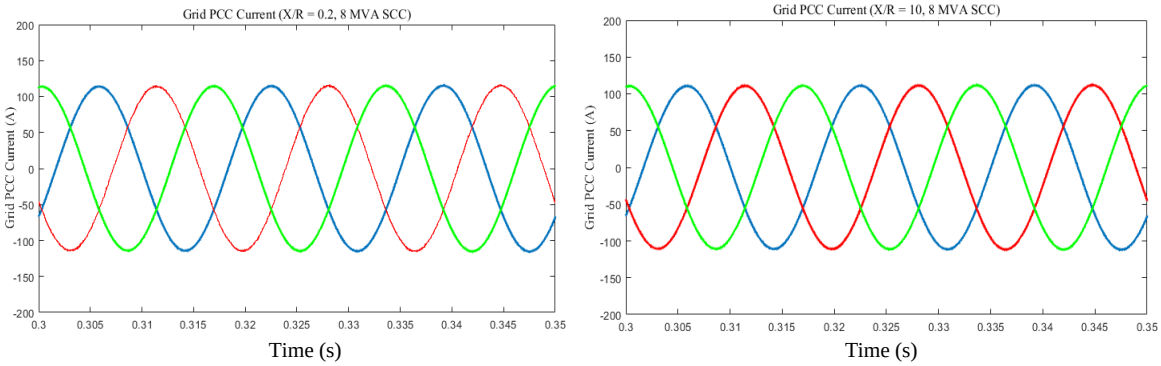

Fig. 4.28 (a) Fig. 4.28 (b)

Fig. 4.28 Comparison of PCC Currents, 8 MVA_{SC} (a) X/R =0.2, and (b) X/R =10

It is observed from Fig. 4.28 that current magnitude is almost same in both the cases. It shows that the impact of X/R ratio reduces with the increase in grid-strength.

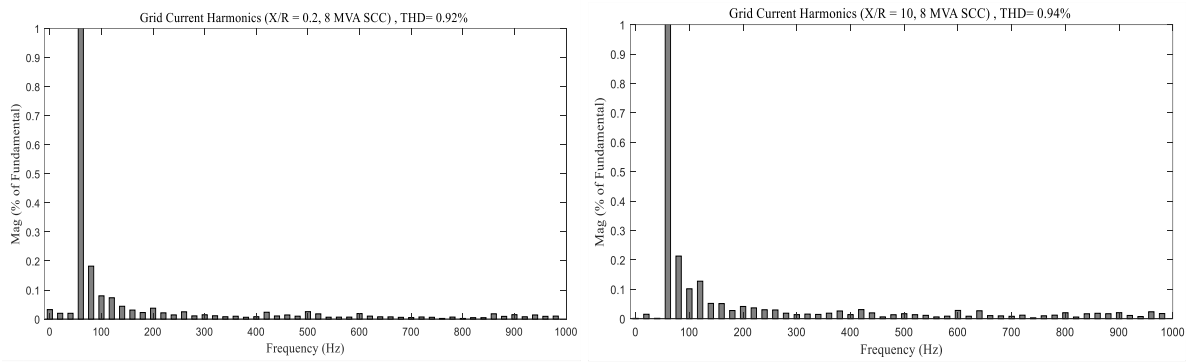

Fig. 4.29 (a) Fig 4.29 (b)

Fig. 4.29 Comparison of THD_I (a), THD_I = 0.92% with X/R =0.2 and 8 MVA_{SC} (b) THD_I = 0.94% with X/R =10 and 8 MVA_{SC}

Fig. 4.29 shows the current harmonic spectra; it is clear from that there is less impact of varying the X/R ratio on the current harmonics (THD_I) in case of strong-grid.

It is observed that strong-grid (8 MVA_{SC}) value makes the system more balanced and efficient, and there is lesser impact of X/R ratio on the system performance. Also, the range of characteristic and non-characteristic harmonics present is much lower with strong-grid. It is clear from the comparison of harmonic spectra (by comparing Fig. 4.23 and Fig. 4.25 with Fig. 4.27 and Fig. 4.29) of weak-grid (2 MVA_{SC}) and strong-grid (8 MVA_{SC}), that there is least impact of X/R ratio on harmonics in case of strong-grid. The higher value of MVA_{SC} results in a more stable and reliable FCS even in the case of low damping.

Scenario II-Fault/Dynamic-state analysis: In this scenario, dynamic-state analysis is done by applying 3-phase fault in case of weak-grid (2 MVA_{SC}), and by varying X/R ratio between 0.2 and 10. In this model, a 3-phase fault is applied at PCC for 5-cycles (0.083 s to 0.1667 s) in case of a weak-grid (2 MVA_{SC}). The results for PCC voltages and PCC currents are presented as follows:

(i) PCC Voltages

The comparison of PCC voltages during 3-phase fault- for X/R = 0.2 and X/R = 10 in case of weak-grid (2 MVA_{SC}) is shown in Fig. 4.30.

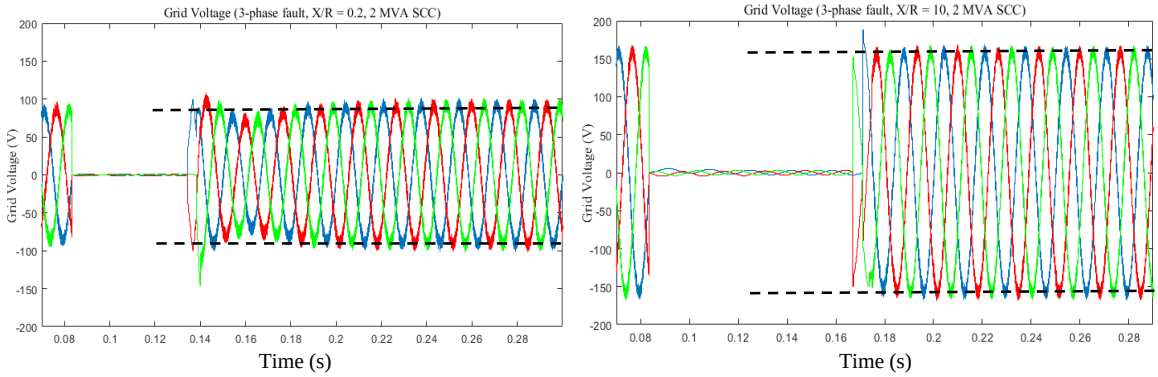

Fig. 4.30 (a) Fig. 4.30 (b)

Fig. 4.30 Comparison of PCC Voltages, dynamic-state (Phase-to-Phase) for (a) X/R = 0.2 and (b) X/R = 10 with weak-grid (2 MVA_{SC})

The comparison shows that there is impact of X/R ratios on the dynamic-state of the system. PCC voltages starts to settle down faster in case of X/R = 0.2, but transients stay in it for longer duration as compared to X/R = 10. This phenomenon is shown with the help of dotted lines in Fig. 4.30. Transients dies down early in case X/R = 10. Low damping in case of X/R = 0.2 is the reason of longer period of transients.

Excessive voltage-harmonics during the fault period may result in damage to the system if fault persists for longer time. Therefore, this kind of FCS require proper insulation and protective gear. These sophsticated equipment adds up in the cost of the system.

(ii) PCC Currents

The comparison of PCC currents during fault-analysis is shown in Fig. 4.31.

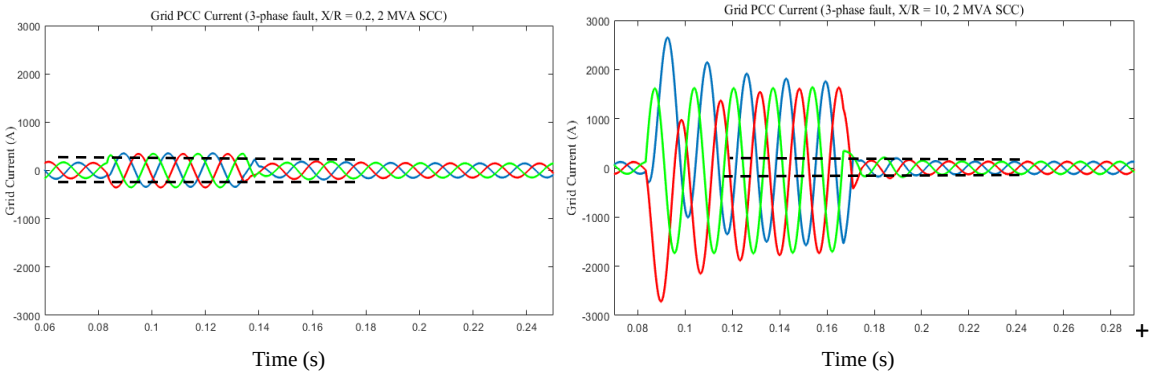

Fig. 4.31 (a) Fig. 4.31 (b)

Fig. 4.31 Comparison of PCC Currents, dynamic-state (a) X/R = 0.2 and (b) X/R = 10

It shows that level of fault current is very high in case of X/R = 10 (reaches up to 2400 A) as compared to X/R = 0.2 (reaches up to 600 A). Fault currents are almost 4-times higher in case of X/R = 10 during fault period. The settling period is also higher in case of X/R = 10.

Short-circuit current is made up of AC and DC component. The decay in DC component directly depends upon value of X/R ratio. It is shown from Fig. 4.31 that the level of DC component is high in case of X/R = 10 which results in more transients and currents take longer time to settle down to steady-state. High damping during X/R = 10 results in large value of transients and long time response in settling down to normal-state.

It has been observed from that the larger X/R ratio results in higher values of fault currents (Fig. 4.31) in case of dynamic-state. Presence of DC component and longer decay time in case of X/R = 10. These transients created during the fault-state needs attention for the design of protective equipment. It is learnt that FCS perform better in case of higher X/R ratio, but excessive fault currents have impact on the age of costly equipment like DT, and may damage the system if same situation prolong and proper protective devices are not used.

Short Circuit Ratio (SCR) and X/R ratio are related to one another and vital to determine the grid strength. The grid with very low SCR (less than 1) is susceptible to voltage instability, and termed as a weak grid. Similarly, grid with very high value of SCR (>10) may result in more harmonics. The harmonic percentage can also be determined through the SCR ratio as given in Table 2.1. As per this table, TDD can be calculated from SCR values. For both the cases (X/R = 0.2 and 10), SCR comes as follows:

For X/R = 0.2, SCR(I_{SC}/I_L) = 12 (I_{SC} = 600 A, I_L = 50 A)

For X/R = 10, SCR(I_{SC}/I_L) = 48 (I_{SC} = 2400 A, I_L = 50 A)

According to Table 2.1, the TDD for X/R = 0.2 and SCR = 12 will be 5%, and for X/R = 10 and SCR = 48 will be 8%. As there will be more distortions (TDD = 8 %) in the system with SCR = 48, so it requires high rating and expensive protective devices.

This investigation by varying X/R ratio and grid-strength shows that higher value of X/R ratio results in higher charging speed and better performance, but also requires more expenses on insulation, protective equipment.

4.1.6 Case VI- Grid-connected DC FCS with a PV-panel

In this section, grid-connected FCS with a PV-panel is compared with the grid-connected FCS without a PV-panel. This investigation is performed by considering a DC FCS connected with 5 EV bays. The inclusion of a PV-panel into the grid-connected FCS (Fig. 4.3) makes the system more flexible and environmentally friendly.

There are different types of PV-panels available in the market. The output power of the solar panels depends upon solar irradiance, module temperature and characteristics of solar-panel. In this Simulink model, Sunpower SPR-315E-WHT-U PV-panel is used. The details of the solar-panel and FCS are covered in chapter-4. Two scenarios considered for this investigation are as follows:

(a) Comparison of grid-connected FCS (without PV-panel) and grid-connected FCS (with PV-panel)

(b) Comparison of SoC of in grid-connected FCS (without PV-panel) and Islanded-mode (with only PV-panel)

(a) Comparison of grid-connected FCS (without PV-panel) and grid-connected FCS (with PV-panel)

In the following results, the comparison of grid-connected DC FCS with (Fig. 3.3) and without PV-panel (Fig. 3.1) is shown. In this investigation, weak-grid rating (2 MVA_{SC}) with 5 EV bays as load are used.

The following results are presented next.

(i) SoC,

(ii) PCC Voltages and THD_V,

(iii) PCC Currents and THD_I.

(i) SoC

The SoC of grid-connected FCS with PV-panel and without PV-panel is shown in Fig. 4.32. This comparison is important to realize the impact of inclusion of PV-panel into the grid-connected FCS.

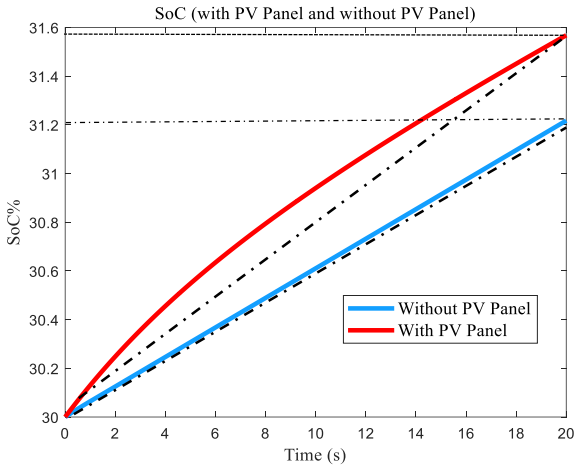

Fig. 4.32 Comparison of State of Charge (SoC) in Grid-connected FCS with PV-panel and without PV-panel

This comparison shows that battery charging reaches from 30% to approx. 31.6% (Red line in Fig. 4.32) in 20 seconds in the case of grid-connected FCS with PV-panel while it reaches up to approx. 31.2% (Blue line in Fig. 4.32) in case of grid-connected FCS without PV-panel. If this approximate rate is maintained, then battery will get charged from 30% to 90% in about 12 minutes for FCS with PV-panel and takes about 17 minutes for grid-connected FCS without PV-panel. Results shows that charging speed get approx. 9-10% faster in case of FCS with the PV-panel.

The inclusion of PV-panel increases the reliability of system, but there are chances of an increase in the harmonics on the grid-side due to addition of the solar-panel generation. This phenomenon is investigated in the next results.

(ii) PCC Voltages and Voltage Harmonics (THD_V)

A comparative analysis of PCC voltages of grid-connected FCS with PV-panel and without PV-panel is presented in Fig. 4.33. The comparison is to show the impact of inclusion of PV-panel into the grid-connected FCS.

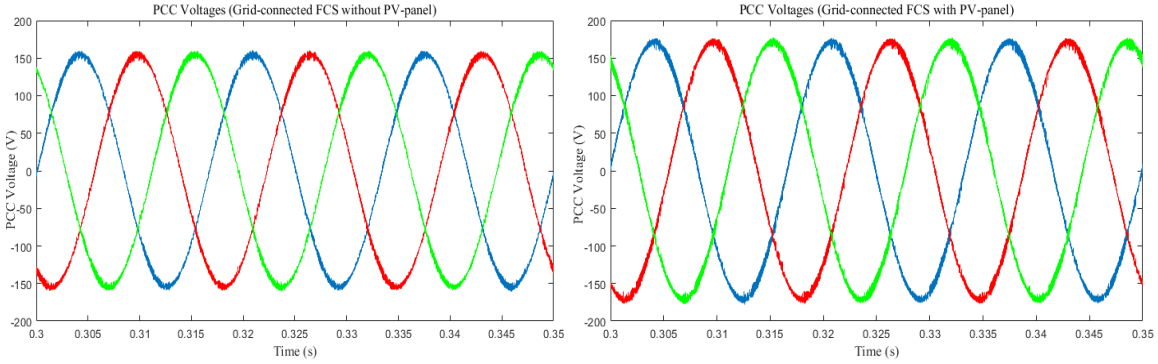

Fig. 4.33 (a) Fig. 4.33 (b)

Fig. 4.33 Comparison of PCC Voltages in Grid-connected FCS (a) without PV-panel (b) with PV-panel, with weak-grid (2 MVA_{SC})

The comparison of PCC voltages shows that the magnitude of voltages is slightly increased from 2.3% to 3.3%, but there are more visible harmonics in case of grid-connected FCS with PV-panel. The magnitude of these harmonics is shown by FFT analysis as in Fig. 4.34.

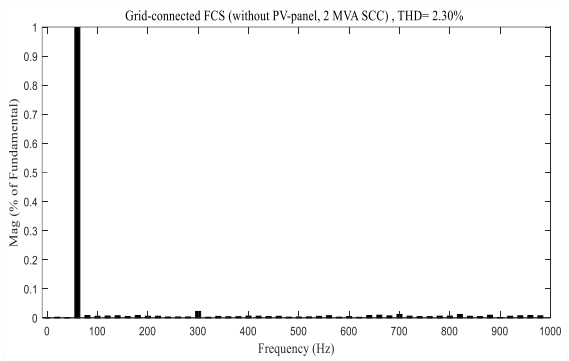

Fig. 4.34 (a)

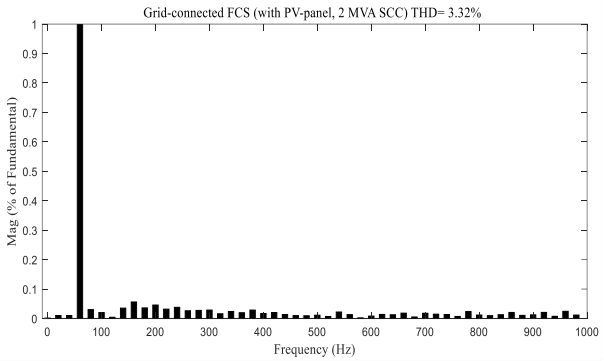

Fig. 4.34 (b)

Fig. 4.34 Comparison of THD_V in Grid-connected FCS (a) without PV-panel, THD_V = 2.30% (b) with PV-panel, THD_V = 3.32%, with weak-grid (2 MVA_{SC})

Fig. 4.34 shows the comparison of THD_V in case of grid-connected FCS without and with PV-panel, respectively. The magnitude of harmonics is approx. 1.02% higher in case of grid-connected FCS with PV-panel. It is due to the inclusion of more power electronics equipment like DC-DC converter with the PV-panel. There is presence of non-characteristics harmonics and inter-harmonics in case of grid-connected DC FCS with PV-panel.

(iii) PCC Currents and Current Harmonics (THD_I)

The comparison of PCC current waveforms and current harmonics (THD_I) for grid-connected FCS with PV-panel and without PV-panel is shown in Fig. 4.35 and Fig. 4.36, respectively.

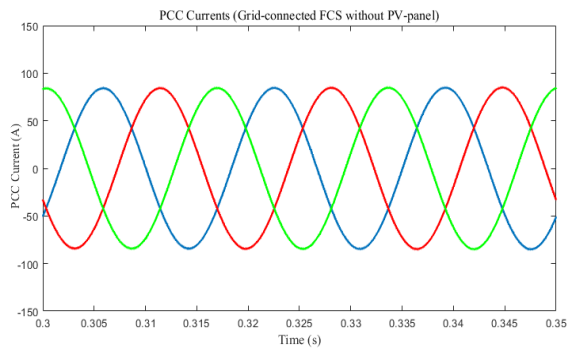

Fig. 4.35 (a)

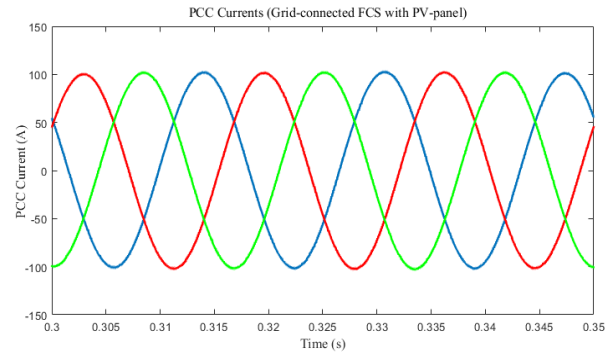

Fig. 4.35 (b)

Fig. 4.35 Comparison of PCC Currents in Grid-connected FCS (a) without PV-panel (b) with PV-panel, with weak-grid (2 MVA_{SC})

It is observed from Fig. 4.35 that current magnitude is approx. 0.5% to 0.9% higher in case of grid-connected FCS with PV-panel and without PV-panel. It shows that whether the current magnitude supplied from grid is almost similar, the charging speed is faster in case grid-connected FCS with

PV-panel (Fig. 4.32). It establishes that inclusion of PV-panel helps in escalating the charging speed of EVs. The harmonic-spectra for THD_I is shown next.

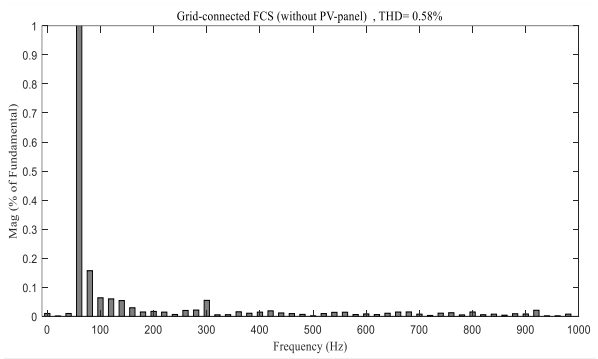

Fig. 4.36 (a)

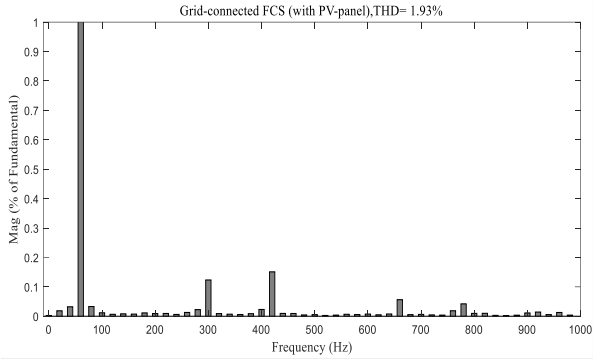

Fig. 4.36 (b)

Fig. 4.36 Comparison of THD_I in Grid-connected FCS (a) without PV-panel, THD_I = 0.58% (b) with PV-panel, THD_I = 1.93%, with weak-grid (2 MVA_{SC})

It is observed from harmonic analysis of both the models that magnitude of current harmonics is 1.35% higher in case of grid-connected FCS with PV-panel. The magnitude of 3rd and 5th order harmonics are 10% to 15% in case of grid-connected FCS with PV-panel. But, THD_I values for both the models are under the safe limits as prescribed in IEEE-519 standards.

It has been observed from the SoC profile (Fig. 4.32) that charging becomes faster in case of grid-connected FCS with PV-panel. It shows that inclusion of PV-panel in grid-connected FCS gives more strength to the system, and charging operation becomes faster in case of weak-grid. But, there is slight increase in harmonics due to the insertion of PV-panel which could increase with the inclusion of high rated PV-panel. This problem must be addressed before the inclusion of high-rated PV-panel system into the grid-connected FCS.

(b) Comparison of SoC in grid-connected FCS (without PV-panel) and Islanded-mode (with only PV-panel)

In the Fig. 4.37, comparison of SoC is done in case of grid-connected FCS (without PV-panel) and during Islanded-mode (when charging is only by PV-panel) with 5 EV bays as load. In Islanded-

mode, FCS is supplied only by PV-panel. This kind of operation is possible in remote areas and installation of FCS is possible even without connecting to electric grid.

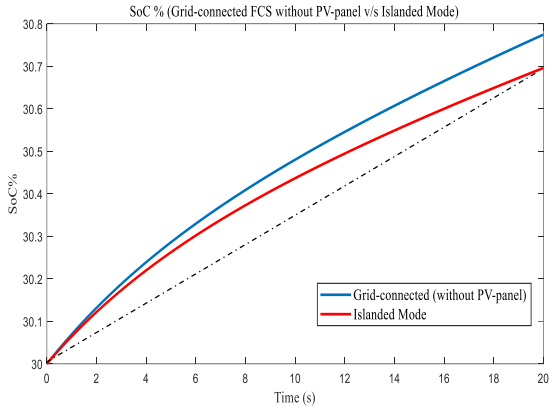

Fig. 4.37 Comparison of State of Charge (SoC) of Grid-connected FCS without PV-panel and Islanded-mode

It is clear from the Fig. 4.37 that EV battery charges 7% to 8% faster in case of grid-connected FCS mode as compared to Islanded-mode. This comparison shows that battery charging reaches from 30% to approx. 30.8% (Blue line in Fig. 4.37) in 20 seconds in the case of grid-connected FCS without PV-panel while it reaches up to approx. 30.7% (Red line in Fig. 4.37) in case of Islanded-mode. If this approximate rate is maintained, then battery will get charged from 30% to 90% in about 25 minutes for grid-connected FCS without PV-panel and takes about 29 minutes for Islanded-mode. The P & O algorithm (explained in chapter 3 (section 3.2.3)) plays an important role in case of Islanded-mode. The charging profile depends upon the solar irradiance, rating of PV-panel and MPPT operation in case of Islanded-mode.

4.1.7 Case VII-Comparison of DC FCS by comparing Super-Capacitor (SC) with Conventional- Capacitor (CC) as a common DC-link capacitor

In this section, comparison of Super-Capacitor (SC) versus a Conventional-Capacitor (CC) as a common DC-link energy storage element in the DC FCS is done. The common DC-link capacitor acts as an important component to control the charging operation in DC FCS. The SC has a larger

capacitance as compared to the CC. This higher capacitance helps in maintaining the DC voltage at a constant value. The motivation to do this comparison arises due to the following reasons:

i. SC is a double layer capacitor having higher energy density and capacity.

ii. SC has higher charging and discharging rate and longer life-cycle (1-million cycles or 30,000 hours) as compared to the CC and batteries.

iii. SC can work more efficiently at low temperatures such as below freezing temperatures (-40 to 65oC).

iv. SC has a comparatively longer life-span than CC and batteries. As an example, its capacity falls to 80% from 100% approx. in 10 years [153].

The rating of SC and CC used in the MATLAB/Simulink® model (Fig. 3.1) is shown in Table 4.6:

Table 4.6: SC and CC Parameters [153] [154]

Parameter	Value (SC)	Value (CC)
Rated Capacitance	100 F	3300 μF
Equivalent DC series Resistance	2.1 mΩ	0.01 Ω (approx.)
Rated Voltage	350 V	350 V
Number of series capacitors	6	1
Number of parallel strings	2	NA

(1) Comparison of grid-connected FCS by using CC and SC

The comparison is made under steady-state and dynamic-state (3-phase fault) conditions.

(a) Steady-state analysis

The simulation is performed by using the system with 10 EV bays (i.e. full-load conditions) and a weak-grid (2 MVA_{SC}) source rating. The results are presented next.

(i) SoC

SoC is an important parameter to compare the DC FCS with CC and SC. This simulation is performed for 20 seconds time-window due to the computational limitation.

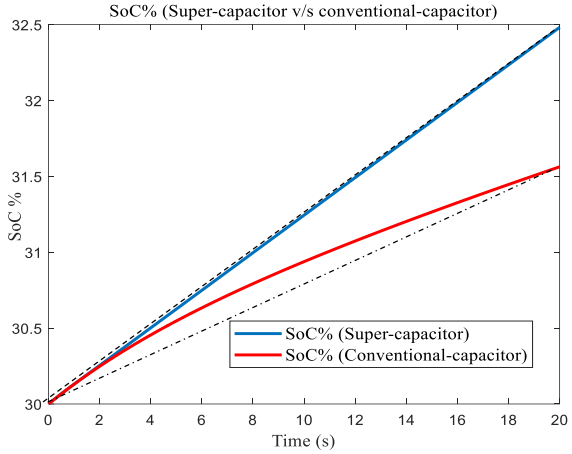

Fig. 4.38 Comparison of State of Charge (SoC) of Grid-connected FCS with SC and CC

The waveform in Fig. 4.38 shows that battery is initially at 30% and charges up to approx. 31.6% (red line in Fig. 4.38) in case of DC FCS with SC while it reaches up to 32.5% (blue line in Fig. 4.38) in case of DC FCS with CC. The charging with the CC is more exponential than linear while charging proceeds linearly in case of SC as shown by dotted lines in the Fig. 4.38. If this approximate constant rate is maintained, the battery will get charged from 30% to 90% in about 12 minutes with CC and takes approx. 8 minutes with SC. This means that battery charging speed is approx. 7% high in case of SC as compared to CC, this is considered a noteworthy improvement.

(ii) PCC Voltages and THD_V

In the following results, PCC voltages and voltage harmonics (THD_V) are compared for both the models.

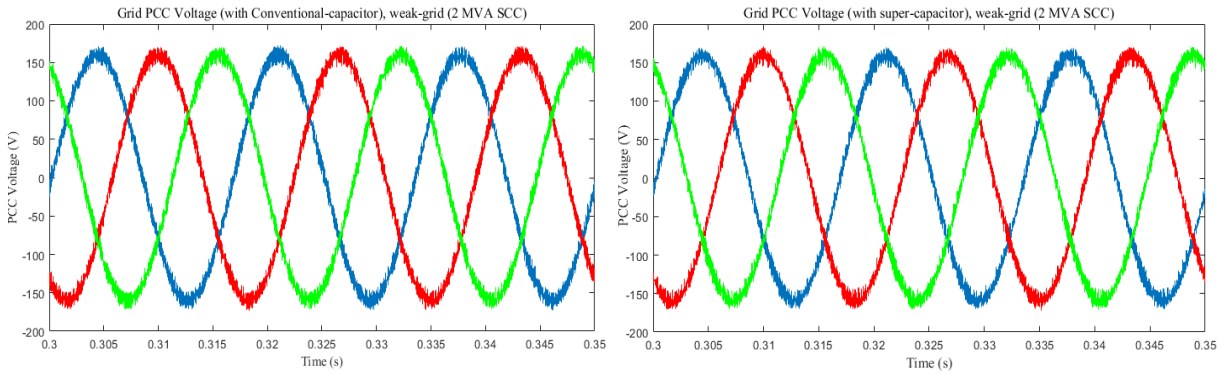

Fig. 4.39 (a) Fig. 4.39 (b)

Fig. 4.39 Comparison of PCC Voltages in Grid-connected FCS (a) with CC (b) with SC

The comparison of PCC voltages shows that magnitude of voltages is almost the same in both the systems. The voltage harmonic (THD_V) analysis is shown in Fig. 4.40.

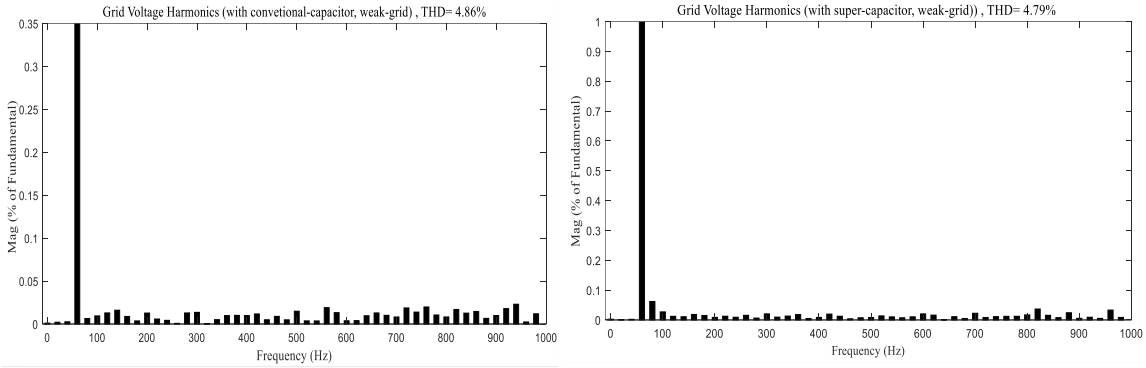

Fig. 4.40 (a) Fig. 4.40 (b)

Fig. 4.40 Comparison of THD_V in Grid-connected FCS (a) with CC (THD_V = 4.86%) (b) with SC (THD_V = 4.79%)

Fig. 4.40 shows the comparison of voltage harmonics in case of grid-connected FCS with CC and, with SC is shown. The magnitude of harmonics is 0.07% higher in case of grid-connected FCS with CC, this is quite marginal difference.

(ii) PCC Currents and THD_I

In Fig. 4.41, PCC currents in case of both grid-connected FCS with CC, and with SC is compared.

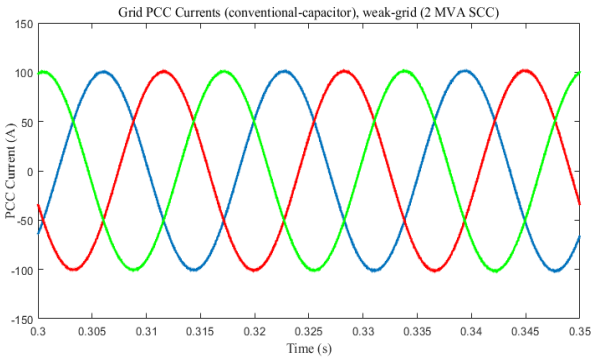

Fig. 4.41 (a)

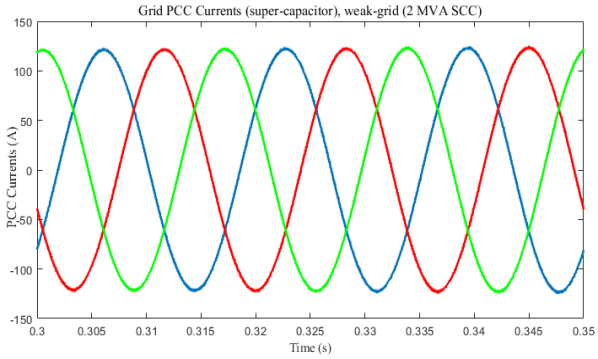

Fig. 4.41 (b)

Fig. 4.41 Comparison of grid PCC currents in grid-connected FCS (a) with CC (b) with SC

It is observed from comparison that PCC currents are 20% higher in case of grid-connected FCS with SC. This higher current results in faster speed of charging as shown in Fig. 4.41.

It has been clear from the comparison that addition of SC increases the charging current which ultimately escalates the charging speed of EVs. The system gives better performance in terms of charging speed. Current harmonics (THD_I) analysis is shown next.

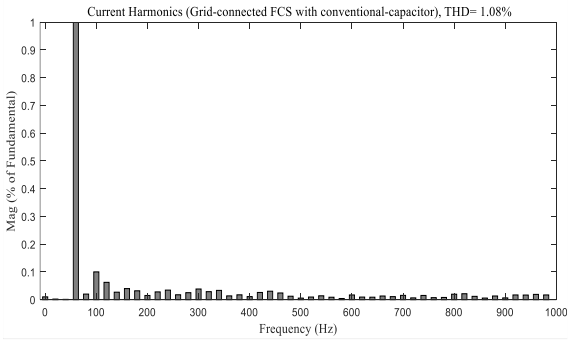

Fig. 4.42 (a)

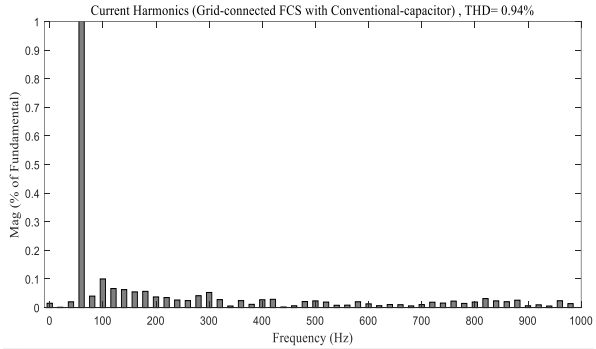

Fig. 4.42 (b)

Fig. 4.42 Comparison of THD_I in case of Grid-connected FCS (a) with CC (THD_I = 1.08%) (b) with SC (THD_I = 0.94%)

In Fig. 4.42, comparison of PCC current harmonics (THD_I) of grid-connected FCS with CC and, with SC is shown. It is observed that current harmonics are 0.14% lesser in case of grid-connected FCS with SC, while charging speed is high.

(b) Fault/Dynamic-state analysis: Dynamic-state analysis is done by applying 3-phase fault in case of grid-connected FCS with CC, and SC. In this model, a 3-phase fault is applied at PCC for

5-cycles (0.083 s to 0.1667 s) in case of a weak-grid (2 MVA_{SC}). The results for PCC voltages and PCC currents are presented as follows:

(i) PCC Voltages

The comparison of PCC voltages during 3-phase fault for grid-connected FCS with CC, and with SC is shown in Fig. 4.43.

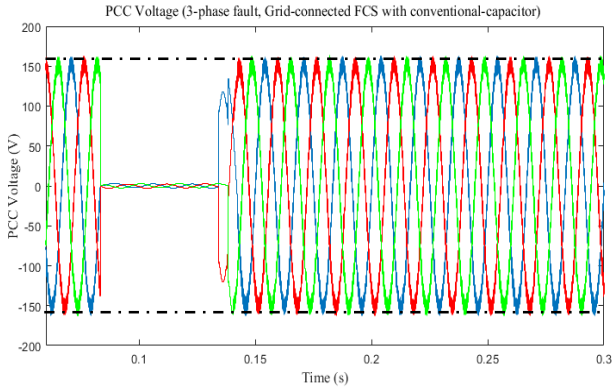

Fig. 4.43 (a)

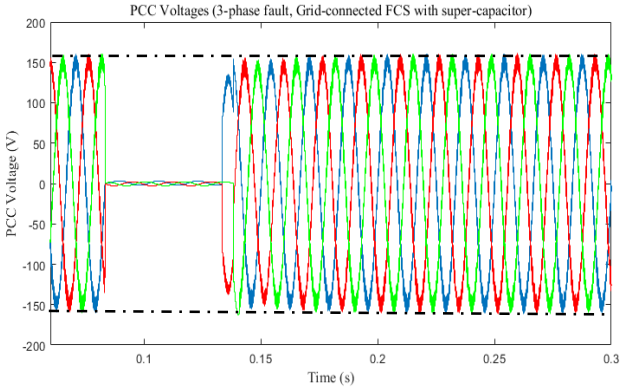

Fig. 4.43 (b)

Fig. 4.43 Comparison of PCC Voltages, 3-phase fault (Phase-to-Phase) for (a) with CC and (b) with SC

The comparison shows that there is little or no impact of CC and SC on the dynamic-state of system. PCC voltages settles almost at same time for both the cases. It shows that behavior of SC is similar in dynamic-state with the CC. Voltages during 3-phase fault does not rise beyond the limit and settle down in same time as in case of CC.

(i) PCC Currents and THD_I

The comparison of PCC currents shown in Fig. 4.44.

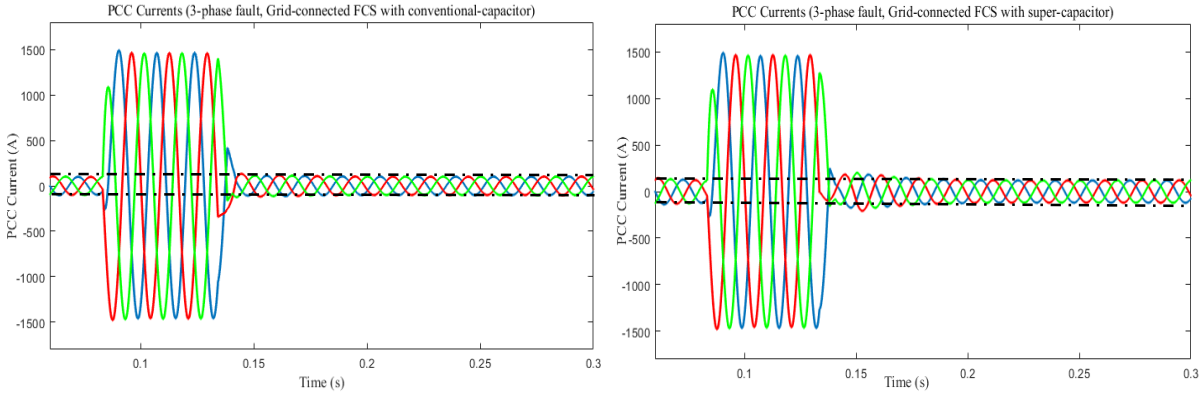

Fig. 4.44 (a) Fig. 4.44 (b)

Fig. 4.44 Comparison of PCC Currents, 3-phase fault (Phase-to-Phase) for (a) with CC and (b) with SC

In Fig. 4.44, comparison of PCC currents during 3-phase fault is shown. It is observed that magnitude of fault currents is similar in both the cases, while it takes a little more time (0.02 to 0.03 s) to settle down in case of SC.

It shows that SC helps in reducing the overall harmonics in the system, thus improves the power quality and efficiency of the system.

Similarly, comparison of grid-connected FCS with PV-panel by using (a) CC and (b) SC is done. This task is performed because it has been seen that magnitude of distortions is high when PV-panel is included in the system. Therefore, the comparison is made by changing the DC-link capacitor with SC if it can reduce the harmonics.

(2) Comparison of THD_V and THD_I in grid-connected FCS with PV-panel by using (a) CC and (b) SC

The comparison of voltage and current harmonics (THD_V and THD_I) for grid-connected FCS with PV-panel (with 5 EV bays) by using CC and SC is presented in Fig. 4.45 and Fig. 4.46.

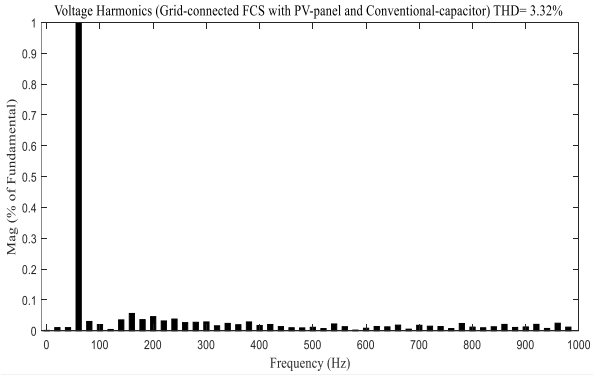

Fig. 4.45 (a)

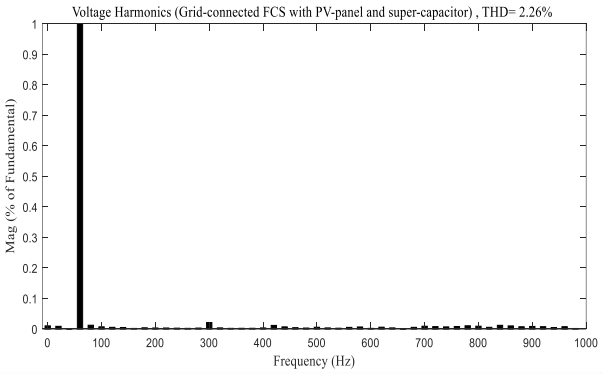

Fig. 4.45 (b)

Fig. 4.45 Comparison of THD_V in grid-connected FCS with PV-panel by using (a) CC (3.32%) (b) SC (2.26%)

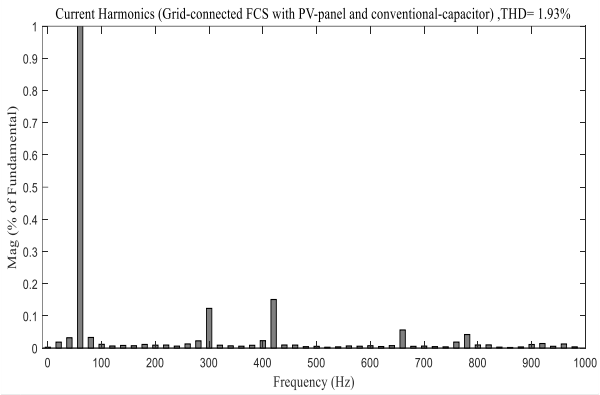

Fig. 4.46 (a)

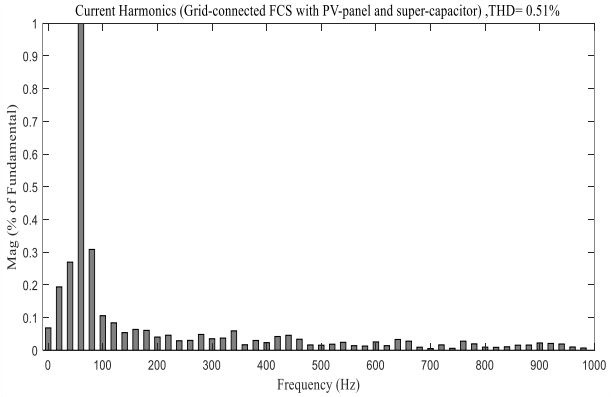

Fig. 4.46 (b)

Fig. 4.46 Comparison of THD_I in grid-connected FCS with PV-panel by using (a) CC (1.93%) (b) SC (0.51%)

This comparison of voltage and current harmonics (THD_V and THD_I) shows that magnitude of harmonics decreases by using SC in case of system with PV-panel. It reduces by 1.06% in case of THD_V and by 1.42% in case of THD_I.

Results shows that replacement of CC by SC reduces the power-quality problems in grid-connected DC FCS with PV-panel and improves the overall efficiency of the system.

The analysis shows that inclusion of SC improves the overall efficiency of the FCS by increasing the speed of charging. As charging speed with fewer harmonics is requirement of EV users and utilities, therefore SC can become a solution for this as a common DC link capacitor. The limitations in case of this technology is cost and very low energy to weight ratio (5 Wh/kg) of the SC. A typical SC costs approximately $ 2,400-6,000 (US) per kWh, which is far higher than the

electrolytic capacitors or even Li-ion batteries ($ 250- $ 1,000). But the service age (10-15 years) of SC is quite higher than the CC and batteries (5-10 years). SC can become a replacement of CC in future FCS if the cost decreases with the new innovations in electrolyte materials.

4.1.8. Case VIII-Comparison of DC FCS and AC FCS in Vehicle to Grid (V2G) Mode

In this section, performance of two architectures CDCB and CACB (Fig. 3.8 and Fig. 3.9, respectively), with partial load operation (i.e. 5 EVs being discharged) is compared in Vehicle to Grid (V2G) operation mode. The advantages and issues related to V2G operation are discussed in chapter-3 (section-3.3). The comparison of CDCB and CACB architectures are made under steady-state and dynamic-state operation.

(i) Steady-state operation

The following results are presented for comparison of CDCB and CACB architectures operating in V2G mode:

(a) State of Discharge (SoD) of battery,

(b) PCC Voltages and THD_V, and

(c) PCC Currents and THD_I.

(a) State of Discharge (SoD) of battery

SoC is a measure of battery charge in G2V mode of operation. It is like the fuel gauge of the battery. The charge leaving or entering the battery is called coulomb counting. It can be represented by the following equation:

$$SoC = \frac{Q_0 \pm \int i_{bt}}{Q_n} \times 100 \quad (4.3)$$

Where Q_0 is the initial charge present in the battery, Q_n is the nominal charge capacity of the battery in Coulombs (C), i_{bt} is the charging/discharging current of battery. This current is deemed positive (i.e. current enters the battery) or negative (i.e. current leaves the battery). This phenomenon of the battery can also be defined by one another term known as State of Discharge (SoD) which is expressed by the following equation:

$$SoD = 1 - SoC \tag{4.4}$$

It is clear from the equation that SoD and SoC always sums up to 1. The comparison of SoD in case of CDCB and CACB architectures is shown in Fig. 4.47.

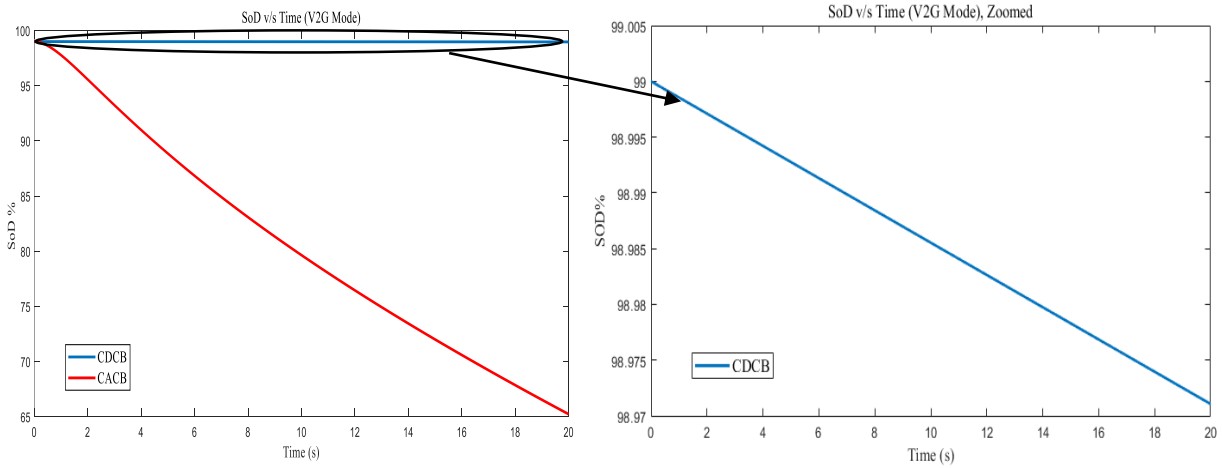

Fig. 4.47 (a) Fig. 4.47 (b)

Fig. 4.47 (a) SoD of CDCB and CACB Architectures (b) zoomed view of SoD of CDCB Arch.

It is shown in Fig. 4.47 that battery SoC is at 99% initially and discharges down to 98.98% in 20 seconds in case of CDCB architecture. It means battery discharges about 0.03% in 20 seconds. If this discharging rate is maintained in a linear fashion, the battery in CDCB architecture discharges in approximately 14 hours down to 20%. But, in case of the CACB architecture, SoD of battery is much faster. It reaches down to 20% approximately in approx. 3-4 minutes. It shows that battery discharge rate is very fast in case of CACB architecture as compared to CDCB architecture. This fast discharging rate results in negative impact on battery life during V2G operation and also not

beneficial for grid-management operation. It means that CDCB architecture is more stable than CACB architecture in terms of retaining the charge in V2G mode. The slow decay in the charging profile of battery is helpful in grid-management operations.

(b) PCC Voltages and THD_V (V2G Mode)

In the Fig. 4.48, comparison of PCC voltages for CDCB and CACB architectures during V2G is shown.

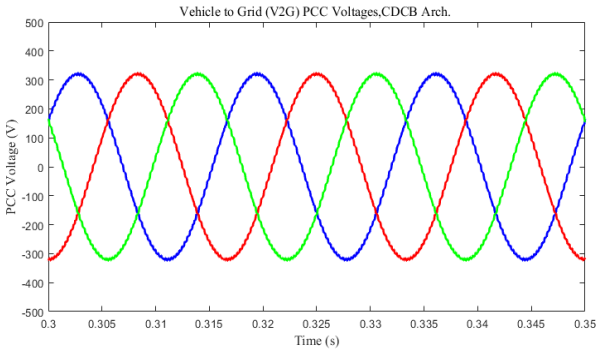

Fig. 4.48 (a)

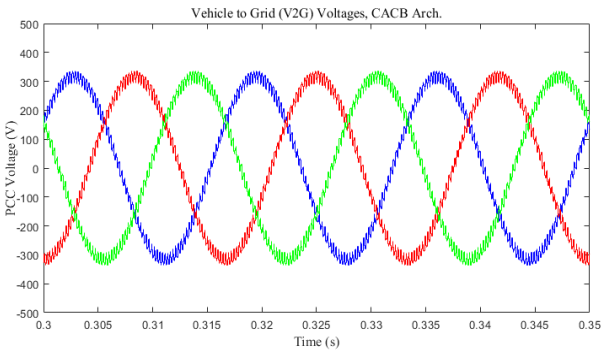

Fig. 4.48 (b)

Fig. 4.48 Comparison of PCC Voltages in V2G mode (a) CDCB architecture, (b) CACB Architecture

The comparison shows that the magnitude of PCC voltages is almost similar in both the architectures, but a high level of disturbances can be observed in the case of CACB architecture (Fig. 4.48 (b)). The PCC voltages of CDCB architecture are more balanced and having fewer harmonics. The magnitude and type of voltage harmonics can be observed from the harmonic spectra shown in Fig. 4.49.

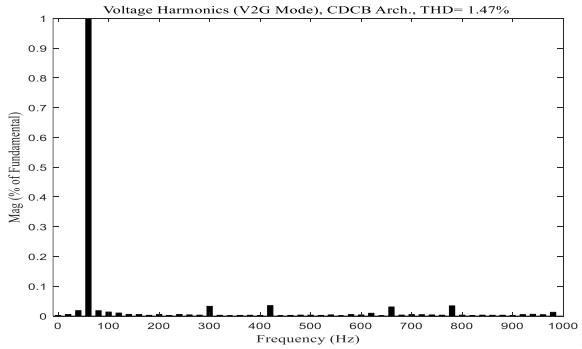

Fig. 4.49 (a)

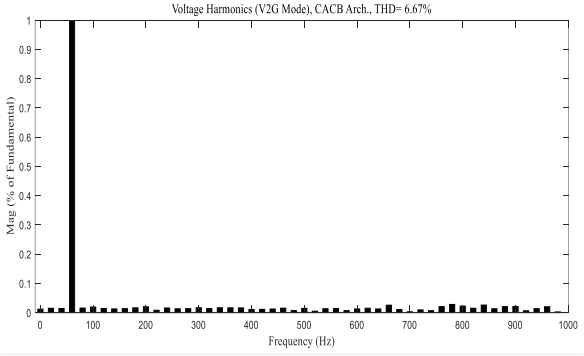

Fig. 4.49 (b)

Fig. 4.49 Comparison of THD_V in Grid-connected FCS during V2G Mode in (a) CDCB Architecture (THD_V = 1.47%) (b) CACB Architecture (THD_V = 6.67%)

It is observed from the harmonic analysis that voltage harmonics are 5.2% higher in case of CACB than the CDCB architecture. These higher quantity of harmonics would not be acceptable in a grid-connected system and extra filtering would be needed to avoid negative impacts on the efficiency and performance of DT and other connected equipment and loads.

(c) PCC Currents and THD_I

In Fig. 4.50, PCC currents for CDCB and CACB architectures are compared.

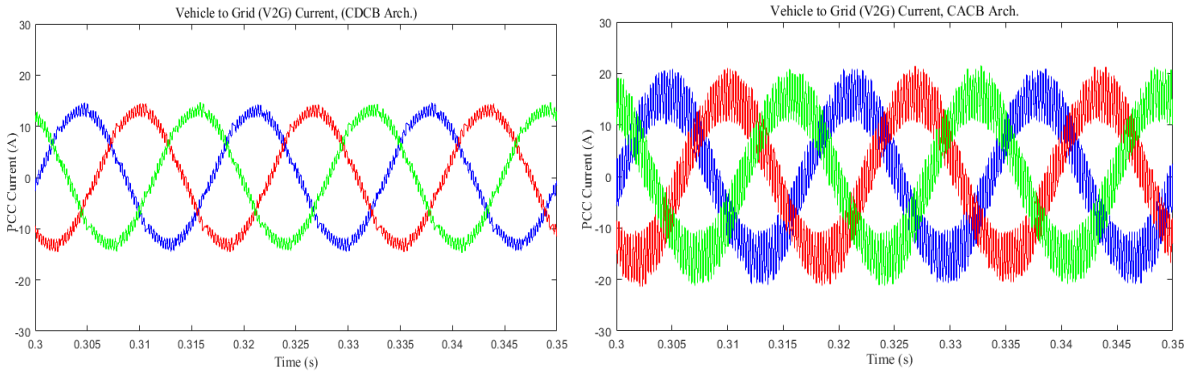

Fig. 4.50 (a) Fig. 4.50 (b)

Fig. 4.50 Comparison of PCC currents in V2G mode (a) CDCB architecture, (b) CACB architecture

It is observed from the comparison of PCC currents in case of CDCB and CACB architectures that magnitude of discharging current is 1.5 to 2% higher in case of CACB architecture, but there is higher order of current harmonics (THD_I) in case of both the architectures. The magnitude of these harmonics is shown in Fig. 4.51.

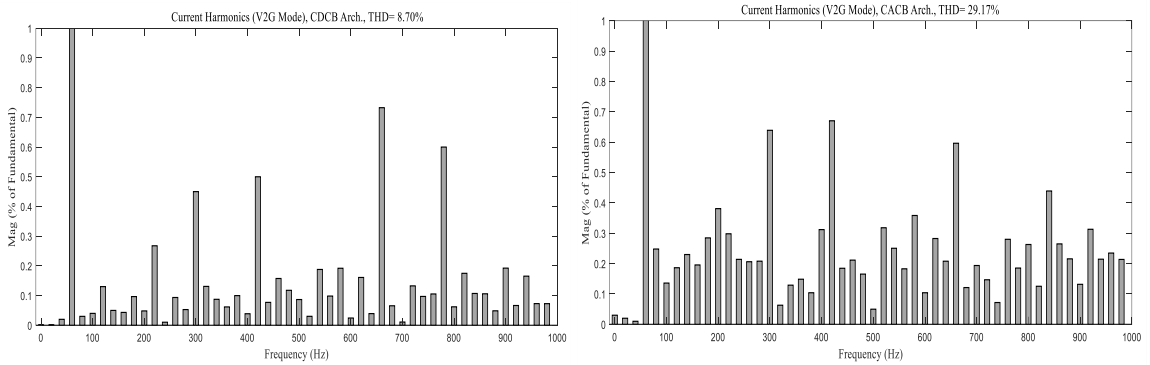

Fig. 4.51 (a) Fig. 4.51 (b)

Fig. 4.51 Comparison of THD_I in Grid-connected FCS during V2G Mode in (a) CDCB Architecture (THD_I = 8.70%) (b) CACB Architecture (THD_I = 29.17%)

It is observed from the harmonic analysis that current harmonics are quite higher in case of both the architectures during V2G mode. There are large amounts of sub-harmonics and inter-harmonics present in the system. Current harmonics are 20.47% higher in case of CACB than the CDCB architecture. These harmonics are beyond the IEEE-519 and IEC standards limits in case of CACB architecture. These higher order harmonics have detrimental impact on the efficiency of the system and may cause overheating in the system.

(ii) Dynamic-state operation

Dynamic-state analysis is done by applying 3-phase fault in case of both the architectures. In this scenario, a 3-phase fault is applied at PCC for 5-cycles (0.083 s to 0.1667 s). The comparative results for PCC voltages and PCC currents are presented for CDCB and CACB architectures as follows:

(a) PCC voltages

The comparison of PCC voltages during 3-phase fault for grid-connected FCS with CDCB and CACB architectures is shown in Fig. 4.52.

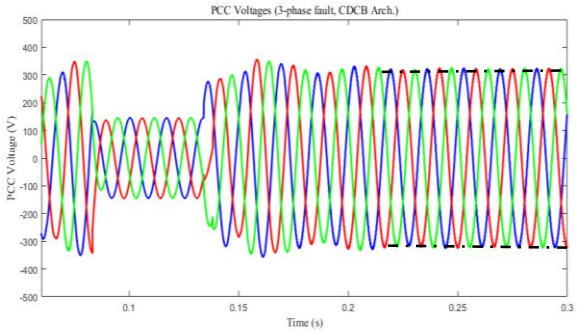

Fig. 4.52 (a)

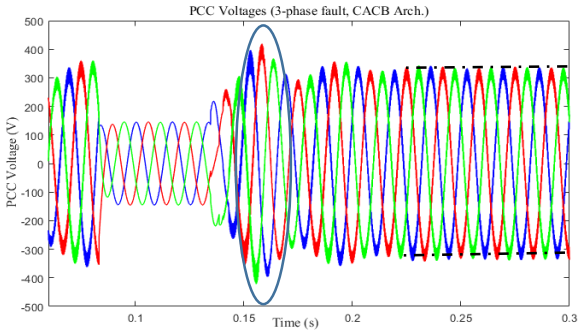

Fig. 4.52 (b)

Fig. 4.52 (a) PCC Voltages (CDCB architecture) (b) PCC Voltages (CACB architecture) in case of 3-phase fault during V2G mode

The comparison during dynamic-state shows that settling time is slightly higher (0.04-0.05 s) in case of CACB than the CDCB architecture. The transient-state is longer in case of CACB

architecture and it rises up to 425 V before settling. The wave shape shows that the sum of harmonics is higher in case of CACB architecture.

(b) PCC Currents

PCC current waveforms during dynamic-state are shown in Fig. 4.53.

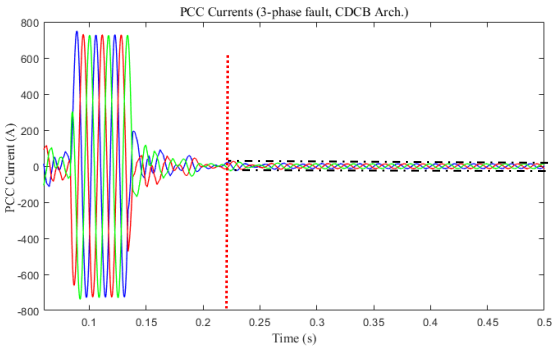

Fig. 4.53 (a)

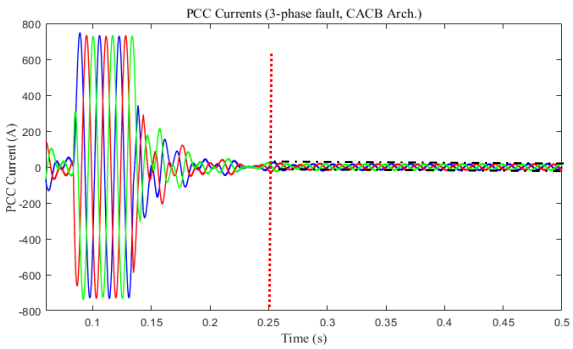

Fig. 4.53 (b)

Fig. 4.53 (a) PCC Currents (CDCB architecture) (b) PCC Currents (CACB architecture) in case of 3-phase fault during V2G mode

It is observed from Fig. 4.53 that PCC currents settles down fast in 0.03s in case of CDCB architecture.

Results shows that there are more transients in CACB architecture, and it takes more time to settle down. Therefore, CDCB architecture is suitable for V2G operation as it is having fewer harmonics in steady-state and also more stable in dynamic-state.

4.2 Summary

In the results and discussions of section-4.1(4.1.1 to 4.1.8), different cases of FCS are discussed. The results include comparison of the impacts on the harmonic emissions of grid-connected common DC bus FCS and common AC bus FCS, steady-state and dynamic-state analysis of FCS, comparison of dq-SRF and UTC strategies for the control operation of AC-DC converter (VSC), comparison of weak and strong-grid and by varying X/R ratio and MVA_{SC}, Inclusion of PV-panel into the FCS, comparison of Super-Capacitor (SC) and Conventional-Capacitor (CC) as a common DC bus link capacitor and Vehicle-to-Grid (V2G) operation.

The results are helpful in understanding the concepts of FCS and particularly harmonic emission assessment in grid-connected system which can arise due to it.

CHAPTER 5

CONCLUSIONS

5.1 Summary of Thesis

This thesis focuses on harmonic emissions assessment relating to grid-connected Fast Charging Station (FCS) for EVs. Two models of grid-connected architectures, Common AC Bus (CACB) and Common DC Bus (CDCB), for FCS are considered. The salient features of both the architecutre are as follows:

a. CACB Architecutre

CACB is a widely popular method for EV charging. In this architecture, separate converter-stages are connected to AC bus through a step-down DT. It is easy to establish this strucutre, as technology is already adopted in many operations. There is requirement of as many VSCs as the number of EV bays. This high number of converters results in increase in unwanted harmonics and poor power factor. This architecture is complex, and expensive and becomes more costly if renewable energy sources included in the FCS.

b. CDCB Architecture

In the CDCB architecture, EVs are connected with the electrid-grid through a step-down DT and common DC bus. This common DC bus feeds individual charging bays. There is requirement of one main AC-DC converter, and several chargers can be tied out with it. Renewable energy sources could also be connected with the FCS through this common DC bus. A DC-link capacitor is used to strengthen the common DC bus. Due to the fewer number of stages and conveters, there is low harmonic content in these stations. Control strategy for main converter is also very important to maintain the system as per global standards.

In these two architectures,a 2-level VSCs are used as a main converter/s and further a DC-DC converter/s are used for voltage regulation in the FCS.

c. VSC Converter

The 2-level VSC is used as main AC-DC converter/s in both the architectures. CDCB architecture requires only one converter, while separate converters are required for each bay in a CACB architecture.

d. DC-DC Converter

The SoC of EV battery is controlled with the help of DC-DC converters. Each EV is connected to the main converter through DC-DC converter in both the architectures. CC-CV method is used to control the charging by using DC-DC converter. Buck-boost operation is employed for the control of the DC-DC converter and bi-directional operation of the FCS is possible with it.

e. Control Strategies for VSC

Unit-template based control (UTC) strategy is used to control and generate the switching pulses for VSC. The reference signals are generated by obtaining active and reactive unit templates. These reference signals act to generate desired switching pulses for VSC with the help of Hysteresis Current Controller (HCC). In this thesis, UTC strategy is compared with the dq-SRF control method.

The results are compared in G2V and V2G modes in terms of (i) PCC voltages, (ii) PCC currents, (iii) THD_V, and (iv) THD_I.

The main contributions of the said-work is listed next.

5.2 Main Contributions and Conclusions

The main conclusions made from this thesis is as follows:

1. In FCS, Common DC Bus Architecture is better than common AC Bus Architecture because of

i. Fewer transformation stages as there is only one main AC to DC converter (VSC) as compared to Common AC bus (separate VSC for each bay). It results in a simpler system and requirement of fewer number of power electronic devices.

ii. The charging rate (SoC) is fast in the case of CDCB FCS as compared to CACB FCS.

iii. The PCC voltage and PCC current waveforms are better and having fewer distortions in case of CDCB architecture.

iv. Low THD_V and THD_I, and as a result, better power quality (low harmonic emissions) is obtained in the case of CDCB FCS.

v. There is an impact of the number of EV bays on the harmonic emissions. THD_V and THD_I increases with the increase in the number of EVs on the same rated system.

vi. The system efficiency of the Common DC bus improves due to better power quality (low harmonic emissions) and power factor.

vii. The CDCB is more stable in a dynamic-state as compared to the CACB.

viii. Reduced circulating currents in between converters, which results in low DC Component in case of CDCB FCS.

2. Star-Delta (Y- Δ) configuration of DT is the method (Table 4.3 and Table 4.4) as it gives low THD_V and THD_I in both the architectures during charging-mode.

3. In the comparison of dq-SRF and UTC control strategies, UTC strategy came as more robust, stable, and has a low impact on THD_V and THD_I. The PCC voltage and current waveforms are more sinusoidal and having fewer disturbances in case of UTC strategy implementation during steady-state and dynamic-state. The settling time of UTC is faster than the dq-SRF control strategy.

4. The comparisons were made by varying X/R ratio and Short Circuit Capacity (MVA_{SC}) in steady-state and dynamic-state. The following conclusions are made.

i. There is visible impact of variation of X/R ratio on the performance of grid-connected DC FCS in case of weak-grid (low value of MVA_{SC}).

ii. The higher X/R ratio increases the charging speed, and decreases the THD_V and THD_I in steady-state. But there are more transients in the FCS during the dynamic-state in case of higher X/R ratio. The value of SCR is higher in case of X/R = 10 (high value), and results in more disturbances. Similarly, increase in MVA_{SC} (strong-grid) rating of the grid decreases the THD_V and THD_I values.

5. The comparison of grid-connected FCS with and without PV-panel is made. The addition of PV-panel in the grid-connected FCS results in flexibility and reliability of the system. The comparison is also made in Islanded-mode operation. The SoC is compared by inclusion of PV-panel in grid-connected DC FCS with and without PV-panel. Comparative analysis shows increase in the charging speed of batteries and smoothening of the charging curve which ultimately results into more battery life. There is slight increase in THD_V and THD_I, with the inclusion of PV-panel. But, harmonics are under the limits as per IEEE-519 and IEC standards.

6. The comparison is done by replacing common DC-link Conventional-Capacitor (CC) with Super-Capacitor (SC).

i. The operation with SC results into faster response, high charging rate and low harmonic content. It may increase the life of connected EV batteries and improves the overall efficiency of the system.

7. Vehicle to Grid (V2G) mode is studied to compare both CDCB and CACB, FCS architectures. In this analysis, State of Discharge (SoD), PCC voltages, PCC currents, and comparison of

THD_V and THD_I has been done. Results shows that CDCB architecture is more robust, having better voltage and current waveforms and low harmonics (THD_V and THD_I) than the CACB architecture in V2G mode. The harmonics (THD_V and THD_I) are unacceptable in case of CACB architecture as per IEEE-519 limits.

These conclusions establish that CDCB architecture is a better technology in FCS and can be employed easily with distributed generation too. There are fewer harmonics in case of grid-connected CDCB FCS. This thesis also gives insight to impact of X/R ratio and MVA_{SC} on grid-connected FCS, inclusion of PV-panel and super-capacitor.

5.3 Future Scope

1. The FCS architectures could be made by using multi-level converter topologies like Neutral-point Clamped (NPC) 3-level converter which can offer a better performance.
2. Other control strategies should be employed for the VSC (main-converter) to compare it with the proposed strategy. Artificial intelligence (AI) based control schemes, direct power control method and model-predictive control techniques can be employed. Similarly, new control methods should be used for DC-DC converter except proposed CC-CV control strategy for further study.
3. Other kind of renewable sources (wind, geothermal etc.) should be included to study the impact on the performance of FCS and smart-grid.
4. The hardware implementation of the simulated work could be done to validate the results.

REFERENCES

[1] Intergovernmental panel on climate change report, https://www.ipcc.ch [accessed 12 February 2020].

[2] World Health Organization report [online], https://www.who.int [accessed 12 February 2020].

[3] V.V. Chernysheva, A.M. Zakharenkoa, S.M. Ugaya et. al, "Morphological and chemical composition of particulate matter in buses exhaust," Elsevier International Journal of Toxicology Reports, Volume 6, pp.120–125,2019.

[4] International Energy Agency (IEA) Annual Report, https://www.iea.org/reports/global-energy-and-co2-status-report-2019 [accessed 12 February 2020].

[5] United Nations Climate Change (UNFCC), https://unfccc.int/ [accessed 12 February 2020].

[6] Global EV Outlook 2019 [online], Available: https://www.iea.org/reports/global-ev-outlook-2019

[7] The World Bank, "An Engagement Paper from The World Bank and The International Association of Public Transport, [online] Available: http://documents.worldbank.org/

[8] Joeri van Mierlo, J. The World Vehicle Journal, The Open Access for Electric the e-Mobility Scene Journal for the e-Mobility Scene. *World Electr. Veh. J.* 2018, 9, 1.

[9] Hydro Quebec, "Electric Vehicle Charging Stations-Technical Installation Guide", Hydro Quebec, ETS, [online] Available: http://www.hydroquebec.com/data/electrification-transport/pdf/technical-guide.pdf

[10] Doug Kettles, "Electric Vehicle Charging Technology Analysis and Standards", Electric Vehicle Transportation Centre, February 2015.

[11] Moradewicz A. J., On / Off – board chargers for electric vehicles, Przegląd Elektrotechniczny, ISSN 0033-2097, R. 95 NR 2/2019.

[12] Hydro Quebec, "Electric Vehicle Charging Stations-Technical Installation Guide", Hydro Quebec, ETS, [online] Available: http://www.hydroquebec.com/data/electrification-transport/pdf/technical-guide.pdf.

[13] Charge Point,"Driver's Checklist: A Quick Guide to Fast Charging", [online] Available: https://www.chargepoint.com/files/Quick_Guide_to_Fast_Charging.pdf

[14] Doug Kettles, "Electric Vehicle Charging Technology Analysis and Standards", Electric Vehicle Transportation Centre, February 2015.

[15] Electric vehicle charging modes [online]: https://www.virta.global/blog/ev-charging-modes.

[16] Electric Vehicle Communication Standards, Testing and Validation – Phase I: SAE J2847/1, "U.S. Department of Energy Report September 2011" [online] Available: https://www.pnnl.gov/main/publications/external/technical_reports/PNNL-20913.pdf

[17] CHAdeMO. What is CHAdeMO [Online]. Available: https://www.chademo.com/about-us/what-is-chademo.

[18] Mohd Rizwan Khalid, Mohammad Saad Alam, Adil Sarwar, M.S.Jalim Asghar, " A comprehensive review on electric vehicle charging infrastructures and their impacts on power-quality of the utility grid", *Elsevier eTransportation*, Volume 1, August 2019.

[19] V. T. Tran, D. Sutanto and K. M. Muttaqi, “The state of the art of battery charging infrastructure for electrical vehicles: Topologies, power control strategies, and future trend,” in Proc. of AUPEC, Melbourne, VIC, Australia, 2017, pp. 1-6.

[20] Hall, D.; Lutsey, N. Emerging Best Practices for Electric Vehicle Charging Infrastructure; The International Council on Clean Transportation (ICCT): Washington, DC, USA, 2017.

[21] G. Naveen, I. H.-I. Yip, Y. Xie, “Modeling and protection of electric vehicle charging station,” in Proc. of 2014 6th IEEE Power India International Conference (PIICON), Delhi, India, 2014, pp. 1-6.

[22] C. H. Dharmakeerthi, N. Mithulananthan, and T. K. Saha, "Modeling and planning of EV fast charging station in power grid," Power and Energy Society General Meeting, 2012 IEEE, pp. 1-8, 22-26 July 2012.

[23] Gagandeep Sharma, Vijay K Sood, Mohammad Saad Alam and Samir M. Shariff, “Comparison of Common DC and AC Bus Architectures for EV Fast Charging Stations and Impact on Power Quality”, *Elsevier eTransportation*, Volume 5, August 2020.

[24] https://www.globenewswire.com/ [online report] accessed on August 20,2020.

[25] Expansion, challenges and opportunities in the EV market and EVSE industry blog on e-mobility, https://circontrol.com/expansion-challenges-ev-market-evse-industry/ [online] accessed on August 19,2020.

[26] Department of Energy, “The History of the Electric Car”, [online] Available: https://www.energy.gov/articles/history-electric-car

[27] History website, “Charles F. Kettering, inventor of electric self-starter, is born”, [online], Available: https://www.history.com/

[28] The White House, Report of The Environmental Pollution Panel President’s Science Advisory Committee, *“Restoring the quality of our Environment”*, November 1965.

[29] B. K. Bose, “The past, present, and future of power electronics,” *IEEE Ind. Electron. Mag*., vol. 3, no. 2, pp. 7–11, Jun. 2009.

[30] Naoui Mohamed, Flah aymen, Ben Hamed Mouna, and Sbita alassaad, “Review on Autonomous Charger for EV and HEV,” 2017 International Conference on Green Energy Conversion Systems, Mar. 2017, pp. 1-6.

[31] E. Ayisire, A. El-Shahat and A. Sharaf,” Magnetic Resonance Coupling Modelling for Electric Vehicles Wireless Charging,” 2018 IEEE Global Humanitarian Technology Conference (GHTC), San Jose, CA, 2018, pp. 1-2.

[32] Ayob, Afida & Mahmood, Wan & Mohamed, Azah & Che Wanik, Mohd Zamri & Mohd Siam, Mohd Fadzil & Sulaiman, Saharuddin & Azit, Abu & Ali, Mohamed, “Review on Electric Vehicle, Battery Charger, Charging Station and Standards”, *Research Journal of Applied Sciences, Engineering and Technology*, Vol. 7, pp. 364-373, January 2014.

[33] Miwa, T., Sato, H., Takayuki Morikawa, T., 2017, “Range and Battery Depletion Concerns with Electric Vehicles”, *Hindawi - Journal of Advanced Transportation*, Volume 3, pp. 1-12, December 2017.

[34] Erik Figenbaum, “Perspectives on Norway’s supercharged Electric Vehicle Policy,” *Elsevier International Journal of Environmental Innovation and Societal Transitions,* Volume 25, pp. 14–34,2017.

[35] Jameson Dow, “56% of Norway’s New cars had a plug in 2019, Tesla Model 3 Overall best-seller”, News Article, [Online]Available : https://ww.electrek.co/

[36] Bill Chappell, “Electric Cars Hit Record in Norway, Making Up Nearly 60 Percent of Sales in March”, Article [online] Available: https://www.npr.org/.

[37] Cregger J. Charging infrastructure required to support us electric vehicle deployment: A cost estimate through 2025. In: Proceedings of the 2015 IEEE Vehicle Power and Propulsion Conference; 2015 Oct 19-22; Montreal, Canada. IEEE; 2015. p. 1–6.

[38] Yassir Alhazmi, “Planning Model for Implementing Electric Vehicle Charging Infrastructure in Distribution System”, Ph.D. Thesis, University of Waterloo, Waterloo, ON, 2016.

[39] IEEE Report by Intelligent Transportation Systems of the IEEE Vehicular Technology Society, “IEEE Standard Technical Specifications of a DC Quick Charger for Use with Electric Vehicles”, September 2015.

[40] V. T. Tran, D. Sutanto and K. M. Muttaqi, “The state of the art of battery charging infrastructure for electrical vehicles: Topologies, power control strategies, and future trend,” in Proc. of AUPEC, Melbourne, VIC, Australia, 2017, pp. 1-6.

[41] L. Tan, B. Wu, V. Yaramasu, S. Rivera, and X. Guo, "Effective Voltage Balance Control for Bipolar-DC-Bus-Fed EV Charging Station with Three-Level DC–DC Fast Charger," *IEEE Transactions on Industrial Electronics*, vol.63, pp. 4031-4041, 2016.

[42] Ancy Sara Varghsese, Polly Thomos and Shemil Varghese, “An Efficient Voltage Control Strategy for Fast Charging of Plug-In Electric Vehicle,” in Proc. of International Conference on Innovations in Power and Advanced Computing Technologies [i-PACT2017], Vellore, India, April 2017, pp. 1-4.

[43] G. Naveen, I. H.-I. Yip, Y. Xie, “Modeling and protection of electric vehicle charging station,” in Proc. of 2014 6th IEEE Power India International Conference (PIICON), Delhi, India, 2014, pp. 1-6.

[44] C. H. Dharmakeerthi, N. Mithulananthan, and T. K. Saha, "Modeling and planning of EV fast charging station in power grid," Power and Energy Society General Meeting, 2012 IEEE, pp. 1-8, 22-26 July 2012.

[45] Vitor Monteiro ,Tiago J.C. Sousa ,Carlos Couto ,Julio S. Martins ,Andres A. Nogueiras Melendez and Joao L. Afonso, “A Novel Multi-Objective Off-board EV Charging Station for Smart Homes,” in Proc. of IECON 2018-44th Annual Conference of the IEEE Industrial Electronics Society, Lisbon, Portugal.2018, pp. 1983-1988.

[46] V. Monteiro, J. G. Pinto, and J. L. Afonso, “Operation modes for the electric vehicle in smart grids and smart homes: Present and proposed modes,” *IEEE Transactions on Vehicular Technology*, vol. 65, no. 3, pp. 1007–1020, Mar. 2016.

[47] K. Rajashekara, “Present status and future trends in electric vehicle propulsion technologies,” *IEEE J. Emerg. Sel. Topics Power Electron*ics, vol. 1, no. 1, pp. 3–10, Mar. 2013.

[48] D. C. Erb, O. C. Onar, and A. Khaligh, “Bi-directional charging topologies for plug-in hybrid electric vehicles,” in Proc. 25th Annu. IEEE Appl. Power Electron. Conf., 2010, pp. 2066–2072.

[49] Mohammad Nikkhah Mojdehi, Prasanta Ghosh, “An On-Demand Compensation Function for an EV as a Reactive Power Service Provider”, *IEEE Transactions on Vehicular Technology*, vol. 65, no. 6, pp. 4572-4583, 6, June 2016.

[50] A. M. Ben Jar, Neville Watson, Rapid EV chargers: Implementation of a charger, Electric Power Engineering Centre (EPECentre), University of Canterbury (EEA Conference Exhibition 2016, Wellington, 2016).

[51] IEC 62196: ‘Connectors for conductive charging of electric vehicles’, version 2016.

[52] IEC61850: ‘Communication/automation, part 90–8: object model for EV’, 2017.

[53] Enel, “The different EV charging Connector type”, [online], Available: https://evcharging.enelx.com/

[54] Wajahat Khan, Furkan Ahmad, Mohammad Saad Alam, “Fast EV charging station integration with grid Ensuring optimal and quality power exchange,” *Elsevier International Journal of Engineering Science and Technology,* Volume 22, Issue 1, pp. 143–152, February 2019.

[55] Van den Bossche Peter, Turcksin Tom, Omar Noshin and Van MierloJoeri, “Developments and Challenges for EV Charging Infrastructure Standardization”, *World Electric Vehicle Journal,* Volume 8, pp. 1-7, 2016.

[56] Little-fuse Expertise Applied, “EV Charging Infrastructure presentation”, [online], Available: https://www.littelfuse.com//media/electronics/market

[57] S. Haghbin, S. Lundmark, M. Alakula, and O. Carlson, “Grid Connected Integrated Battery Chargers in Vehicle Applications: Review and New Solution,” *IEEE Transactions on Industrial Electronics*, vol. 60, no. 2, pp. 459–473, Feb. 2013.

[58] B. T. Vankayalapati, R. Singh, and V. K. Bussa, "Two stage integrated on-board charger for EVs," in 2018 IEEE International Conference on Industrial Technology (ICIT), 2018, pp. 1807-1813.

[59] O. Veneri, L. Ferraro, C. Capasso, D. Iannuzzi, “Charging Infrastructures for EV: Overview of Technologies and Issues,” *IEEE Electrical Systems for Aircraft, Railway and Ship Propulsion*, pp 1 – 6,2012.

[60] Diogo Varajao, Rui E. Araujo et. al, “Control of an Isolated single-phase bidirectional AC-DC Matrix Converter for V2G applications”, *Elsevier International Journal of Electric Power System Research,* Volume 149, pp. 19–29, 2017.

[61] Deepak, R.; Apoorva, K.; Sheldon, S.W. Extreme Fast Charging Technology—Prospects to Enhance Sustainable Electric Transportation. *Energies* 2019, *12*, 3721.

[62] Gray, M.K., Morsi, W.G.: ‘Power quality assessment in distribution systems embedded with plug-in hybrid and battery electric vehicles’, *IEEE Trans. Power Syst.*, 30(2), pp. 663–671,2015.

[63] N. Shaukat et. al, ‘‘A survey on electric vehicle transportation within smart grid system,’’ Renew. Sustain. Energy Rev., vol. 81, pp. 1329–1349, Jan. 2018. [Online]. Available: https://doi.org/10.1016/j.rser.2017.

[64] Sam Francis, “Top 20 Electric Vehicle Charging Station Companies”, Robotics and automation news report, https://roboticsandautomationnews.com/ [online] accessed on August 21, 2020.

[65] Tan, L., Wu, B., Rivera, S., et al.: “Comprehensive DC power balance management in high-power three-level DC–DC converter for electric vehicle fast charging”, *IEEE Trans. Power Electron.*, 2016, 31, (1), pp. 89–100.

[66] Cai, G.; Liu, D.; Liu, C.; Li, W.; Sun, J. A High-Frequency Isolation (HFI) Charging DC Port Combining a Front-End Three-Level Converter with a Back-End LLC Resonant Converter. *Energies* 2017, *10*, 1462.

[67] Vitor Monteiro, João C. Ferreira, Andres A. Nogueiras Melendez, Carlos Couto, João L. Afonso, “Experimental Validation of a Novel Architecture Based on a Dual-Stage Converter for Off-Board Fast Battery Chargers of Electric Vehicles,” *IEEE Trans. Veh. Tech.*, vol.67, no.2, pp.1000-1011, Feb. 2018.

[68] A.Jimenez,N.Garcia, “Power Flow Modeling and Analysis of Voltage Source Converter-Based Plug-in Electric Vehicles,” IEEE Transactions on Power Systems,2011.

[69] Kulsomsup Yenchamchalit, Yuttana Kongjeen and Krischonme Bhumkittipich and Nadarajah Mithulananthan, “Optimal Sizing and Location of the Charging Station for Plug-in Electric Vehicles using the Particle Swarm Optimization Technique”, 2018 International Electrical Engineering Congress (iEECON), Krabi, Thailand,2018.

[70] Wajahat Khan, Furkan Ahmad and Mohammad Saad Alam, “Fast EV charging station integration with grid ensuring optimal and quality power exchange”, *Elsevier eTransportation*, Volume 22, pp. 143-152,2019.

[71] IEEE, "IEEE Recommended Practice for Powering and Grounding Electronic Equipment - Redline," in IEEE Std. 1100-2005 (Revision of IEEE Std 1100-1999) - Redline ed., 2006, pp. 1-703.

[72] Fuchs E., & Masoum, M.A., “Power Quality in Power Systems and Electrical Machines”, 2nd ed. Elsevier, USA, 2015.

[73] Ahmed R. Abul’Wafa, Aboul’fotouh El’Garably, Wael A.Fatah Mohamed. Uncoordinated vs Coordinated Charging of Electric Vehicles in Distribution Systems Performance. International Journal of Engineering and Information Systems (IJEAIS), 2017, 1 (6), pp.54 - 65.

[74] R.C. Dugan, M.F. McGranaghan, S. Santoso, H.W. Beaty, Electrical Power Systems Quality, third ed., McGraw Hill, 2012.

[75] IEC, "IEC 61000-4-30 Standard", 2007.

[76] IEEE Recommended Practice and Requirements for Harmonic Control in Electric Power Systems, in IEEE Std. 519-2014 (Revision of IEEE Std 519-1992), pp.1-29, June 2014.

[77] IEEE Draft Guide for Applying Harmonic Limits on Power Systems, in IEEE P519.1/D12, July 2012, pp.1-124, 26 Feb. 2015.

[78] M.F. McGranaghan and S. Santoso, “Challenges and trends in analyses of electric power quality measurement data,” EURASIP J. Adv. Signal Process. (Special Issue on Emerging Signal Processing Techniques for Power Quality Applications), 2007.

[79] M.H.J. Bollen *et al*., “Bridging the gap between signal and power,” *IEEE Signal Processing Magazine,* 26(4), 2009, pp. 12-31.

[80] Chudy A., Mazurek P. A., “Electromobility – the Importance of Power Quality and Environmental Sustainability”, Journal of Ecological Engineering, 20(10), 2019, pp. 15-23.

[81] P. T. Staats, W. M. Grady, A. Arapostathis and R.S. Thallam. “A Statistical Analysis of the Effect of Electric Vehicle Battery Charging on Distribution System Harmonic Voltages,” *IEEE Transactions on Power Delivery*, USA, vol. 13, pp: 640-646, 1998.

[82] J. C. Gomez and M. M. Morcos, "Impact of EV battery chargers on the power quality of distribution systems," *IEEE Transactions on Power Delivery*, vol. 18, pp. 975-981, 2003.

[83] Deb, S.; Tammi, K.; Kalita, K.; Mahanta, P. Impact of Electric Vehicle Charging Station Load on Distribution Network. *Energies 2018*, 11, 178.

[84] M. A. Awadallah, B. N. Singh, and B. Venkatesh, "Impact of EV Charger Load on Distribution Network Capacity: A Case Study in Toronto", *Canadian Journal of Computer Engineering*, Vol. 39, 2016.

[85] C.K. Duffey, R.D. Stratford, "Update of Harmonic Standard IEEE-5 19: IEEE Recommended Practices and Requirements for Harmonic Control in Electric Power Systems", *IEEE Trans. Ind. Appl.*, Vo1.25, No.6, 1989, pp.1025-1034.

[86] Jeremy D. Watson and Neville R. Watson, “Impact of Electric Vehicle chargers on harmonic levels in Newzeland”, in Proc. of 2017 7th IEEE Innovative Smart Grid Technologies (ISGT Asia 2017) annual premier smart grid technology meeting, Auckland, Newzeland, December 4-7 2017.

[87] L.R. Limongi, D.Roiu, R.Bojoi, and A.Tenconi, "Analysis of Active Power Filter Operating with Unbalanced Load," in Proc. of 2009 IEEE Energy Conversion Congress and Exposition, San Jose(CA), USA,2009, pp.584-591.

[88] M. Vujacic, M. Hammami, M. Srndovic, and G. Grandi, "Analysis of dc-link voltage switching ripple in three-phase PWM inverters," Energies, vol. 11, no. 2, p. 471, 2018.

[89] R. Erickson, *Fundamentals of Power Electronics*, New York: Chapman and Hall, 1997.

[90] Mathew Keyser et. al, *Design and Analysis of Large Lithium-ion Battery Systems*, Boston: Artech House, 2015.

[91] Iclodean C, Varga B, Burnete N, Cimerdean D, Jurchiş B. Comparison of Different Battery Types for Electric Vehicles. IOP Conf. Ser Mater Sci Eng 2017;252. doi:10.1088/1757-899X/252/1/012058.

[92] Shah F.A., Sheikh S.S., Mir U.I., Athar S.O., "Battery Health Monitoring for Commercialized Electric Vehicle Batteries: Lithium-Ion", in Proc. of the 5th International Conference on Power Generation Systems and Renewable Energy Technologies (PGSRET), Istanbul, Turkey, 26-27 August,2019.

[93] Hannan, M.A., Hoque, M.M., Hussain, A., et al.: 'State-of-the-art and energy management system of lithium-ion batteries in electric vehicle applications: issues and recommendations', *IEEE Access*, 2018, 6, pp. 19362–19378.

[94] Song Y, Minjun P, Seo M, Kim WS, "Improved SOC estimation of lithium-ion batteries with novel SOC-OCV curve estimation method using equivalent circuit model", in Proc. of the 4th International Conference on Sustainable Technologies (SpliTech), Bol and Split, Crotia, June 18-21, 2019.

[95] Jokic, I.; Zecevic, Z.; Krstajic, B. State-of-charge estimation of lithium-ion batteries using extended Kalman filter and unscented Kalman filter. In Proceedings of the 2018 23rd International Scientific-Professional Conference on Information Technology (IT), Zabljak, Montenegro, 19–24 Febulary 2018; pp. 1–4.

[96] Frede Blaabjerg, *Control of Power Electronic Converters and Systems*, Academic Press, Imprint of Elsevier, 2018.

[97] Chang W-Y. The state of charge estimating methods for battery: a review. ISRN Appl. Math 2013; 2013:1–7.

[98] Xu Zhang, Yujie Wang, Zonghai Chen, "Model-Based Remaining Discharge Energy Estimation of Lithium-ion Batteries", in the Proc. of 2017 3rd International Conference on Control, Automation and Robotics, Japan, 22-24 April, 2017.

[99] Feng Y, Meng C, Han F, Yi X, Yu X, "An Online Estimation Algorithm of State-of-Charge of Lithium-ion Batteries", in Proc. of the 44th Annual Conference of the IEEE Industrial Electronics Society, Washington D.C., USA, October 21-23,2018, pp. 3879- 882.

[100] M. Coleman, C. K. Lee, C. Zhu, and W. G. Hurley, "State-of-charge determination from EMF voltage estimation: using impedance, terminal voltage, and current for lead-acid and lithium-ion batteries," *IEEE Transactions on Industrial Electronics*, vol. 54, no. 5, pp. 2550–2557, 2007.

[101] Katyara S, Staszewski L, Musavi A. H, Soomro F. 2017. Short Circuit Capacity: A key to design Reliable Protection Scheme for Power System with Distributed Generation. *International Journal of Mechanical Engineering and Robotics Research*, 6(2), 126-133.

[102] L. D. Aguiar, R. Cardoso, C. Stein, P. D. Costa, and E. Carati. 2016. *Distributed Renewable Power Sources in Weak Grids - Analysis and Control*. London, 199-225, UK: IntechOpen.

[103] S. L. Lorenzen, A. B. Nielsen and L. Bede. 2016. "Control of a grid connected converter during weak grid conditions." In *2016 IEEE 7th International Symposium on Power Electronics for Distributed Generation Systems (PEDG), June 27-30*, pp. 1-6, Vancouver, BC.

[104] Leon Freris, David Infield. 2008. *Renewable Energy in Power Systems*. West Sussex, UK: Wiley.

[105] Sayed, K. Gabbar, H.A. 2016. Electric Vehicle to Power Grid Integration Using Three-Phase Three-Level AC/DC Converter and PI-Fuzzy Controller. *Energies*, 9(532), 1-16.

[106] R. Erickson.1997. *Fundamentals of Power Electronics*, New York: Chapman and Hall.

[107] F. E. U. Reis, R. P. Torrico-Bascope, F. L. Tofoli and L. D. Santos Bezerra. 2020. Bidirectional Three-Level Stacked Neutral-Point-Clamped Converter for Electric Vehicle Charging Stations. *IEEE Access*, 8, 37565-37577.

[108] V. M. Iyer, S. Gulur, G. Gohil and S. Bhattacharya, "Extreme fast charging station architecture for electric vehicles with partial power processing," 2018 IEEE Applied Power Electronics Conference and Exposition (APEC), San Antonio, TX, 2018, pp. 659-665, doi: 10.1109/APEC.2018.8341082.

[109] F. E. U. Reis, R. P. Torrico-Bascopé, F. L. Tofoli and L. D. Santos Bezerra, "Bidirectional Three-Level Stacked Neutral-Point-Clamped Converter for Electric Vehicle Charging Stations," in IEEE Access, vol. 8, pp. 37565-37577, 2020, doi: 10.1109/ACCESS.2020.2976003.

[110] H.-G. Eckel, M. M. Bakran, E. U. Krafft, and A. Nagel, “A new family of modular IGBT converters for traction applications,” in Proc. European Conf. Power Electronics Applications, Dresden, Germany, 2005, pp. 1–10.

[111] Anandarup Das, Design and Implementation of a 3-phase, 2-Level Voltage Source Converter, Report by PEEMD, Research Group, IIT Delhi, Version V. 1.0, 2017.

[112] J. Rodriguez, S. Bernet, B. Wu, J. O. Pontt and S. Kouro, "Multilevel Voltage-Source-Converter Topologies for Industrial Medium-Voltage Drives," in *IEEE Transactions on Industrial Electronics*, vol. 54, no. 6, pp. 2930-2945, Dec. 2007.

[113] Olimpo Anaya-Lara, David Campos-Gaona, Edgar Moreno-Goytia and Grain Adam, *Off shore Wind Energy Generation: Control, Protection, and Integration to Electrical Systems*, First Edition, John Wiley & Sons Ltd., 2014.

[114] Amirnaser Yazdani, Reza Iravani, *Voltage –Sourced Converters in Power System: Modeling, Control and Applications*, Wiley-IEEE Press, 2010.

[115] C. Huang and L. Zhao, "Design of Controller for VSC-HVDC Systems with the alpha beta Stationary Frame," 2012 Asia-Pacific Power and Energy Engineering Conference, Shanghai, 2012, pp. 1-4.

[116] Michael Lindgren, “Modeling and Control of Voltage Source Converters Connected to the Grid” Ph.D Thesis, Chalmers University of Technology, Goteborg, Swedan,1998.

[117] J. Rodriguez et al., "Predictive Current Control of a Voltage Source Inverter," in *IEEE Transactions on Industrial Electronics*, vol. 54, no. 1, pp. 495-503, Feb. 2007.

[118] B. Singh, A. Chandra and K. AL -Haddad, *Power Quality – Problems and Mitigation Techniques*, West Sussex, UK: Wiley, 2015.

[119] A. 1. Rana, C. K. Vasoya, M. H. Pandya, and P. M. Saradva, "Application of Unit Template Algorithm for voltage sag mitigation in distribution line using D-STATCOM," 2016 International Conference on Energy Efficient Technologies for Sustainability (ICEETS), 2016, pp. 756-761.

[120] J. Bangarraju, V. Rajagopal and A. Jayalaxmi, “Unit template synchronous reference frame theory based Control algorithm for DSTATCOM,” *J.Inst. Eng. India Ser. B*, Vol. 95, no.2, pp. 135-141,2014.

[121] A. Verma and B. Singh, “Multi-objective reconfigurable three phase off-board charger for EV,” in IEEE Transportation Electrification Conf. (ITEC-India), Pune, 2017, pp. 1-6.

[122] S. Pulendran, J. E. Tate, "Hysteresis Control of Voltage Source Converters for Synchronous Machine Emulation" in Proceedings of the 15th International Power Electronics and Motion Control Conference, EPE-PEMC 2012 ECCE Europe, Novi Sad, Serbia, 4-6 September 2012, 1-8 pp.

[123] A. Blorfan, P. Wira, D. Flieller, G. Sturtzer and J. Mercklé, "A three-phase hybrid active power filter with photovoltaic generation and hysteresis current control," IECON 2011 - 37th Annual Conference of the IEEE Industrial Electronics Society, Melbourne, VIC, 2011, pp. 4316-4321.

[124] Frede Blaabjerg, *Control of Power Electronic Converters and Systems*, Academic Press, Imprint of Elsevier, 2018.

[125] J. Patel, H. Chandwani, V. Patel and H. Lakhani, "Bi-directional DC-DC converter for battery charging – Discharging applications using buck-boost switch," 2012 IEEE Students' Conference on Electrical, Electronics and Computer Science, Bhopal, 2012, pp. 1-4.

[126] I. Lee and J. Kim, "A high-power DC-DC converter for electric vehicle battery charger," 2017 IEEE 3rd International Future Energy Electronics Conference and ECCE Asia (IFEEC 2017 - ECCE Asia), Kaohsiung, 2017, pp. 1861-1866.

[127] S. Chakraborty, H. Vu, M. M. Hasan, D. Tran, M. El Baghdadi, and O. Hegazy, “DC-DC Converter Topologies for Electric Vehicles, Plug-in Hybrid Electric Vehicles and Fast Charging Stations: State of the Art and Future Trends,” Energies 2019, 12, 1569.

[128] S. Chakraborty, S. Goel, I. Aizpuru, M. Mazuela, R. Klink and O. Hegazy, "High-Fidelity Liquid-cooling Thermal Modeling of a WBG-based Bidirectional DC-DC Converter for Electric Drivetrains," 2019 21st European Conference on Power Electronics and Applications (EPE '19 ECCE Europe), Genova, Italy, 2019, pp. 1-8.

[129] Ke Bao, Shuhui Li, and Zheng “Battery Charge and Discharge Control for Energy Management in EV and Utility Integration,” *IEEE Power and Energy Society General Meeting*, pp. 1-8, 2012.

[130] Serna-Garcés S, González Montoya D, Ramos-Paja C. Control of a charger/discharger DC/DC converter with improved disturbance rejection for bus regulation. *Energies*. 2018; 11: 594.

[131] Marian P. KAZMIERKOWSKI, Krzysztof ZYMMER, “Power Electronic Architecture of Supply Systems for Electric Vehicle Charging,”*Baztech Prace Instytutu Elektrotechniki journal*, Vol. Z 278, pp. 7-19, 2018.

[132] T. M. Blooming, and D. J. Carnovale, “Application of IEEE Std. 519-1992 harmonic limits,” in Pulp and Paper Industry Technical Conference, 2006. Conference Record of Annual, pp. 1-9, 2006.

[133] P. M. Ivry, D. W. P. Thomas and M. Sumner, "Assessment of power quality in a microgrid with power electronic converters," 2016 Asia-Pacific International Symposium on Electromagnetic Compatibility (APEMC), Shenzhen, 2016, pp. 825-827.

[134] P. Thomas and F. M. Chacko, "Electric vehicle integration to distribution grid ensuring quality power exchange," 2014 International Conference on Power Signals Control and Computations (EPSCICON), Thrissur, 2014, pp. 1-6.

[135] A. Arancibia, K. Strunz, Modeling of an electric vehicle charging station for fast DC charging, Electric Vehicle Conference (IEVC), 2012 IEEE International, 2012, pp. 1-6.

[136] Rivera, S., Wu, B., Kouro, S., et al.: ‘Electric vehicle charging station using a neutral point clamped converter with bipolar DC bus’, IEEE Trans. Ind. Electron., 2015, 62, (4), pp. 1999–2009.

[137] Sebastian Andre Rivera Iunnissi, “Architecture and Control of an Electric Vehicle Charging Station using a Bipolar DC Bus,” Ph.D. Thesis, Ryerson University, Toronto, ON, 2016.

[138] T. Mishima, E. Hiraki, T. Tanaka and M. Nakaoka, "A New Soft Switched Bidirectional DC-DC Converter Topology for Automotive High Voltage DC Bus Architectures," in Proc. of IEEE Vehicle Power and Propulsion Conference, Windsor, 6-8 Sept. 2006.

[139] K.Mishra, M.K. Karthlkeyan, A Fast-Acting DC-link Voltage Controller for Three-Phase DSTATCOM to compensate AC and DC loads, *IEEE Transactions on power delivery*, Vol. 24, no. 4, pp. 2291-2299, 2009.

[140] L. Kutt, E. Saarijarvi, M. Lehtonen, H. Molder, and J. Niitsoo, "A review of the harmonic and unbalance effects in electrical distribution networks due to EV charging", in Proc. 2013 IEEE International Conference on Environment and Electrical Engineering.

[141] Robert Bass, Nicole Zimmerman, “Impacts of Electric Vehicle Charging on Electric Power Distribution Systems”, Oregon Transportation Research and Education Consortium Final Report, Tech Report, OTREC-SS-731, October 2013.

[142] Alexandre Lucas, Fausto Bonavitacola, Evangelos Kotsakis and Gianluca Fulli, “Grid Harmonic Impact of multiple electric vehicle charging,” *Elsevier Journal of Electric Power System Research,* Vol. 127, pp. 13-21, October 2015.

[143] Ikram Ullah and Muhammad Ashraf, “Comparison of Synchronization Techniques Under Distorted Grid Conditions”, *IEEE Access Journal*, vol. 7, pp. 101345-101354, August 2019.

[144] F.D. Freijedo, J. Doval-Gandoy, O. Lopez, and E. Acha, “Tuning of phase locked loops for power converters under distorted utility conditions,” *IEEE Trans. Ind. Appl*., vol. 45, no. 6, pp. 2039–2047, Nov./Dec. 2009.

[145] L. N. Arruda, S. M. Silva, and B. J. C. Filho, “PLL structures for utility connected systems,” in Conf. Rec. 36th IEEE IAS Annu. Meeting, Chicago, IL, Sep./Oct. 2001, vol. 4, pp. 2655–2660.

[146] Singh, B., Arya, S.R.: ‘Adaptive theory based improved linear sinusoidal tracer control algorithm for DSTATCOM’, *IEEE Trans. Power Electron*., 2013, 28, (8), pp. 3768–3778.

[147] F. X. Chapman and B. Hammonds, "The effect of DC offset on instantaneous operating characteristics of low-voltage circuit breakers," in *IEEE Transactions on Industry Applications*, vol. 33, no. 6, pp. 1488-1492, Nov.-Dec. 1997, doi: 10.1109/28.649960.

[148] P. Sahu, D. Verma and S. Nema. 2016. “Physical design and modelling of boost converter for maximum power point tracking in solar PV systems.” In *2016 International Conference on Electrical Power and Energy Systems (ICEPES), December 14-16*, pp. 10-15, Bhopal.

[149] Sun power SPR-315E-WHT-D (315 W) Solar panel data-sheet [online], Available: http://www.solardesigntool.com/

[150] T. Chen et al., "A Review on Electric Vehicle Charging Infrastructure Development in the UK," in *Journal of Modern Power Systems and Clean Energy*, vol. 8, no. 2, pp. 193-205, March 2020.

[151] W. Kempton and J. Tomic, “Vehicle-to-grid power implementation: From stabilizing the grid to supporting large-scale renewable energy,” J. Power Sources, vol. 144, no. 1, pp. 280–294, Jun. 2005.

[152] Chairul Gagarin Irianto and R. Setiabudy, "Design Dtz transformer that compatible with nonlinear load in modern electrical systems," Proceedings of the 2011 International Conference on Electrical Engineering and Informatics, Bandung, 2011, pp. 1-6, doi: 10.1109/ICEEI.2011.6021751.

[153] L. M. P. Fanjul, "Some New Applications of Super-capacitors in Power Electronic Systems," Master of Science, Dept. Electrical Engineering, Texas A&M University, College Station, 2003.

[154] Super-capacitor Simulink component description, Available: https://www.mathworks.com/